A MATHEMATICAL MODEL DEVELOPMENT AND SENSITIVITY ANALYSIS OF TWO PHOTON POLYMERIZATION FOR 3D MICRO/NANO FABRICATION

by

NITIN UPPAL

Presented to the Faculty of the Graduate School of
The University of Texas at Arlington in Partial Fulfillment
of the Requirements
for the Degree of

DOCTOR OF PHILOSOPHY

THE UNIVERSITY OF TEXAS AT ARLINGTON

August 2008

ACKNOWLEDGEMENTS

I would like to thank my principal advisor, Dr. Panos S. Shiakolas for the valuable guidance and generous support that he provided throughout the course of my graduate studies. I learnt from him how to independently tackle the research problem and to formulate theoretical concepts and bridging them with practical applications. I consider myself lucky to be a part of his research group and to work with someone who is genuinely passionate about research. Many thanks to Dr. Pranesh Aswath whose valuable inputs have helped me make a better researcher and an engineer. His emphasis on the underlying theories helped me acknowledge the fundamental phenomenon that sometimes we take for granted. I would like to thank Dr. Jian Yang who introduced me to the interesting world of polymers and polymerization. I would also like to thank Dr. Seiichi Nomura and Dr. Kytai Nguyen for their interest in my research and being an integral part of the dissertation committee.

I acknowledge the support and help received from my colleagues at the BioMEMS and MARS laboratories: Dr. Sunil Belligundu, Dr. Mohammad Mayyas, Mr. Mohsin Rizwan, Mr. Nikhil Kavadia, Mr. Krishanu Saha and Mr. Vijay Sarathy. I also graciously acknowledge Stephanie Autrey, for her assistance in modifying the originally developed simulation program to address our needs relative to multiple pulses and result plotting and her suggestions fro improving the simulation algorithm. I would also like to thank the staff of Mechanical Engineering department, Mr. Tom Leeds, Mr. Michael Baker, Mrs. Barbara Sanderson, Mrs. Donna Woodhead and Mrs. Janet Gomber for their support, assistance and encouragement throughout my graduate studies. I would also like to thank Dr. Jiechao Jiang for providing access to the SEM and optical microscope for the characterization and measurement of micro/nano structures.

Finally, I would like to express my deep gratitude to my parents and sister for their ever-present and unconditional support and encouragement. They have always been a source of inspiration for me. Without their support, love, patience and encouragement it would have been really tough to finish this research.

July 1, 2008

ABSTRACT

A MATHEMATICAL MODEL DEVELOPMENT AND SENSITIVITY ANALYSIS
OF TWO PHOTON POLYMERIZATION FOR
3D MICRO/NANO FABRICATION

Nitin Uppal, PhD.

The University of Texas at Arlington, 2008

Supervising Professor: Panos S. Shiakolas

Two photon polymerization (2PP) is an effective technique for the fabrication of complex polymeric 3-D micro/nano features using ultrashort pulses from a NIR laser source. The photosensitive material absorbs two photons and initiates the chain polymerization reaction. The interaction of laser pulses with photo responsive resin creates a voxel (volumetric pixel) which defines the resolution of 2PP process. In this work, a mathematical model of the polymerization process that considers the effects of molecular diffusion and polymerization kinetics on the formation of voxel. The increase in temperature upon polymerization and their effect on the polymerization kinetics and molecular diffusion is also considered in the model. The model adheres to the 3D confinement and nonlinear photophysical and photochemical changes that take place in the confined volume.

A Design of Experiments methodology is employed to evaluate the sensitivity of the 2PP process on the applied laser power, scanning speed (or exposure time) and photoinitiator concentration. The proposed statistical model is checked for interaction between the process

parameters, and multiple comparisons are laid out for evaluating the statistically significant differences. A regression model is developed for the prediction of polymerization resolution based on the experimental data. The developed statistical model is experimentally verified and along with the understanding acquired through the statistical analysis was used for the successful prototyping of various micro/nano structures. Feature sizes of ~1.5 μm in radial direction and ~20 μm in axial direction are fabricated using the existing laser system and 0.4 NA microscope objective.

A novel approach for fabricating high aspect ratio in a single laser scan is also presented. Aspect ratios of ~ 100 and higher can be easily achieved with a single laser scan of loosely focused laser pulses. The fabricated structures show good structural integrity, high aspect ratio and fabricated in a single laser scan at moderate laser powers. Also, the deformation and collapse of the polymerized pattern due to cohesive forces and remedial measures are discussed. The presented work demonstrates the ability of low repetition rate laser systems and loosely focused laser pulses for fabrication of high aspect ratio structures in a single laser scan.

TABLE OF CONTENTS

LIST OF ILLUSTRATIONS

LIST OF TABLES

LIST OF NOMENCLATURES

n_a ..... Number of photons absorbed per molecule per sec

δ ..... Two photon absorption cross-section

P_{avg} ..... Average applied power

τ_p ..... Pulse width of laser system

$\hbar$ ..... Planck's constant

c ..... Speed of light

λ ..... Laser wavelength

f_p ..... Pulse repetition rate of laser system

I ..... Applied laser intensity

v ..... Laser frequency

N ..... Number density of excited radicals

S_o ..... Ground state

S_1 ..... First excited state

T_1 ..... Triplet state

F ..... Fluorescence emission

Ph ..... Phosphorescence emission

P ..... Photoinitiator concentration

R ..... Radical concentration

I ..... Inhibitor concentration

T ..... Temperature distribution

M ..... Monomer concentration

H ..... Enthalpy of polymerization

k ..... Thermal conductivity

ρ ..... Monomer density

α ..... Molar absorption coefficient

c_p ..... Monomer specific heat

x ..... distance along x-axis

y ..... distance along y-axis

z ..... distance along z-axis

t ..... time

r ..... radial distance

I_o ..... Laser intensity at the center of the beam

ω_o ..... Theoretical beam waist

z_r ..... Rayleigh length

$\omega(z)$ ..... spatial distribution along axial direction

Φ ..... Applied photon flux

d ..... Diffusion constant

d_o ..... Pre-exponential factor for diffusion

R_g ..... Gas constant

E_{pa} ..... Activation energy for propagation

E_{za} ..... Activation energy for inhibition

E_{ta} ..... Activation energy for termination

ψ ..... Quantum yield

k_t ..... Combination termination constant

k_p ..... Propagation constant

k_z ..... Inhibition termination constant

k_{to} ..... Pre-exponential termination constant

k_{po} ..... Pre-exponential propagation constant

k_{zo} ..... Pre-exponential inhibition constant

f ..... Trapping factor

Y ..... Dependent variable

β ..... Photoinitiator concentration main effect

γ ..... Speed main effect

ω ..... Power main effect

$\beta\gamma$ ..... Interaction between photoinitiator and speed

$\beta\omega$ ..... Interaction between photoinitiator and power

$\gamma\omega$ ..... Interaction between speed and power

$\beta\gamma\omega$ ..... Interaction between photoinitiator, speed and power

ε ..... Probability of committing type 1 error

c_{ijk} ..... Contrast coefficients

H_o ..... Null Hypothesis

w_t ..... Tukey coefficient

τ ..... Treatment mean

w_s ..... Scheffé coefficient

μ ..... Actual mean

y_{ijk} ..... Estimated mean

w_{ijkt} ..... Weights used for weighted least square analysis

s^2_{ijk} ..... Sample variance

d ..... Distance between the polymerized walls

σ .... Surface tension

F .... Cohesive force

θ .... Angle of contact

LIST OF ABBREVATIONS

2PP	Two photon Polymerization
FLM	Femtosecond laser micromachining
3D	Three dimensional
UV	Ultraviolet
NA	Numerical Aperture
MPA	Multiphoton Absorption
µTM	Micro transfer molding
SDG	Synchronization and delay generator
GVD	Group velocity dispersion
CCD	Charged couple device
GM	Göppert Meyer
HQ	Hydroquinone
MEHQ	Hydroquinone mono methyl ether
FOM	Figure of merit
PDE	Partial differential equation
FDM	Finite difference method
FTCS	Forward time centered space
DPR	Dynamic power range
ANOVA	Analysis of variance
mSE	Mean square error
MSD	Minimum significant difference

WLS ..... Weighted least square

AVP ..... Added variable plots

LISW ..... Light induced self-written waveguides

NIR ..... Near infrared

CHAPTER 1

INTRODUCTION

The ever increasing advancements in MEMS applications require the development of truly three dimensional micro structure fabrication technologies is ever increasing. Technological advancements and the need to reduce the component size, novel micro/nano fabrication processes have and are being developed that push the limit of achievable process resolution. Microelectronics, boosted by more than half a century of research, has already reduced the size of silicon based components to mere tens of nanometers. Apart from silicon based fabrication methods, some non traditional processes are also being explored to include other materials in the realm of micro/nano advancements. Polymers are used increasingly for bioengineering, microfluidics and photonics applications due to their flexibility, good optical properties, biocompatibility and their ability for tailored properties [1, 2]. Polymer based micro/nano components are gaining popularity because of their conformability and ease of fabrication without the use of harsh processing conditions.

Extensive work has been done with LIGA and photolithography for fabricating three dimensional microstructures but these methods require either secondary operations or masks, making them less desirable for rapid prototyping applications [1]. Though, photolithography is extensively used in semiconductor industry and is a very mature technology. In photolithography, light is used to transfer the geometric pattern from a mask to a photoresponsive resist. Chemical etching is usually employed that removes the regions that are not protected by photoresist. In photolithography, a negative or positive tone photoresist is used on which the geometric pattern from the mask is transferred. In negative tone photoresist, the exposed resist withstands the developing phase, whereas the positive tone photoresist is

etched away. Primarily, the optical source used for mask transfer is UV light, but various other alternatives are being explored such as electron beam lithography, X-ray lithography, extreme ultraviolet lithography, ion projection lithography, projection lithography, nanoimprint lithography etc. that are pushing the achievable resolution of the process. High index lithography is a new development in the real of photolithography micro/nano fabrication that has pushed the feature sizes smaller than 30 nm [3]. Though, these methods are very efficient for fabricating high resolution features their major drawback is that they are mostly limited to planar geometries.

For 3D fabrication, stacking of different layers has been tried, but alignment and number of stacked layers puts a limitation on the aspect ratio of the micro component. Various other techniques, chemical deposition, proton beam writing etc. are also employed for 3D fabrication, but these methods are also limited to mostly planar structures with high aspect ratios [4, 5]. Microstereolithography is another method that is commonly employed to polymerize a photo resin, layer-by-layer to build up microstructures by focusing an ultraviolet laser beam on the resin surface. Microstereolithography is based on single photon absorption process where the photoinitiator molecule decomposes into radicals that initiate the polymerization process on the absorption of UV light. Microstereolithography is a very common rapid prototyping technique extensively used in industry for the fabrication of 3D structures [6]. The focused laser beam is absorbed by liquid resin that polymerizes and forms a solid feature. By scanning the laser beam in a predefined pattern and by lowering the vat in a step-by-step manner, a complete 3D structure is fabricated. The schematic of microstereolithography process is shown in figure 1.1.

The main limitation of the microstereolithography is the absorption of the laser beam on the surface because of single photon absorption mechanism. As the laser is absorbed by the surface of photoresponsive resin, the vat has to be lowered after every exposure setting so that the liquid resin can form a fine layer on top of polymerized feature. This layer is a gain polymerized by the UV laser source and the process is repeated till the final component is

fabricated. The limitation comes as the thickness of the smallest layer defines the resolution of this process and is generally depend on the surface tension of employed resin system. This layer-by-layer fabrication methodology can fabricate complex 3D structures but the achievable resolution of the process is no match to the photolithographic techniques mentioned earlier.

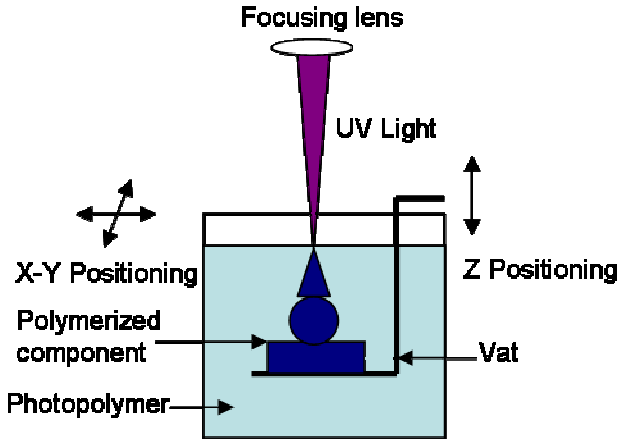

Figure 1.1 Schematic of microstereolithography process

1.1 Two Photon Polymerization for 3D fabrication

Two Photon Polymerization, 2PP, is a powerful and fairly new (mid 1990s) technique for fabricating complex 2D and 3D microstructures by polymerizing the photo responsive liquid resin. The principle of 2PP is somewhat similar to stereolithography, but in 2PP process the laser beam is focused inside the liquid consisting of defined concentrations of monomer and photoinitiator and the polymerization reaction takes place at the point of focus. The unexposed resin can be removed by washing with a solvent leaving behind the polymerized structure. The polymerization can be spatially and temporally controlled because radical species that initiate the polymerization reaction are produced only at the point of focus [7, 8]. 2PP has many advantages as a technique for the direct fabrication of complex 3D structures which might be difficult to fabricate using conventional miniaturization technologies.

In 2PP, two photons are used to initiate the photochemical changes and the polymerization can be localized within the focal volume of ultrashort laser pulse that has passed

through a focusing lens. The absorption of two photons by the photoinitiator molecule should take place in a very short time interval (generally in sub femtosecond range). The photoiniator decomposes and generates radicals which initiate the chain polymerization process, converting liquid resin into solid features. The number of photons absorbed per molecule per pulse (n_a) of an ultrashort laser beam is represented by equation 1 [9, 10]. In equation 1, δ_2 is the two photon absorption cross-section of the photoinitiator molecule, P_{avg} is the applied average laser power, NA is the numerical aperture of the microscope objective, τ_p is the pulse width of laser system, f_p is the pulse repetition rate of laser source, $\hbar$ is the plank's constant, c is the speed of light, and λ is the laser wavelength in vacuum.

$$n_a \approx \frac{\delta_2 P_{avg}^2}{\tau_p f_p^2}\left(\frac{NA^2}{2\hbar c\lambda}\right)^2 \quad (1)$$

As presented in equation 1, the absorption of photons by the photoinitiator molecules has a quadratic dependence on the applied input laser power, where single photon absorption assisted fabrication has a linear dependence on the input laser power. The quadratic dependence is advantageous in confining or defining a volume where photon absorption and subsequent chemical changes take place. The intensity distributions for a single and a two photon absorption process are presented in figure 1.2. The difference between the linear and quadratic dependence on intensity is represented through spatial distribution and contour plots in figures 1.2(a) to 1.2(d) respectively. High laser intensity is achieved by ultrashort lasers at the focal volume that enhances the probability of two photon absorption and subsequent initiation of the polymerization process. Though, the confinement produced by quadratic dependence does not always represent the minimum feature size produced by 2PP process, since there are other molecular and kinetic phenomena that have a strong effect on the achievable resolution of 2PP process. A complete discussion on these phenomena along with the intensity dependence will be presented in following sections.

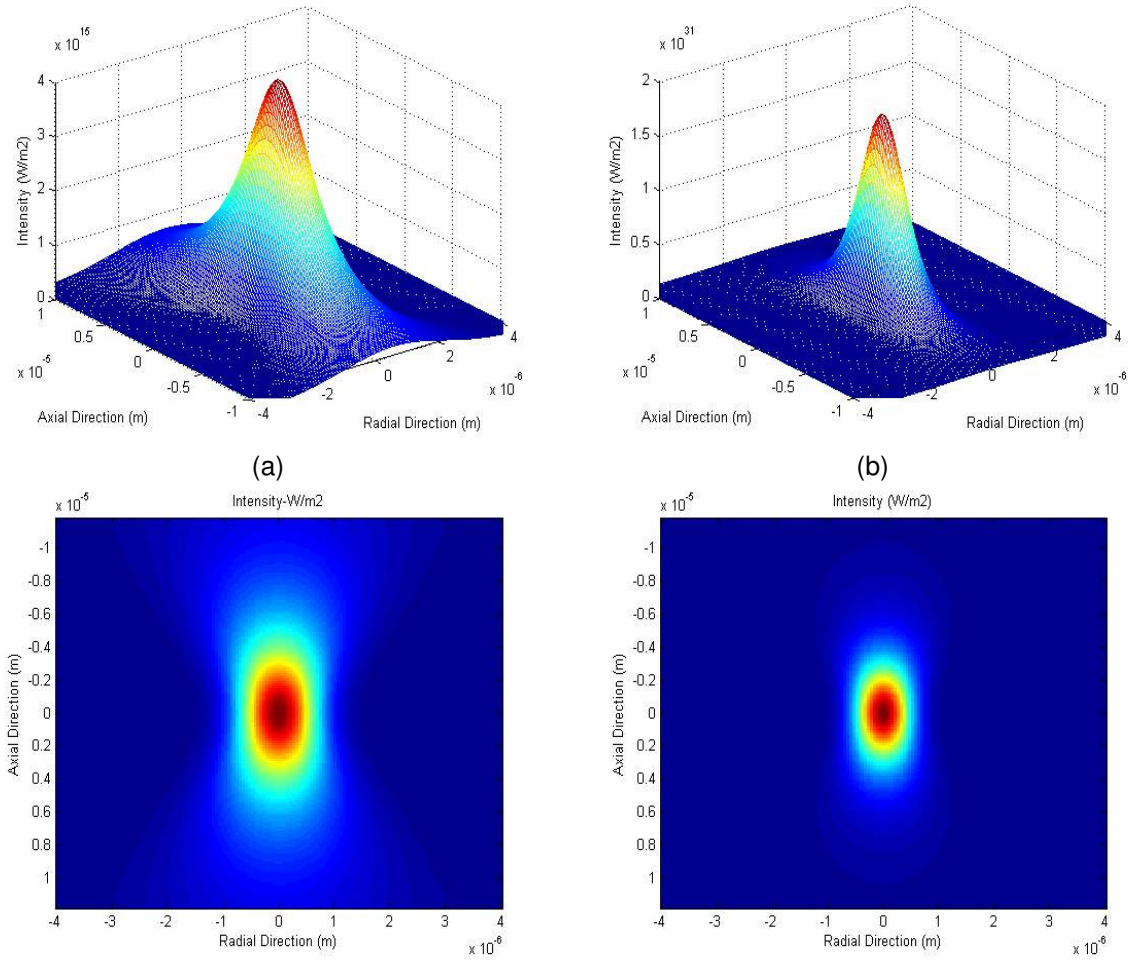

Figure 1.2 Point spread function of single and two photon absorption (a) Single photon absorption 3D plot, (b) Two photon absorption 3D plot, (c) Single photon absorption contour plot, and (d) Two photon absorption contour plot

The quadratic intensity dependence of 2PP process leads to higher flexibility compared to the single photon absorption assisted fabrication. The nonlinear dependence on intensity leads to localization of polymerization volume and helps in achieving much higher resolution compared to single photon process [9, 10]. The two photon absorption region is defined by the intersection of inverted cones that is basically the focal volume created by the focusing optics as shown in figure 1.3. Hence, the region where the polymerization reaction initiates depends on the high intensity regions defined by this focal volume. Also, because of the nonlinear

dependence on input laser intensity and nonlinear photophysical and photochemical changes, focal volumes as small as few atto-liters can be initiated leading to achievable fabricated feature sizes much smaller than the diffraction limit of the focusing optics [11].

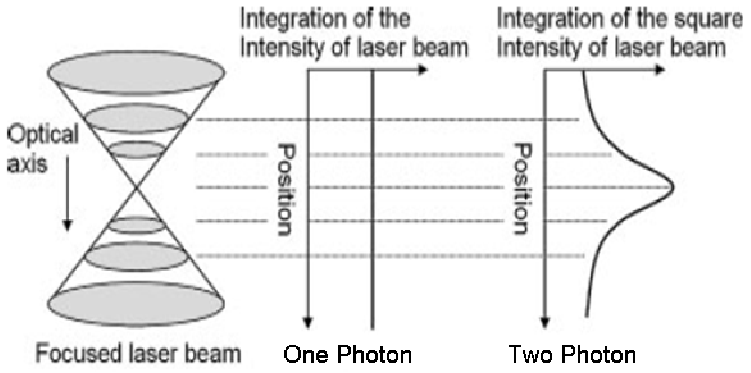

Figure 1.3 One photon and two photon process [11]

Hence, 2PP provides an effective process for fabricating complex 3D structures with very high resolution not achieved with single photon or other fabrication processes. The photopolymerization reaction initiated in the irradiated region and the gradual conversion of monomer into high molecular weight polymer take place, while off focus regions stay in the liquid phase. This provides an advantageous situation where complex 3D structures can be fabricated inside the liquid resin with the scanning of laser irradiation in a predefined pattern. The idea of 2PP assisted 3D fabrication is presented in the schematic shown in figure 1.4.

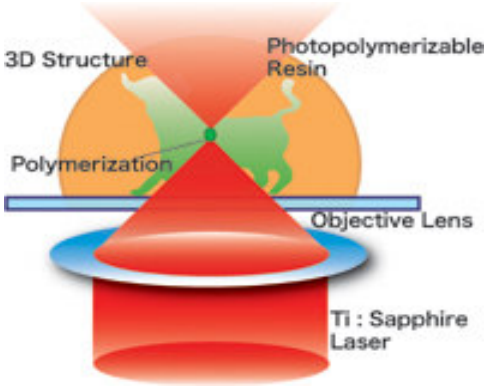

Figure 1.4 Two Photon Polymerization process [11]

The resolution of 2PP process is defined by the volume in which monomer conversion takes place. The propagation of chain polymerization reaction polymerizes a small volume referred to as a *voxel* (volumetric pixel). A complete 3D structure can be easily fabricated by stacking these voxels together as presented in figure 1.4. Thus, it is important to understand the physical phenomena responsible for the evolution of voxel as functions of various process and material dependent parameters to achieve high resolution and good control over the polymerization process.

1.2 Two Photon Absorption process

As discussed in the previous section, 2PP is initiated by the absorption of two photons in a quasi-simultaneous event. Two-photon absorption defines a quantum event when a molecule of an absorber simultaneously absorbs two photons, where quasi-simultaneous event means a temporal window of 10^{-16} sec (0.1 fs) [9]. This makes the two photon absorption a rare event and its probability of occurrence depends on the applied photon flux. The rarity of this event was reported by Denk et al where they compared the absorption of single and two photons of sunlight. An absorber absorbs single photon by one photon interaction process once every one second but the simultaneous two photon absorption of a photon pair of sunlight takes place once every 10 million years [12]. Hence, this small temporal window makes the two photon absorption a rare event but it can be achieved by using high photon fluxes. That is why the experimental work could only be performed with the evolution of laser sources in the early 60's. The initial two photon absorption applications were limited to spectroscopic studies. The development of mode-locked ultrafast high repetition rate laser sources made two photon absorption possible for scanning microscopy [10, 12].

Commendable work by Denk et al at the W.W. Webb laboratory at Cornell University provided a breakthrough for multi-photon absorption for fluorescence microscopy, data storage and micro/nano fabrication [10, 13]. Multi photon absorption was first demonstrated by the group for fluorescence microscopy using a NIR mode-locked ultrafast laser source for the

molecular excitation and subsequent fluorescence microscopy. J.H. Stickler also perform pioneering work in optical data storage in the early nineties [13], which was later adapted by various research groups across the world. Mazur et al from the Department of Physics at the Harvard University performed extensive research in optical changes induced in transparent materials with multi photon absorption [14].

The mechanism of two photon absorption process relates to the single photon absorption where the molecules are brought to an excited state with the absorption of photon/s. In single photon absorption, the molecules absorb the energy from incident irradiation that matches the energy requirement for transition and transits to higher energy states. At the higher energy state, the molecule looses energy due to thermal relaxation and relaxes back to the ground state. During the transition from higher to ground state the molecule emits a photon of lower energy. With the transition and relaxation of enough molecules a strong fluorescence signal can be generated that becomes the source for fluorescence microscopy. The same idea is extended to multiphoton absorption process. But, in multiphoton absorption more than one photon is required to raise the molecules to an excited state, as a single photon does not have enough energy for a direct transition, their interaction raises the molecules to a virtual state. The virtual state has a very short life time (10^{-15} to 10^{-16} sec) and the subsequent photon absorption should take place within this time frame to raise the molecule to excited state. Once excited, the molecules relax similar to the one photon absorption process producing fluorescence signal or radical species depending upon the application [10, 12]. A schematic comparing the one and two photon processes is presented in figure 1.5.

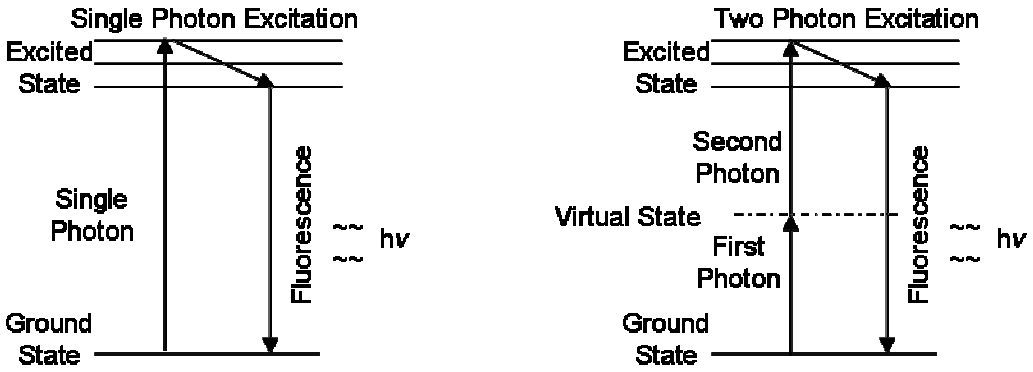

(a) (b)

Figure 1.5 Single and two photon absorption process (a) Single photon excitation process, (b) Two photon excitation process

The simultaneous absorption of multiphoton absorption is possible only by focusing ultrafast lasers that are capable of producing high intensities. The average number of molecules that are excited per unit volume per unit time, R_{nhv} is given by equation 2 [7].

$$R_{nhv} = \frac{\delta^{(n)} N I^n}{n(\hbar v)^n} \tag{2}$$

Where, $\delta^{(n)}$ is the absorption cross-section of the photoinitiator, $\hbar$ is Planck's constant, N is the number density of excited radicals, v is the frequency of laser, I is intensity and n is the order of excitation process. For 2PP to initiate, the intensity must be high enough so that there is a high probability of more than one photon arriving simultaneously at the species to be excited. This is where femtosecond lasers are able to initiate the 2PP process because of achievable high intensity due to ultrashort pulsewidths. Typical cross sections for one and two photon processes are $\delta^{(1)}$ = 10^{-17}cm^2 and $\delta^{(2)}$ = 10^{-47}cm^4 s/photon respectively [7]. To achieve almost the same average number of molecules per unit volume per unit time generated by one photon and two photon excitation ($R_{1hv} \approx R_{2hv}$), the intensity, $I = 2hv\ \delta^{(1)} / \delta^{(2)}$ required and is equivalent to 500 GW/cm^2 (500x10^9 W/cm^2). A femtosecond laser of 800 nm wavelength and pulse width of 100 fs having pulse energy of 0.125 nJ and a focal lens generating a spot size of 0.5 µm, has an intensity of ~200x10^9 W/cm^2 which is same order in magnitude as a one photon process. This

illustrates the need for using ultrafast laser pulses that can increase the probability of two photon absorption resulting in the radical generation.

In a photopolymerization process, the liquid polymer is converted into solid phase by crosslinking or polymerization induced by the incident light of appropriate wavelength only in the focal volume. The achievable 3D confinement in 2PP is attributed to the nonlinear photophysical and photochemical changes that take place only in that confined volume with the photoresponsive resin system. Most monomers and oligomers commonly used for photopolymerization do not possess reactive species with high enough quantum yield. A photoinitiator is used that absorbs the incident radiation and breaks down into reactive species. Though, the mechanism of decomposition of photoinitiator and subsequent generation of radicals is quite complex, it can be explained by electronic states transition of the molecules and is pictured by Perrin-Jablonski diagram [15]. In two photon polymerization, when the laser pulses interact with the photoinitiator molecules in the resin, the molecules absorb the first photon and move from the ground state (S_0) to the virtual state. The virtual state has a very short life time and the second photon has to be absorbed in a quasi-simultaneous event that can raise the molecule to the first excited state (S_1) as shown in figure 1.6. The quasi-simultaneous event requires high photon fluxes that increase the probability of two photon absorption. The required high photon fluxes can be created by temporal and spatial confinement of laser pulses. The tight focusing using a high N.A. lens satisfies the requirement of spatial confinement but the temporal confinement is achieved by using ultrashort laser pulses. The pulses from a femtosecond laser source along with tight focusing conditions produced high incident photon fluxes that increase the probability of two photon absorption. Though the supplied energy should match the energy requirement for electronic state transition, the combined energy of two photons should be equal to the energy requirement for transition. The photoinitiator molecules after the absorption of two photons rise to the first excited state (S_1). The time period of S_1 is generally short and the molecules relax to the triplet state (T_1) due

to the collisions with other molecules. The triplet state (T_1) has a little lower energy than S_1. In the triplet state, the radical generation takes place when the excited photoinitiator molecules undergo bond cleavage and decompose into radical species [15]. These reactive species then react with the monomer and initiate chain polymerization forming a high molecular weight polymer. But the number of radicals generated in the triplet state depends on other competing radical termination processes. It is not necessary that the excited molecules in S_1 make an inter system transition to T_1. These excited molecules in S_1 can relax to the ground state by fluorescence emission (F) or from T_1 to ground state by the phosphorescence emission (Ph) [11]. These relaxed molecules do not undergo bond cleavage processes and have no contribution in the generation of radicals. So, the photoinitiator is chosen such that it has minimum fluorescence and phosphorescence emission and most of the excited molecules undergo bond cleavage and subsequent radical generation. Even if the excited photoinitiator molecules make an inter system crossing to T_1 and undergo bond cleavage and subsequent radical generation, these generated radicals can be deactivated either by monomer or inhibitor quenching processes [11, 15]. The quenching of radicals depends on the concentration of quencher media in the resin system and can be controlled to a certain extent by varying its concentration. One of the common quenching processes is the combination of a radical molecule with oxygen which is a strong inhibitor. The combination with inhibitor molecules deactivates the reactive radicals and renders it ineffective for initiating the chain polymerization process. The generation of radicals and their effective use for the initiation of polymerization reaction has to compete with the radical deactivation mechanisms (fluorescence, phosphorescence and quenching). The efficiency of the polymerization process can be increased by minimizing these deactivating processes and increasing the number of generated radicals with input laser energy. Note, that deactivation by quenching can be advantageously employed to increase the polymerization threshold and reduce the size of polymerized features and will be discussed later.

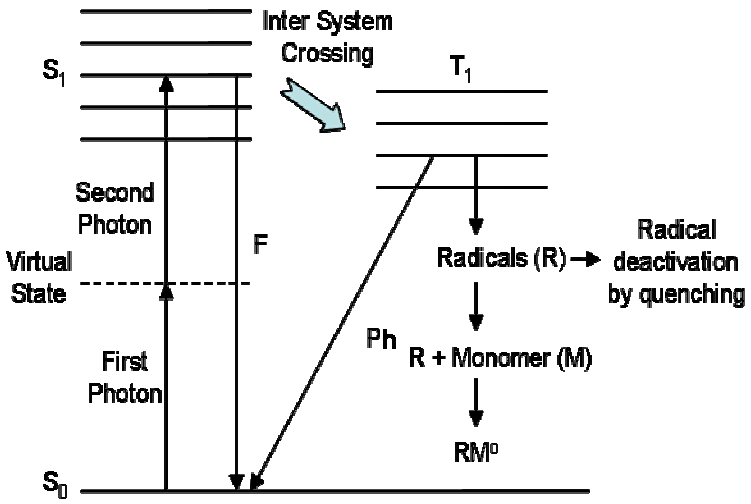

Figure 1.6 Two Photon Polymerization mechanism.

Most of the 2PP work is conducted using negative tone photopolymer systems consisting of acrylate monomer and photoinitiator in controlled concentrations. The polymerization undergoes a free radical chain polymerization reaction where monomer molecules interact with the active radicals and produce a reactive center that propagates the polymerization reaction converting monomer into high molecular weight polymer. The radical chain polymerization consists of a sequence of three steps: Initiation, Propagation and Termination [16]. In initiation, the photoinitiator molecules generate active radicals as discussed earlier. The initiation process can be represented by equation 3.

$$P \xrightarrow{h\nu} 2R^{\bullet} \qquad (3)$$

The generated radicals combine with monomer molecules and create reactive center ($M_1^{\bullet}$) that then combines with available monomer molecules to form a polymer chain. The propagation of polymer chain depends upon the availability of monomer molecules and the kinetic constant for propagation, k_p. Propagation continues with the growth of reactive center with successive addition of large number of monomer molecules. The propagation step can be represented by equation 4.

$$M_n^{\bullet} + M \xrightarrow{k_p} M_{n+1}^{\bullet} \quad (4)$$

The conversion of monomer molecules to high molecular weight polymer takes place very rapidly but at some point the propagating chain stops growing and terminates. The termination can take place by three mechanisms: 1) termination by radical combination, 2) termination by trapping, or 3) termination by inhibition. These competing mechanisms partially control the size of propagating chain and the percentage of monomer conversion. The rate of termination depends upon the termination rate constants, k_t and k_z, and the available concentration of active radicals. Without termination, the propagating chain polymerization will continue until all the monomer is completely exhausted and the whole volume will polymerize. But termination kinetics limit the volume where polymerization reaction progresses and monomer conversion takes place. The termination step is presented by equation 4.

$$M_n^{\bullet} + M_m^{\bullet} \xrightarrow{k_t} \textit{Dead Polymer} \quad (5)$$

The advantage of using the photoinitiator polymerization is that the reaction can be controlled both spatially and temporally. The molecular weight of polymer gradually increases and provides the structural integrity to the polymerized features. The lower molecular weight polymer and non reactive monomer molecules are washed away during the developing process leaving the polymerized feature.

1.3 Literature Review

2PP is derived from the Multiphoton Absorption (MPA) phenomenon that has a nonlinear dependence on the input photon flux. The origin of MPA dates back to 1931 when Maria Göppert-Mayer predicted this phenomenon in her doctoral dissertation [7, 9]. But at that time, MPA was just a theory as there were no lasers to validate the absorption of two or more photons. With the advent of laser systems in early 60's, the experiment to validate the MPA process was performed on CaF_2: Eu^{2+} [9]. But initial experiments were mostly performed for spectroscopic studies and limited to few materials because of long pulse laser sources available

at that time. With the development of ultrashort pulse laser system in the early 90's, Denk et al at the W.W. Webb laboratory at the Cornell University utilized the two photon absorption mechanism for fluorescence microscopy applications [10, 12]. They coupled the two photon excitation with scanning microscope that revolutionized the field of fluorescence microscopic imaging. Strickler et al also at the W. W. Webb laboratory used the multiphoton absorption phenomena for 3D optical data storage and also used the two photon absorption for the fabrication of the first 2PP microstructure [13, 17]. Since then, various groups across the world have effectively employed 2PP for complex 3D micro/nano fabrication applications [18-20].

1.3.1 Applications of 2PP

2PP has been an active research area in recent years because of its many advantages over conventional miniaturization technologies. The polymerization patterning does not require a mask, the material properties can be tailored, and true three dimensional features can be fabricated that makes the process applicable for a diverse range of applications. Since the seminal work at the W. W. Webb lab at the Cornell University, two photon absorption was adapted for the fabrication of microstructures by S. Maruo and S. Kawata of the Department of Applied Physics at Osaka University, Japan [18]. They fabricated a micro spiral and a tube using commercially available urethane acrylate oilgomer also known as SCR 500 and were able to attain a lateral and depth resolution of 0.62 µm and 2.2 µm respectively. In the coming years, research in the development of efficient two photon photoinitiators with high two photon absorption cross-section was intensified. Kuebler et al at the University of Arizona worked on developing various new photoinitiator molecules that show very high two photon absorption cross-section [19]. Some very important work in 3D fabrication using 2PP has been performed at laser Zentrum Hannover, Germany by the research group of Dr. B.N. Chichkov. In most of Dr. Chichkov's work, a photosensitive inorganic-organic hybrid polymer (ORMOCER) has been used for the fabrication and rapid prototyping of different photonic structures and integrated optical devices [20, 21]. ORMOCER is an acronym for ORganically MOdified CERamic

consisting of Si-O-Si (Silicone) backbone. Even in the recent years, 2PP is extensively used for fabrication of 3D photonic crystals because of the achievable nanoscale resolution with this process. Photonic crystals are materials that have periodicity in their dielectric constant and can strongly modulate light or may produce a photonic bandgap [22]. Direct writing of woodpile structures using 2PP that act as photonic crystals is an efficient method because of achievable resolution and flexibility in fabricating complex periodic structures. Various groups have used 2PP for the fabrication of these woodpile structures for photonic applications [22-24]. Metallization of these photonic crystals is also reported by first patterning the polymeric crystal using 2PP and then using electroless electroplating of copper for metallization [25].

2PP has also been used for various other applications beside photonic applications. Simple microstructures like microsprings and microturbines have been fabricated that are driven optically by laser beam trapping. These movable microcomponents are directly fabricated through an assembly-free process using 2PP inside the photocurable resin [26]. Also, selective functionalization of fabricated polymeric structures is reported by depositing of wide range of materials on selected areas on polymerized structures [27]. In selective functionalization, features were fabricated of acrylate and methacrylate monomer and because of the differential reactivity of these materials, deposition reaction was performed only on the regions consisting of only one type of polymer. 2PP is also used for biomedical patterning applications. 2PP is effectively used for the prototyping of transdermal microneedles for drug delivery using ORMOCER as the material for fabrication [28]. 2PP is also used for the fabrication of scaffolding structures for tissue engineering applications [29]. The main limitation with the use of 2PP for the fabrication of implantable biomedical devices is the availability of very few biocompatible monomer and photoinitiator systems that can be employed for prototyping applications. As the living cells are very sensitive to external media, even small concentrations of toxic photoinitiator commonly employed for 2PP can cause cytotoxicity and killing of living cells.

Though, new photoinitiator and monomers are being developed in laboratory settings, there are only a few commercially available photoinitiator and monomer systems that can be effectively used for 2PP applications. Another challenge for 2PP is the serial nature in which the components are fabricated. As components are fabricated one at a time, the throughput of the process is small. Multiple processing and micro transfer molding (μTM) are two common techniques employed to increase the throughput of 2PP. In multiple processing, a microlens array is used to create multiple focal volumes where polymerization can initiate. By scanning the microlens array in predefine patter similar to the serial 2PP process, multiple features can be fabricated that increase the effective throughput of the process [30]. Another method is μTM that is a soft lithographic technique used for replicating microscopic structures. The master mold created by 2PP is covered with PDMS that forms an elastomeric solid mold. The PDMS mold can be poured with molding material and produce the replica of original structure [31]. By combining, multiple processing and μTM, the throughput of 2PP can be tremendously increased.

The realm of 2PP is ever expanding and various new applications or materials are constantly being developed. Due to its 3D fabrication capability, 2PP is emerging as a novel and efficient micro/nanofabrication technology that can change the way in which features are fabricated. Though there are various challenges that are still associated with this technology, they will be overcome with constant effort from the active research groups in this area.

1.3.2 Materials for 2PP

Photopolymerization is primarily performed using UV irradiation of a photoresponsive liquid resin that contains a defined concentration of monomer and photoinitiator. The UV light initiates the polymerization process by decomposing photoinitiator molecules into radicals. These radicals combine with the present monomer molecules and propagate the chain polymerization process. Similar free radical chain polymerization reaction governs the 2PP process. The 2PP, like any photo-polymerization process is characterized by the steps of

initiation, propagation and termination but the polymerization mechanism is quite different because of quadratic dependence on applied laser intensity and the polymerization is initiated by ultrashort pulsed laser source. 2PP has been used for the patterning of micro/nano features in both negative and positive tone photoresists [7, 32]. Most of the work has been performed in the patterning of negative tone photoresists using the Two Photon polymerization (2PP) technique. Epoxy based cationic photoresists (SU8), acrylates (SR499, PEGdma) and inorganic based materials are routinely used for 2PP fabrication [32-35]. Epoxy based photoresists are mostly solid and polymerization reaction only takes place after the laser irradiation (during post baking process) but acrylate based and inorganic materials the polymerization reaction initiates during the laser irradiation and carries on until the active radicals terminate [32]. Acrylates are commonly used for the 2PP process and upon initiation go through a free radical chain polymerization reaction. Unlike epoxy based photoresists, acrylates are mostly liquid at room temperature and mixed with a controlled amount of photoinitiator. Complex 2D and 3D microstructures can be fabricated from this photo responsive liquid resin by scanning ultrashort laser pulses and subsequent polymerization of a *voxel* (a volumetric pixel). Scanning the laser pulse inside the liquid resin, true 3D structures can be fabricated with micron and submicron resolution. 2PP has been performed on both negative and positive tone photoresist materials. In negative photoresists, the two photon exposure causes crosslinking of the exposed volumes and provides enough structural rigidity to withstand the developing process. The unexposed resin is washed away during the developing step leaving behind polymerized features. Whereas, in positive tone materials, the exposure causes a chain scission reaction and creating shorter chains that are washed away during the developing process leaving behind unexposed regions. Most of the work in 2PP has been performed using the negative tone photoresponsive media. The negative tone materials come either in liquid or solid forms. Some of the common negative tone materials are acrylate based which are extensively used for photopolymerization in the industry. Acrylates have high rate of polymerization and show good mechanical properties

because of strong crosslinking. Also, various multifunctional acrylates are commercially available that can enhance the degree of crosslinking and provide toughness and structural integrity of polymerized features.

Some groups have also used negative tone solid photoresists for 2PP process. The solid photoresponsive materials are epoxy based cationic photoresists that undergo ring opening polymerization. One of the commonly used material is SU8 that generates lewis acid on laser irradiation. The polymerization does not take place during the laser irradiation process and only takes place during the post baking process. One of the advantages of using cationic based photoresists is the achievable process flexibility because of the solid nature of photoresist material. As the polymerization does not take place in liquid environment, but the problems due to scanning stage acceleration and deceleration are minimized. Also, with the exposure to laser pulses the refractive index of the material does not change, thus allowing for a flexible irradiation strategy. But because of being a multistep process (pre bake, exposure and post bake), generally fabrication time is significantly increased [32].

Liquid negative tone photoresists are used extensively and are generally prepared by mixing monomer and photoinitiator together in defined concentrations. The acrylate family is the most commonly used monomer materials commonly used for photopolymerization applications. Acrylates are also available as sidebands with various other monomers that allow them to be photopolymerized. Acrylates side bands are commonly employed with urethane, polyethylene glycol that allows them to be polymerized for biomedical applications. Acrylates are most commonly used in industry because they are available with varying functionalities, sizes and compositions. Also on polymerization, acrylates are inert to harsh solvents and elevated temperatures. Acrylates are very frequently used for 2PP application because of all these properties. Other advantage of acrylate based negative tone liquid monomers for 2PP is that the real time monitoring of polymerization process is possible as the polymerization takes place during the laser irradiation [34].

2PP has also been performed using the inorganic-organic hybrid polymers such as ORMOCER [20, 21]. The physical and chemical properties of ORMOCER can be tailored effectively that gives an added advantage for certain applications. ORMOCER is processed using sol-gel process with the attachment of inorganic units to the organic moieties. The organic moieties like methacryl, styryl, or epoxy functionalities allow the material to be patterned through photopolymerization. ORMOCER's combine the properties of both organic polymers and glass like materials. They allow processing at low temperatures and functionalities but also show thermal and chemical stability, hardness, and transparency. ORMOCER is extensively used at the Laser Zentrum Hanover for applications in photonics and biomedical engineering, attributed to its good optical and mechanical properties [20, 21, 28, 29].

Another key component of a photoresponsive resin is the photoinitiator. Since most of the monomers commonly used for polymerization do not generate sufficient concentrations of radicals that can initiate the chain polymerization process, the monomer is mixed with small concentrations of photoinitiator that absorb the incident photons and decompose into radicals that initiate the polymerization process. Most of the commercially available photoinitiators have absorption in UV range and are primarily employed for 300-400 nm wavelength range. These photoinitiators have strong absorption for single photon but generally do not generate high enough concentration of radicals to initiate the polymerization process. Only a handful of commercially available photoinitiators are effectively employed for 2PP process. Though these photoinitiators do initiate the polymerization process on two photon absorption, sometimes energies close to the damage threshold of the resin system have to be used because of their weaker two photon absorption coefficients. The smaller *dynamic power range* (power levels between the polymerization threshold and damage threshold value) constraints in flexibly choosing the power levels for polymerization. Sometimes, the distinction between the polymerization threshold value and damage threshold value is lost because of very small *dynamic power range* [7].

Some groups have synthesized photoinitiators with high two photon absorption coefficients in laboratory settings. Cumpston et al designed D-π-D based photoinitiator systems where D is an electron donor group and π represents π-conjugated backbone [19]. The presence of D-π-D structures provide effective intramolecular charge transfer within the photoinitiator molecule from the donor groups to the π center. Extended structures based on D-A-π-A-D, D-A-D-A-D and D-D-A-D-D where A represents an acceptor molecule are also designed with improved charge transfer characteristics. Some of these photoinitiator molecules represent very high two photon absorption cross-section (~5500 GM) and provide a user with a very high *dynamic power range* [19]. Various other groups have also designed photoinitiators with high two-photon absorption cross-section based on octupolar and dendritic chromospheres [36]. The limitation of these photoinitiator molecules is that they are not commercially available, thus restricting their widespread use for 2PP applications.

There are few photoinitiators that are commercially available and are efficient in generating radicals by two photon excitation. Two of the commonly used commercially available photoinitiators are Lucirin TPO-L and Irgacure 819 DW from BASF and Ciba respectively. Both of these photoinitiators have an absorption band around 400 nm wavelength that makes them suitable for two photo absorption applications. Also, other important property of these photoinitiators is that they are liquid at room temperature and are readily soluble in most of the monomers. The molecular structure of these photoinitiators is presented in figure 1.7. These photoinitiators molecules go through bond cleavage in the triplet state that generates active radicals that initiate the polymerization process.

Both developed and commercially available monomer and photoinitiator systems have pushed the domain in which 2PP can be effectively employed. The right combination monomer and photoinitiator are very critical for certain applications. Also, the employed process parameters and the resultant polymerization dynamics have a strong dependence on material properties of monomer and photoinitiator system. Hence it becomes essential to choose from a

wide range of materials that are suitable for the process. New materials are constantly added to the 2PP domain with the development and commercialization of highly sensitive two photon excitation motifs that can possibly improve the efficiency of the process and also explore other applications.

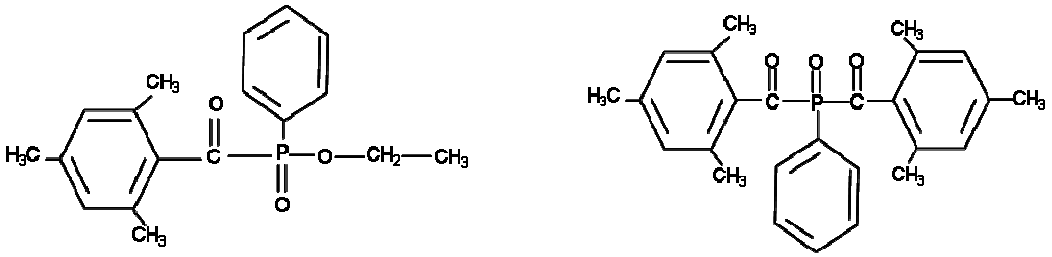

(a) (b)

Figure 1.7 Commercially available photoinitiators for 2PP (a) Lucirin TPO-L, (b) Irgacure 819

1.4 Limitations of Published Research and Motivation

2PP has been effectively employed for the fabrication of complex 3D micro/nano structures by various groups across the world. The current state of research in the area of 2PP and some of the seminal work has been discussed in section 1.3. As discussed, research in 2PP is focused on developing new photoinitiators and materials that are highly efficient for two photon absorption. But good materials alone do not lead to high level and control on the micro/nano fabrication as the process and material dependent parameters also have a strong effect on the 2PP process. Most of the work that has been performed in 2PP is based on experiments. The role of various user controllable process parameters (applied laser intensities, exposure time, and concentration of photoinitiator) is discussed and how they affect the polymerization process. In 3D fabrication of any microstructure using 2PP, knowledge of the voxel size is very critical, since the voxel is the building block of any microstructure and essentially controls the spatial resolution of the process. A good understanding of the voxel shape and size and how it is affected by various process and material parameters essentially provides a good platform from where components with micro and submicron resolution can be accurately fabricated.

Various groups have performed detailed experiments to understand the effect of various process parameters on the development of voxel [37-40]. Most of the experimental studies were performed by modulating applied laser power and exposure time and evaluating their effects on the voxel shape and size. Experiments to characterize the voxel were performed by fabricating voxels at various levels of applied laser power and exposure time. The difficulty in measuring the voxel dimensions is voxel truncation if the laser is focused near the substrate surface. Also, the voxels can get flushed away while developing if they are not firmly attached to the surface of the substrate. To counter this problem, the ascending scan method was proposed by Sun et al [39]. In ascending scan method, a series of voxels are produced at the same exposure conditions but by first focusing the laser beam below the substrate and then ascending it with a constant distance. In this way, there are always some complete 3D voxels that remain even after developing at the exposure site. The schematic of ascending scan method is shown in figure 1.8.

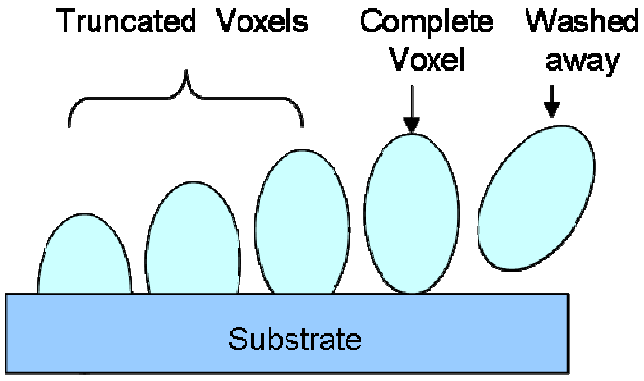

Figure 1.8 Ascending scan method

But due to the very small size of voxel, sometimes it becomes extremely difficult to correctly measure the width and height of a fabricated voxel. Another method to measure the effect of applied laser power and exposure time is the suspended bridge method [37]. In this method, polymer walls are fabricated that are suspended with support from polymeric pillars. The problem of truncation and loss of voxels is avoided, but with this method the shape of voxel

can not be evaluated as they are stacked together to form walls which are used for height and width measurements.

These, these methods are effective in evaluating the effect of applied laser power and exposure time on the size of voxel. But power and exposure time are not the only factors that have an effect on voxel shape and size. There are other material dependent parameters and transport phenomena that also have a strong effect on voxel formation and hence the resolution of 2PP process. As the photophysical and photochemical processes initiate in a very small volume, the effects of molecular diffusion and polymerization kinetics become very important. Also, because of the involvement of various process and material dependent parameters, it becomes almost impossible to understand the role of these parameters on the sixe of voxel and the dynamics of polymerization from the experimental data. Some of the important process parameters that affect the 2PP are applied laser power, microscope objective, pulse repetition rate, pulse width of laser system and exposure time. The important material dependent parameters that also have significant effect are monomer and photoinitiator concentration, two photon absorption cross-section and quantum yield of photoinitiator, polymerization kinetic constants, physical parameters (specific heat, density and thermal conductivity) of monomer and photoiniator systems, and the molecular diffusion constants to name just a few. Because of the involvement of so many different parameters and the fact that the polymerization progresses with a fine balance between all these parameters, the role of single parameter on the 2PP dynamics and the resulted resolution is hard to extract from experiments.

To understand how the nonlinear photochemical and photophysical changes take place in 2PP, a mathematical approach is needed that can help in simulating the polymerization conditions and also extract the role of various involved process and material dependent parameters. In the published literature, there is no single mathematical model that can fully simulate the role of these parameters on the process resolution and adheres to the nonlinear behavior of the 2PP process. A theoretical model presented by Kawata et al related the voxel

formation on two mechanisms: beam spot duplication and voxel growth [40]. The initial voxel takes the size of beam spot and is called beam spot duplication. After the initial duplication, the voxel grows in size because of radical diffusion. As the generated radicals diffuse outward from the irradiated volume because of the concentration gradients, the region in which the polymerization initiates becomes bigger. This theoretical model tries to depict the role of molecular diffusion and gives an insight on the underlying phenomena that have an effect on the voxel size and shape. But because of being theoretical in nature, the role of diffusion can not be quantified.

Few simple mathematical models are presented in the open literature that can be used to estimate or predict the width and height of voxel. A simple mathematical model to evaluate voxel size is presented by Serbin et al by predicting the change in radical concentration both spatially and temporally [21]. This model though does not consider or include the effect of molecular diffusion, polymerization kinetics and the effect of temperature on the polymerization process which are believed to have significant effects on voxel growth and hence the resolution of the process. Another mathematical model developed by Xing et al by considers the time integral spatial distribution of excited photoinitiators [41]. The model is similar to the Serbin's model, but it considers the effect of radical kinetics on the degree of polymerization. The limitation with this model is that it simplifies 2PP as a steady state problem and does not consider the effect of temperature rise and molecular diffusion on the polymerization process.

The current state of research does not provide tools to correctly depict the polymerization process, thus the motivation to implement a mathematical model that can correctly represent the 2PP process along with its 3D confinement and all the nonlinear changes that take place in and around that volume. The model should consider the effects of molecular diffusion and polymerization kinetics on the evolution and growth of voxel. Also, as the laser pulses irradiate the resin volume, the temperature of the system increases because of the absorption of laser energy by monomer and photoinitiator molecules and due to the

generation of heat because of the exothermic nature of polymerization reaction. The effect of temperature is ignored by the most 2PP models published in the literature but it has to be correctly depicted as it strongly affects the polymerization dynamics.

Also, a statistical analysis will be performed to relate the simulation results with experimental work. The understanding gained from the mathematical analysis should be helpful in bridging the gap between published and experimental work with the underlying theory of 2PP process. The statistical analysis will also be used to easily evaluate the effect of considered controllable process parameters on the voxel growth and hence the resolution of the process. Most of the published experimental work uses contrast plots for evaluating the effect of exposure time and applied powers on the 2PP resolution [21, 36-40]. However, these contrast plots do not provide much information about the relevant role of individual parameters and often provide their combined effect on the voxel growth. To analyze the role of user controlled process parameters (applied power, exposure time and photoinitiator concentration), a Design of Experiments methodology will also be employed to evaluate statistical significant differences between the various levels of considered process parameters.

The understanding gained from both the mathematical and statistical analysis will attempt to answer open-ended questions that have appeared in the published literature but cannot be answered due to the experimental nature of work. The mathematical analysis will also effectively demonstrate the role of molecular diffusion and polymerization kinetics on the underlying 2PP dynamics that has until now only proposed theoretically without detailed understanding. Once correctly implemented, the model should also be used use as a simulation engine to predict the size of voxel and for the automation of 2PP process.

1.5 Thesis Outline

2PP is a powerful technology and is very efficient in fabricating complex 3D micro/nano features. Great control on the fabrication process can be achieved by understanding the role of process and material dependent parameters and also the heat and mass transport phenomena

that take place during polymerization. The following chapters will present the mathematical model development and experimental analysis of 2PP process. But before presenting the mathematical model, a complete discussion on the experimental setup and the materials used for the experiments is presented in chapter 2. Detailed discussion on the development of the mathematical development that includes the heat and mass transport effects and their effects on the polymerization dynamics is presented in chapter 3. The numerical simulations and results obtained from the mathematical analysis for both the low (1 kHz) and high (80 MHz) repetition rate laser system are presented and discussed in chapter 4. Chapter 5 presents a discussion on the experimental analysis and subsequent statistical approach for evaluating the role of considered process parameters on the resolution of 2PP process and an explanation on the phenomena noticed from the experiments, and relates the discussion to the information obtained from the mathematical analysis. In chapter 6, a novel approach to fabricate high aspect ratio structures using loose focusing conditions for both amplified and low energy laser pulse is presented. This single scan fabrication saves a lot of fabrication time that can increase the throughput of this process. The conclusion and recommendations for future work is presented in chapter 7 along with some key issues and questions that still need attention.

CHAPTER 2

EXPERIMENTAL SETUP AND MATERIALS

The two most important components of a 2PP system are the ultrashort laser source and photoresponsive resin system. The micro/nano structures are fabricated by scanning the laser pulses inside the photoresponsive media in a predefined pattern. The complexity of experimental setup can vary, but the core of the system remains an ultrashort laser source. In this chapter, a discussion on the experimental set up that was used for experiments and subsequent micro/nano fabrication is presented. Also, a discussion on the materials (monomer and photoinitiator) and the corresponding free radical chain polymerization reaction is also presented that leads to the understanding for mathematical model development. Both these components have a strong effect on the fabrication and achievable resolution of 3D micro/nano structures.

2.1 Ultrashort Laser Source for Microfabrication

The laser system that was used for the experimental verification and subsequent micro/nanofabrication is a femtosecond laser system housed at the BioMEMS lab in The University of Texas at Arlington. The polymerization reaction for 2PP is initiated by focusing of ultrashort laser pulses inside the photoresponsive resin. Most of the 2PP work is performed using the femtosecond laser source working at 800 nm wavelength, 80 MHz pulse repetition rate and about 100 fs pulsewidth [7, 32]. In this work, the Hurricane femtosecond laser system by Newport-Spectra Physics was employed for experimental characterization and fabrication. The Hurricane system consists of a Ti:Sapphire oscillator, a pump laser and a regenerative amplifier. The Hurricane laser system is based on chirped pulse amplification and has an output of 0.75 μJ/pulse at 1 kHz pulse repetition rate. The system is ideal for subtractive fabrication

processes and is used extensively for performing ablation studies and micromachining on various engineering materials [42, 43]. The low pulse repetition rate high energy ultrashort pulses generate very high peak intensities that ablate the material without causing detrimental heating effects. The main elements of the Hurricane system are a seeding laser (Mai-Tai), a pump laser (Evolution), regenerative amplifier, optical pulse stretcher and compressor and synchronization and delay generator (SDG).

Most of published 2PP work is conducted by the tight focusing of low energy pulses from the Mai-Tai oscillator [7, 32]. The Mai-Tai oscillator consists of two lasers, a continuous wave diode pumped solid state laser working at 532 nm acting as a pump source. The neodymium yattrium vanadate ($Nd:YVO_4$) crystal is the driving engine of the Mai Tai pump laser. Two laser diode bars are used to pump the $Nd:YVO_4$ crystal. The output from the pump chamber is used to pump the Ti:Sapphire rod that produces a modelocked ultrashort pulse around 100 fs pulse, 750-850 nm wavelength and average pulse energy in few nanojoules range. Modelocking is the key to achieve stable and ultrashort laser pulses that have a strong effect on 2PP process. All lasers produce light over a range of frequencies defined by the gain-bandwidth of the laser medium. The Ti:Sapphire laser has a bandwidth of 128 THz that corresponds to a 300 nm wavelength range centered around 800 nm [44]. The resonant cavity of the laser consists of two end mirrors encompassing the gain medium. The laser light reflects off the end mirrors and forms a standing wave with a discrete set of frequencies that are know as the longitudinal modes of the cavity. Only these frequencies that correspond to the longitudinal modes are allowed to oscillate in the cavity and all other frequencies are suppressed by destructive interference. In a free-running laser, the laser output consists of various randomly phased mode frequencies that lead to output fluctuation and multi-mode output pulses. The modelocking ensures that all the longitudinal modes are locked in phase and constructively interfere at one point in a cavity and destructively interfere everywhere else thus creating a single circulating pulse. There are various approaches that are used for obtaining a

train of modelocked pulses from an oscillator. But by far, active modelocking is the most common approach to obtain shortest pulse from solid state laser [44]. The most common active modelocking method is by placing an acousto-optic modulator in the laser cavity that ensures reliable modelocked operation and provides smooth wavelength tuning [44].

Since, Ti: Sapphire has a wider bandwidth, the pulse contains frequencies over a wider range. As the index of refraction of any material is frequency dependent, each frequency in a pulse experiences different index of refraction and hence dispersion as it propagates. This dispersion is often termed as Group Velocity Dispersion that causes broadening of laser pulse width. The lower frequencies (red) travel faster than higher frequencies (blue) and causes broadening of the pulse. Broad pulses are not desirable for 2PP applications and leads to an ineffective fabrication process. The broadening of laser pulses is compensated by introducing a set of prism pair in the Mai-Tai cavity that compensates for the positive GVD and maintains the temporal distribution of laser pulses [44]. The output from the Mai-Tai has low energies (sub nanojoules) and high repetition rate. These pulses can be effectively used for 2PP process by tightly focusing inside the photoresponsive resin.

As the laser system is also used for subtractive process and the low energy pulses do not produce high enough fluences required to exceed the threshold for ablation. The energy of the output pulses from the oscillator is increased by passing it though a regenerative amplifier. But before the laser pulses go to the amplifier, they are broadened to avoid any damage to the optics within the amplifier. The low energy output from the Mai-Tai oscillator is passed through pulse stretcher circuit that consists of a diffraction grating that causes the different frequencies to disperse. The grating in the stretcher is so configured that makes the higher frequencies to travel a longer path length compared to the lower frequencies. This causes the lower frequencies to exit the stretcher first and stretches the pulse. The stretched pulse is then fed to the regenerative amplifier where the energy of the pulse is amplified. The regenerative amplifier consists of a Ti:Sapphire laser rod that is optically pumped by the evolution laser. The evolution

uses Nd:YLF as the gain medium that is pumped by a four laser diode array, and is capable of producing Q-switched pulses with average power greater than 6 W at 527 nm and at a repetition rate of 1 kHz. These pulses then excite the Ti:Sapphire laser rod in the regenerative amplifier. The pulse from the pulse stretcher is directed into the amplifier cavity where it makes 16 round passes and gets amplified. Once the laser pulse is amplified it exits the regenerative amplifier by switching on the pockel cells at correct timing [45]. The switching on of pockel cells is controlled by Synchronization and Delay Generator (SDG). The SDG contains the high speed electronics that control the switching of pockel cells and allows the user to adjust the amount of time the beam stays in the amplifier, thus controlling the output power.

The amplified pulse from the regenerative amplifier is then compressed in the pulse compressor circuit. The grating in the circuit is adjusted so that the higher frequencies travels a shorter distance and catch up with the lower frequencies, resulting in the compression of the pulse. The compression of the pulse reduces the pulse width and amplifies the energy. The schematic of the Hurricane system with its sub-components is presented in figure 2.1.

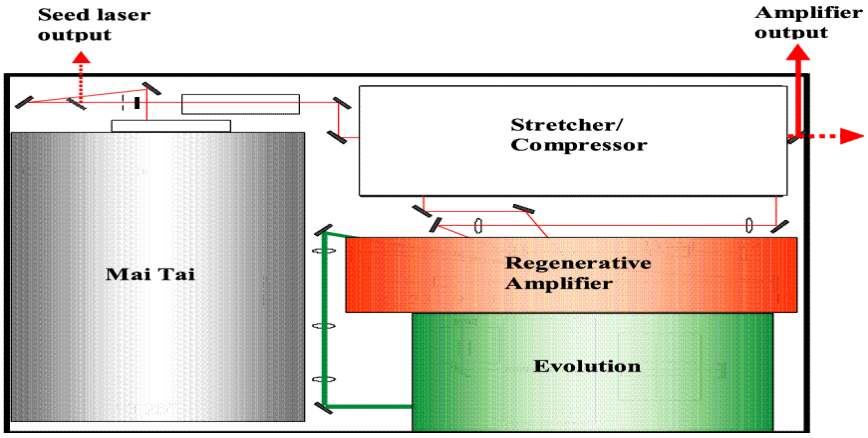

Figure 2.1 Schematic of Hurricane laser system

The 2PP can be performed with either 80 MHz low energy pulses from the oscillator or using amplified laser pulses from the amplifier source working at 1 kHz. Most of the work on 2PP is performed using the low energy pulses from the oscillator in tight focusing conditions. The 80 MHz source has been primarily used for fluorescence microscopy where 80 MHz

repetition rate is essential for keeping the fluorescence intensity relatively constant that provides good source for 3D image synthesis. As the 2PP is based on the same mechanism where radicals are generated instead of fluorescence, only the high repetition rate oscillator was employed by most of the groups working with 2PP fabrication. In our laboratory, we use both the oscillator and the amplifier for two photon assisted micro/nanofabrication. To use the oscillator alone, the seeding pulses were picked out from the system using a flipping mirror. The picked pulses were then navigated through mirrors and allowed to pass through the power attenuator where output energy can be modulated. Also, 5% of the output from attenuator is directed to a CCD camera interfaced with Beamview® beam analyzer for real time pulse monitoring [46]. The pulses are than directed downwards by a 45^0 mirror and through the focusing objective mounted on the Z-stage. The pulses are focused inside the holder containing the photoresponsive resin which is mounted on the linear X-Y stages. These Aerotech linear stages have a resolution of 0.01 µm and controlled by NL Drive amplifier interfaced with A3200 software provided by Aerotech Inc. The software enables users to execute laser scanning path based on industry standard G-codes [46].

In this work, we have also employed the laser pulses from the amplified source working at a much lower repetition rate of 1 kHz compared to the oscillator. But energy of output pulses from the amplifier is generally a couple of orders or more in magnitude higher than the oscillator. The amplified laser pulses are generally employed for micromachining and ablation applications and are not readily used for 2PP process. Focusing of amplified pulses leads to excessive heat generation and may cause the burning of monomer. But we have employed amplified laser pulses in an innovative way for 2PP polymerization resulting in high aspect ratio structures in a single laser scan. To use the amplified source, the seeding pulse is directed through the stretcher, regenerative amplifier and compressor before it comes out of the front end of Hurricane system. The output pulse than passes through an optical configuration to reduce the size to match the input beam size requirement of the power attenuator. After passing

though the power attenuator, the laser pulses go through the same optical setup as discussed of high repetition rate system and are used for polymerization. The schematic of FLM system that can be used with both low and high energy conditions for 2PP is presented in figure 2.2.

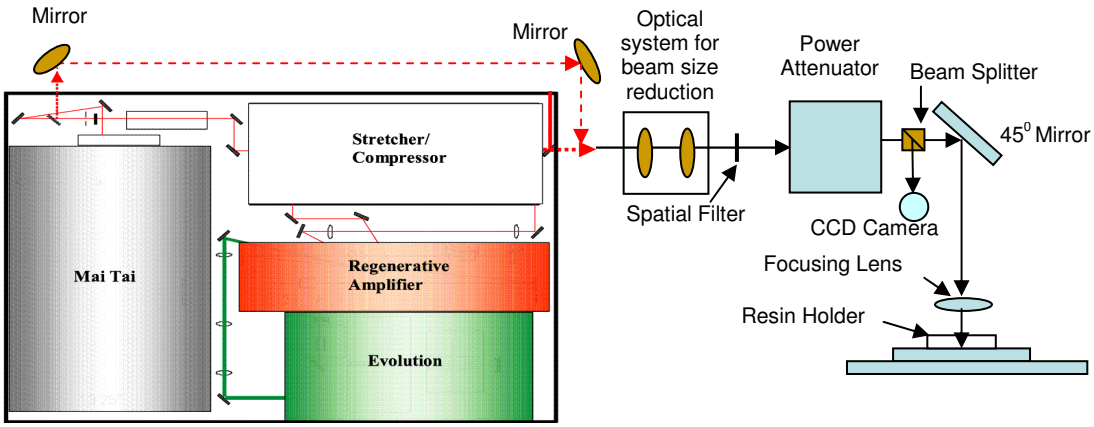

Figure 2.2 Schematic of Femtosecond laser system

Hence, the femtosecond laser system produces both low energy pulses at high pulse repetition rate (80 MHz) and amplified pulses at low repetition rate (1 kHz) and both these pulses can be used for 2PP process. It is advisable to use shortest pulses from the laser source, which is obtained by modelocking and introducing prism setup for negating group velocity dispersion. We have used linear stages that move the resin in a predefined pattern while the laser remains stationary. The linear stages provide the user with bigger scanning area which is beneficial for fabricating multiple structures in a single setting. Other groups have used scanning galvanometers or piezoelectric stages and that have an advantage of achieving high resolution and repeatability [7, 32, 36]. But the total scanning region obtained by galvanometers and piezoelectric stages is generally very small. Another difference in our laser system is the way we focus the laser pulses. Most of the laser systems that are used for 2PP use a microscope for focusing the laser pulses. The microscope is used either in an inverted or upright position, where the laser pulses are focused through the objective into the photoresponsive resin. But in our lab, the laser system is used for both subtractive and additive

processes and this allows us to use a lens holder that is mounted on the z-stage. This setup provides an effective solution for using the system either for subtractive or additive process.

2.2 Materials used in this Research

Another important part of 2PP process is the material used for fabrication. As discussed, a photoresponsive resin is prepared by mixing defined weight percentages of monomer and photoinitiator material. The monomer alone cannot generate high concentration of radicals that can lead to polymerization. A photoinitiator is added that decomposes into active radicals on laser irradiation (free radical polymerization) or after the laser irradiation (catatonic polymerization) [7, 32]. In this work, free radical chain polymerization is employed that is initiated by the absorption of two photons by the photoinitiator molecule. A commercially available monomer and photoinitiator is used for experiments and all the experiments and subsequent fabrications were performed using the discussed laser system. It is important to understand how the chain polymerization reaction progresses as it provides the framework for developing the mathematical model and also enhances the understanding on the 2PP process.

The monomer used in this work is a trifunctional acrylate, commercially available from Sartomer with commercial name SR499 [47]. It is a six mole ethoxylated trimethylolpropane triacrylate commonly used for free radical chain polymerization. The trifunctionality gives the polymer structural rigidity that is usually not obtained from mono acrylates. SR499 is a clear liquid with low formulation viscosity and low shrinkage upon polymerization attributed to the ethoxylation [47]. The chemical formula of SR499 is presented in figure 2.3.

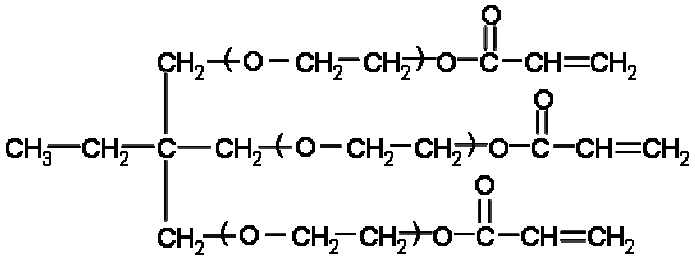

Figure 2.3 SR499 (Ethoxylated (6) trimethylolpropane triacrylate)

In this work, a commercially available photoinitiator from BASF under the name of Lucirin TPO-L is used for experiments and micro/nano fabrication. The advantage of Lucirin TPO-L is that it is liquid at room temperature and is readily soluble in most of the monomers. Lucirin TPO-L is commonly used as a UV initiator for resins containing acrylic groups and unsaturated polyesters containing styrene. Though it has a peak absorption at 375 nm but it also shows good absorption of 400 nm wavelength light. This makes it an excellent candidate for radical generation while working at 800 nm wavelength employed for 2PP. Lucirin TPO-L generate radicals once excited to the triplet state. Though the two photon absorption coefficient of Lucirin TPO-L is small (~1 GM) compared to some of the synthesized photoinitiators, but it has a high quantum yield (0.99) that generate high number of radicals which can efficiently initiate the polymerization process [48]. The good physical properties and high polymerization efficiency makes Lucirin TPO-L an efficient photoinitiator for polymerization for NIR ultrashort laser system. The chemical formula of Lucirin TPO-L is presented in figure 2.4.

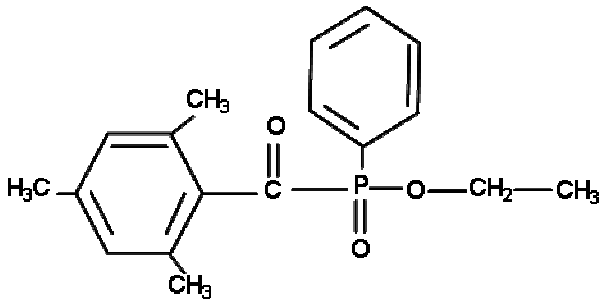

Figure 2.4 Lucirin TPO-L (Ethyl 2,4,6 trimethyl benzyol phenyl phosphinate)

In a free radical chain polymerization process the photoinitiator molecule generate active radicals by chemical decomposition that follows the absorption of incident photons. The decomposition of photoiniator into active radicals generally takes place in the triplet state by undergoing various decomposition modes (Norrish I photoscission, intermolecular hydrogen abstraction, Norrish II processes, electron-proton transfer etc.) depending on the type of employed photoinitiator [15, 16]. Lucirin TPO-L undergoes the bond cleavage reaction in the triplet state resulting into two radicals as shown in figure 2.5.

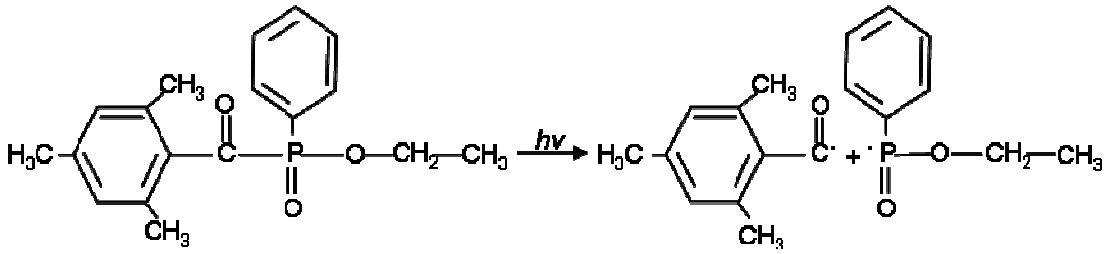

Figure 2.5 Decomposition of Lucirin TPO-L

The bond between the phosphorous and carbon is cleaved in the excited sate and generates 2,4,6 trimethylbenzoyl and ethyl phenyl phosphinate radicals. Both these radicals can initiate polymerization reaction but based on the high reactivity of phosphorous based radical, a large concentration of polymer is expected to contain ethyl phenyl phosphinate at the chain ends [49]. The generated radicals combine with the present monomer molecules at the unsaturated sites thus creating a reactive center. For simplicity, the combination of radical with a monoacrylate is shown in figure 2.6 to avoid complex chemical reaction that results with multifunctional acrylate actually used for experiments. The generated reactive center combines with the other monomer molecules and initiates the chain polymerization process.

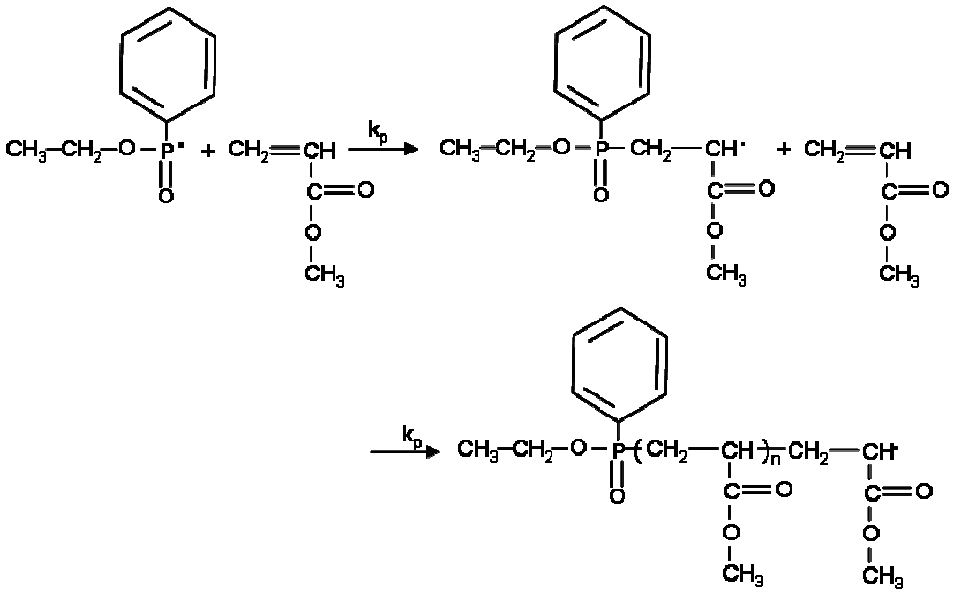

Figure 2.6 Propagation of chain polymerization reaction

The molecular weight of the polymer increases with the growing polymer chain and the chain keeps on growing until it terminates by various radical terminating mechanisms. It should be considered that not all the polymer chains have same length and hence same molecular weight. Some chains terminate pretty early in the reaction and some keeps on growing depending on when they encounter the termination mechanism. This is why the molecular weight of polymerization is always referred as average molecular weight that includes the effect of varying degrees of chain lengths in the polymerization reaction. Generally the growing polymer chain terminates by either combining with an active radical, inhibitor molecule or by trapping within dead monomer. These termination processes are competing in nature and define the volume in which polymerization takes place.

Termination of reactive center of the growing polymer chain by combination depends on the probability of encountering an active radical. Radicals are generated by the decomposition of photoinitiator molecules and are responsible for the initiation of polymerization reaction. But, these radicals can also lead to the termination of growing polymer chain. The radical species combine with the reactive center and undergo electron transfer that converts the growing chain into dead polymer. This dead polymer is non-reactive and do not participate further in the chain polymerization process. The termination reaction as it relates to the acrylate chain and ethyl phenyl phosphinate is presented by figure 2.7.

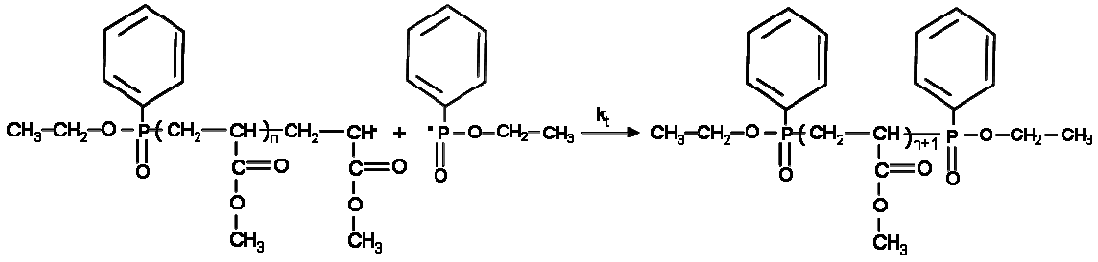

Figure 2.7 Termination by combination

Another mode of termination is the radical quenching by the inhibitor molecules. Inhibitor is commonly added to the monomer in small concentrations to prevent the undesired

polymerization reaction to propagate and increase the monomer shelf life. The two most commonly added inhibitor molecules are hydroquinone (HQ) and hydroquinone mono methy ether (MEHQ) [50]. The inhibitor scavenges the free radicals that are produced during the manufacturing process or extreme storage conditions. Side reactions can occur during monomer production that can produce hydroperoxide side chains that decompose over time to generate radicals. These radicals can initiate chain polymerization reaction that can lead to premature polymerization [50]. To avoid this, HQ and MEHQ are added to the monomer which stabilizes radicals before they can react with the unsaturated sites and initiate undesirable polymerization. The molecular structure of HQ and MEHQ are presented in figure 2.8.

(a) (b)

Figure 2.8 Inhibitor molecules in monomer (a) Hydroquinone (HQ), and (b) Hydroquinone mono methyl ether (MEHQ)

Either of these inhibitor molecules is present in small concentrations in the monomer system. The presence of inhibitor puts the thresholding conditions for the polymerization process as the concentration of active radicals have to exceed and eventually survive the inhibition effect before that can initiate the polymerization reaction. Other than these inhibitor molecules, presence of oxygen also acts as a very strong inhibitor [16]. The oxygen molecules also react with the active radicals and render them inactive. The inhibition reaction of the propagating chain with MEHQ and oxygen molecules is presented in figure 2.9.

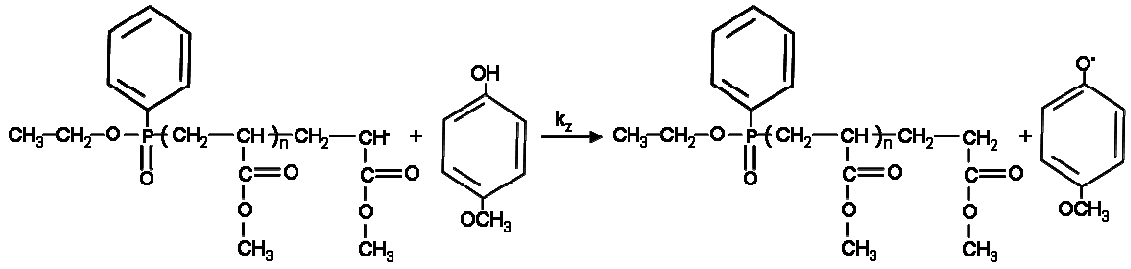

(a)

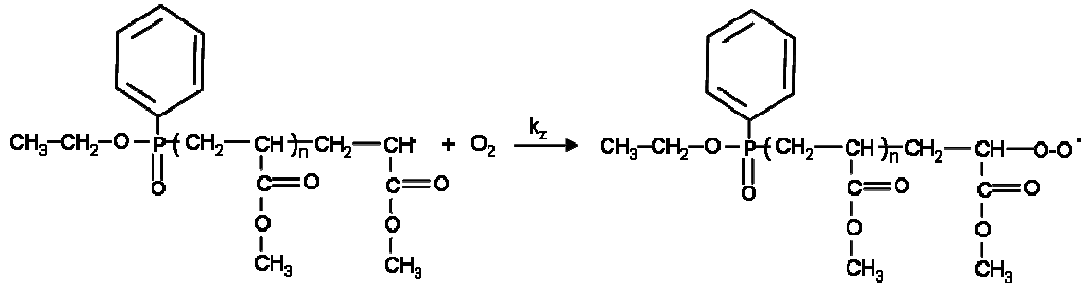

(b)

Figure 2.9 Inhibition reactions with propagating polymer chain (a) Inhibition with MEHQ, and (b) Inhibition with oxygen

All these processes (photoinitiator decomposition, propagation and radical termination) in combination represent a typical chain polymerization process. As discussed, in 2PP the photophysical and photochemical processes are confined in a very small volume defined by the focusing power of microscope objective. The decomposition of photoinitiator and subsequent generation of radicals takes place in this volume. The time integral spatial concentration of radicals defines an envelope where chain polymerization propagates and monomer conversion takes place. This transition of liquid monomer into high molecular weight polymer defines the size and shape of polymerized feature which eventually represents the resolution of 2PP process. Though the polymerization process in 2PP is a typical free radical chain polymerization that involves initiation, propagation and termination kinetics, but the dynamics of the process is very different partially because of the temporal and spatial confinement of induced photochemical and photophysical changes.

CHAPTER 3

MATHEMATICAL MODEL DEVELOPMENT

Two photon polymerization (2PP) is an inherently nonlinear process because of the nonlinear behavior of molecular excitation and subsequent photo-conversion. 2PP is characterized by the spatial confinement of polymerization reaction that takes place because of tight focusing conditions and nonlinear polymerization kinetics. As discussed in chapter 1, the 2PP has a quadratic dependence on the applied laser intensity that initiates the polymerization in the irradiated volume [7,8,10-13]. Because of the quadratic dependence, the polymerization reaction can be initiated inside the photoresponsive resin without any polymerization on the surface or areas away from the focal volume. The sectioning capability makes the 2PP process ideal for 3D micro/nano fabrication. Modeling of 2PP process is inherently different compared to single photon polymerization because of the spatial confinement, non-linear polymerization and pulsed nature of the laser source [7, 32].

Most of the published literature/research on 2PP focuses on employing this novel process for prototyping applications. Research has also been performed in characterizing and inventing new or improved photoinitiators with high two photon absorption cross-section [19, 36, 38]. However, in order to have a controlled polymerization process, understanding of the parameters that influence the voxel (volumetric pixel) formation is important. Voxels are the microstructure building blocks and define the achievable spatial resolution of 2PP process. Experimental work has been performed for voxel characterization to understand the change in size and shape of voxel by varying power, speed and photoinitiator concentration levels [39]. It is also demonstrated that there is a size mismatch in axial and lateral resolution which widens with the increase of power and irradiation time. This mismatch often leads to high aspect ratio

voxels which for certain applications are not desirable as they reduce the process resolution in axial direction. Though, this mismatch can be eradicated by utilizing the thresholding behavior of polymerization and adjusting the applied power and irradiation time close to the threshold values. This behavior can not be explained just from experiments and an understanding of various underlying polymerization kinetics becomes important that can provide information about the growth of voxel at various time scales. The thresholding behavior is proposed by various groups working on 2PP process, but the actual mechanism of thresholding is not completely understood because of the experimental nature of their work [7, 32, 38].

Voxels with dimensions in the order of few hundred nanometers are often fabricated using high N.A. lenses combined with low power and exposure conditions. Ascending scan method and suspended bridge methods are often employed to characterize the shape and size of voxel [37, 40]. But with the improvements in resolution of 2PP process the actual measurement of single voxel is becoming more challenging. In addition, the size of voxel depends upon various other physical and chemical factors that can not be identified and precisely controlled in experiments. A good understanding of the various process parameters and their effect on the voxel formation is difficult to analyze just experimentally. Thus mathematical formulation of the 2PP process is required to connect various physical and chemical factors that affect the voxel size and shape.

Limited theoretical modeling is published in open literature that evaluates the effect of process and material dependent parameters on the voxel formation and size. It is estimated that the voxel size depends on the N.A. of focusing lens, applied energy, two photon cross-section and concentration of photoinitiator and the irradiation time. At the small spatial resolutions generally obtained by 2PP process, the diffusion of active radicals and the polymerization kinetics play an important role in determining the resolution of the process and should be considered [32, 40]. No mathematical model in the published research attempts to incorporate the affect diffusion and polymerization kinetics along with other process parameters as they

relate to the 2PP process. Though, steady state mathematical models have been presented but they simplify the problem by assuming no diffusion and temperature effects [21, 41]. The idea of beam spot duplication and voxel growth tries to theoretically depict the role of radical diffusion on the size of polymerized voxel. This theoretical model also tries to explain the mismatch in voxel's axial and radial dimensions with increasing input power levels [40]. But it is not possible to employ this model to quantify and understand the dynamics of 2PP process and the affect of various material and process dependent parameters on the resolution of 2PP process.

The majority of the 2PP research involves radical polymerization which is governed by three substeps: initiation, propagation and termination [16]. Though, research has been performed on epoxy based systems where polymerization is initiated by the production of Brønsted acid and polymerization process begins on subsequent baking process [41, 51]. But, this work only tries to model free radical chain polymerization process that dominates most of the published work in the area of 2PP. The initiation of polymerization begins with the irradiation of a photoresponsive resin that produces active radicals which combine with monomer molecules to produce live reactive centers. Subsequently, the live monomer radicals combine with other monomer molecules in a chain like fashion to form high molecular weight polymer. The polymerization and voxel growth progresses until the reaction ceases or terminates. Thus, to better understand the 2PP process, it is important to evaluate the role of initiation, propagation and termination and how they are affected by employed process parameters. The dynamics of these polymerization phases change with time and may affect the voxel growth. Also, it is imperative to analyze the role of molecular diffusion that may lead to the propagation of radicals from the irradiated volume and increase the voxel size. Note that the polymerization and diffusion kinetics are dependent on the resin temperature which changes with monomer conversion and increasing number of pulses. Hence, the diffusion and reaction kinetics parameter values changes in space and time with respect to the temperature distribution.

Mathematical modeling of free radical chain polymerization has been performed for think/thick film polymerization and stereolithography [52-56]. The think/thick film polymerization is generally performed using UV lamps [52, 53]. The polymerization is not spatially controlled and thickness of polymerized film depends on the intensity of the applied irradiation from UV lamp. The photoinitiators used in the photoresponsive resin system have strong absorbance for UV light and undergoes single photon absorption. The polymerization starts from the surface and the degree of crosslinking decreases with depth as the light intensity decreases defined by the Beer-Lambert law [52-56]. A comprehensive model is presented by Goodner et al that present a mathematical formulation to thick film polymerization process [52]. The model includes the effect of temperature on reaction kinetics and diffusion constant. This model considers most of the important phenomena that relate to thick film polymerization and is referred in this work to understand the effect of some of the phenomenon that also relate to the 2PP process. But because of ultrashort pulses, nonlinear excitation and small spatial confinement, the mathematical formulation of 2PP process is challenging and is very different from homogeneous thin/thick polymerization.

Mathematical modeling of microstereolithography is also been performed but similar to thin/thick film polymerization, microstereolithography also depends on single photon absorption [56]. Microstereolithography is based on well established stereolithography method that is commercially used for the prototyping of macro size components [55]. Microstereolithography tries to reduce the achievable feature size by using tight focusing of UV laser light. In microstereolithography, the polymerization initiates on the surface of the photoresponsive resin because of single photon absorption. A mathematical model of microstereolithography is presented by Fang et al that includes the effect of diffusion on the polymerization resolution [56]. But the developed model does not consider the effect of radical trapping and inhibition that have a significant effect in defining the actual concentration of radicals that participate in the polymerization process. The model also does not include the effect of temperature change on

the molecular diffusion and polymerization kinetics that can significantly change the polymerization dynamics.

In this chapter, a discussion on the development of mathematical model is presented that tries to incorporate various material and process parameters employed for 2PP process along with molecular diffusion and nonlinear excitation of photoinitiator molecules. The mathematical model describes the 2PP process by including the initiation, propagation and termination kinetics of free radical polymerization. The model incorporates the generation of radicals as it relates to the *figure of merit* (FOM) of photoinitiator that is defined by the two photon absorption cross-section, quantum yield and concentration of photoinitiator in the resin system [7]. The model depicts the termination kinetics as it is governed by the combination, trapping and inhibition of radicals. The mathematical formulation of 2PP process also includes the affect of increased temperature conditions because of laser irradiation and monomer conversion. The temperature affects the kinetic and diffusion constants and should be considered to correctly depict the polymerization process.

In this chapter, a detailed discussion on the development of mathematical model is presented. All the critical governing processes in 2PP polymerization are depicted and their mathematical formulations are presented. The model focuses on evaluating the temporal and spatial species distribution as it affects the polymerization process and the resulting dynamics, and attempts to depict the actual 2PP process by the spatial confinement of irradiated volume. The model assumes a Gaussian intensity distribution for the applied laser pulses and focuses on evaluating the spatial and temporal variation in the concentration of photoinitiator, radicals and monomer after irradiation with femtosecond laser pulses.

3.1 Temperature Distribution

In a 2PP process, the laser pulses irradiate the photoresponsive resin. Though the pulses normally used for 2PP have very low energies (< 0.25 nJ for 80 MHz system), but the accumulation of heat can take place due to very high repetition rate and heat generation from

the polymerization reaction. The resin system absorbs some part of the incident energy dependent on the absorption coefficient of the material. Also, heat is produced by the monomer conversion because of the exothermic nature of the reaction. The temperature of the monomer changes as the reaction progresses and more energy is added with increasing number of pulses. The tightly focused ultrashort pulses generate very high intensities which are not possible when employing UV lamps. Also, because of local confinement of polymerization reaction, temperature can be high enough to cause polymer degradation and/or boiling.

Though, the monomer and the photoinitiator do not have strong absorption of laser energy at 800 nm wavelength, it is important to include the temperature gradient produced by the absorption of ultrashort laser pulses because of the high intensities. Hence, the absorption of laser energy is related to the monomer concentration that changes both spatially and temporally. As the polymerization reaction progresses, the concentration of both the monomer and photoinitiator decreases from the irradiated volume. The decrease in their concentration affects the rate of heat generation and the temperature distribution of the resin system. Hence, it is important to incorporate the time and space dependent resin concentration that changes with each time step. Also, the amount of heat produced because of the exothermic nature of the reaction is dependent on the rate of change of monomer concentration. The rate of change in monomer concentration is time dependent and changes as the polymerization reaction progresses. Hence, these two process in combination causes heat generation with the resin system that leads to temperature increase of the system. Because of the induced local temperature gradients, thermal diffusion also affects the system state by spreading heat out in the resin system. All these three processes: thermal diffusion, laser energy absorption, heat generation because of monomer conversion produce temperature gradient that affects the polymerization kinetics. The energy balance equation relating the temperature gradient as a function of thermal diffusion, input laser energy and the exothermic nature of polymerization process is given by equation 1.

$$\frac{\partial T}{\partial t} = \frac{k}{\rho c_p}\left(\frac{\partial^2}{\partial x^2} + \frac{\partial^2}{\partial y^2} + \frac{\partial^2}{\partial z^2}\right)T + \frac{\alpha.I.[M]}{\rho c_p} + \frac{H}{\rho c_p}\frac{\partial M}{\partial t} \quad (1)$$

Where T is the temperature, x, y and z are the respective spatial distances, k is thermal conductivity, ρ is monomer density, c_p is monomer specific heat, H is enthalpy of polymerization, α is the molar absorption coefficient for the monomer, $[M]$ is the spatial and temporal monomer concentration and I is the laser intensity distribution. In this research, the spatial intensity distribution of laser pulse is approximated by a Gaussian distribution as shown in equation 2, where, I_o is the laser intensity at the center of the beam at its waist, ω_0 is the theoretical beam waist, z_R is the Rayleigh length, and r and z are the radial and axial distances.

$$I = I_o\left(\frac{\omega_0}{\omega(z)}\right)^2 \exp\left(\frac{-2r^2}{\omega^2(z)}\right) \quad (2)$$

$$\text{Where } r = \sqrt{x^2 + y^2} \text{ and } \omega(z) = \omega_0\sqrt{1 + \left(\frac{z^2}{z_R^2}\right)} \quad (3)$$

The mathematical formulation of temperature distribution primarily incorporates thermal diffusion caused by conduction and assumes no convection. The assumption of no convection is reasonable as the polymerization is confined in a very small volume and takes place in a liquid system without any direct contact with the outside environment. The temperature increase is also discussed in polymerization models that represent think or thick film polymerization that takes place with the absorption of UV light from lamp source [52, 53]. Even the intensity of incident UV light from lamps are very small compared to ultrashort laser source but the bigger polymerization volume causes significant rise in the temperature primarily because of the exothermic nature of reaction. Temperature in these systems can easily to 200°C that have significant affect on the polymerization dynamics [52, 53]. In 2PP, though the irradiated volume is very small but because of high intensity laser pulses the temperature of the irradiated volume is expected to increase significantly. Also because of the pulsed nature of the laser source the

absorption of laser energy takes place only during the laser irradiation period and the release of energy generally occurs during the period when the laser pulse is off. The pulsed nature of laser source provide enough time for thermal diffusion to occur especially for low repetition rate laser systems, but heat accumulation is expected with high repetition rate system. The information about spatial and temporal temperature distribution is subsequently used to determine the species distribution (photoinitiator, radicals, monomer and inhibitor) and dependent kinetic parameters and how it may affect the 2PP process.

3.2 Photoinitiator Concentration Distribution

The next step in the mathematical model development is to formulate the change in both spatial and temporal photoinitiator concentration distribution. The photoinitiator molecules in the resin absorb incident laser pulses and decompose into active radicals. In this work, the photoinitiator decomposes into active radicals through homolytic dissociation [16]. Because of the quadratic intensity dependence and induced spatial confinement, the decomposition of photoinitiator takes place only in the focal volume. The active radicals combine with the monomer molecules to generate reactive centers which initiate the chain polymerization process. The initiation rate can be very high in photopolymerization and depends upon laser pulse intensity and the two photon absorption cross-section of the photoinitiator [48]. The photoinitiator concentration at the focal volume decreases with increasing number of pulses and as the polymerization reaction progresses. The produced gradient in photoinitiator concentration leads to molecular diffusion that attempts to replenish the photoinitiator molecules to the depleted volume. The influx of photoinitiator molecules from the surrounding regions also changes the photoinitiator concentration at the non-irradiated volume. The depletion and diffusion of photoinitiator molecules causes an induced gradient in the concentration that affect the polymerization process with subsequent pulses. The spatial and temporal change in photoinitiator concentration, $[P]$, after the laser irradiation is presented by equation 4. The first term on the right side of equation 4 represents the diffusion of photoinitiator molecules that is

driven by the induced concentration gradients. The second term on the right side represents the decomposition of photoinitiator molecules that in the 2PP process, depends on the two photon absorption cross-section of the photoinitiator molecules, δ, square of applied photon flux, Φ, and the concentration of available photoinitiator, $[P]$, in the resin system. The photon flux represents the number of photons irradiating a unit area in one second and is related to the applied laser intensity by equation 5 where $\hbar$ is Plank's constant and ν is the laser frequency.

$$\frac{\partial P}{\partial t} = [d].\left(\frac{\partial^2}{\partial x^2} + \frac{\partial}{\partial y^2} + \frac{\partial^2}{\partial z^2}\right)P - \delta.\Phi^2.[P] \tag{4}$$

$$\Phi = \frac{I}{\hbar \nu} \tag{5}$$

The diffusion of photoinitiator molecules is governed by the concentration gradients and the rate of diffusion is dependent on the molecular diffusion constant, $[d]$. The molecular diffusion constant depends on the temperature of resin system. The molecular diffusion constant has an Arrhenius relationship as a function of temperature as presented in equation 6 where d_o is pre-exponential factor for diffusion, R_g is the gas constant and E_a is the activation energy [16, 52]. As temperature increases, it causes the molecular diffusion constant to increase and leading to a higher molecular diffusion rate. The dependence of molecular diffusion on temperature distribution has a affect on the polymerization process and

$$d = d_o \exp\left(\frac{-E_a}{R_g.[T]}\right) \tag{6}$$

The absorption of laser intensity depends on the two photon absorption cross-section δ that represents the ability of a photoinitiator molecule to produce radicals on absorption of two photons within a very short amount of time required to raise the electron from the ground state to an excited state. Most of the photoinitiators used in 2PP process have strong absorption for single photon as they are optimized for UV light but do not absorb effectively in the NIR range

because of their small two-photon absorption cross-section. Hence, the change in concentration of photoinitiator also depends on how strongly the photoiniator absorbs the laser irradiation and decomposes into active radicals. Most of the commercially available photoinitiators have very limited absorption for NIR wavelength. The two photon absorption cross-section of commonly used off the shelf photoinitiators is around 1 GM [48]. Although, there are photoinitiators with three orders of magnitude higher absorption cross-section, they are not commercially available and they are custom synthesized in a laboratory setting [19]. In this research, the two photon absorption cross-section of a commercially available photoinitiator (Lucirin TPO L) was used since this photoinitiator was used for the experimental verification of the proposed mathematical model.

3.3 Radical Concentration Distribution

Radicals are generated by the decomposition of photoinitiator molecules and their concentration varies both spatially and temporally depending on various kinetic processes. The generation of radicals during the pulse width also depends upon how fast the bond cleaving and nuclear rearrangement takes place. The rearrangement time varies with the type of photoinitiators used in the 2PP process and can vary from few picoseconds to nanoseconds (compared to the femtosecond pulse width). Once the radicals are generated, they combine with monomer molecules to initiate the chain polymerization reaction. The conversion of monomer into high molecular weight polymer partially depends upon the concentration of active radicals as the radicals propagate the polymerization reaction. Solid polymerized volumes are produced once the monomer conversion ratio is high enough to exceed the gelation point [16]. Hence, the size of polymerized volume or the 2PP process resolution also depends upon the spatial distribution of generated radicals. Though, the concentration of active radicals changes as they are also consumed during the polymerization reaction. The active radicals terminate leading to a reduction in their concentration. Also, apart from generation and termination, the radicals diffuse spatially to compensate for the variation in spatial concentrations. These three

processes of generation, termination, and diffusion define the change in radical concentration over time and are mathematically modeled as a partial differential equation (PDE) represented by equation 7.

$$\frac{\partial R}{\partial t} = [d]\left(\frac{\partial^2}{\partial x^2} + \frac{\partial^2}{\partial y^2} + \frac{\partial^2}{\partial z^2}\right)R + \psi.\delta.[P]\Phi^2 - 2[k_t][R]^2 \ldots$$
$$\ldots - (1-f)[k_p][M][R] - [k_Z][Z][R] \qquad (7)$$

It is important to consider the role of various factors that may lead to radical termination and change the dynamics of polymerization process. The spatial and temporal change in radical concentration depends upon the molecular diffusion, generation of radicals, and their termination, as represented on the right side of equation 7. The termination of radicals can be attributed to radical combination, radical trapping and the presence of inhibitor in the resin mixture [16, 52, 54]. In radical termination, the generated radicals terminate by combining with other active radicals or reactive centers that render them useless. The termination constant, $[k_t]$, relates to the rate at which radical termination occurs by combination and is represented as the third term on the right side of equation 7.

The other mode of termination is radical trapping, where the active radicals get trapped in entangled non-reactive polymer chains and can not take part in the polymerization reaction. As the polymerization progresses when the active radicals combine with monomer molecules and propagate the polymerization reaction which partially depends on the propagation rate constant $[k_p]$. But due to radical trapping, only a portion of the radicals actually take place in the propagation phase [54]. The ratio of radicals that get trapped is defined by the trapping factor, f which varies between $0 < f \leq 1$, where $f = 1$ represents that radical trapping is insignificant. Generally the effect of trapping depends upon the kinetics of polymerization reaction, size of polymer chains and radical molecules, and the viscosity of the resin system. In this research, trapping is modeled as a constant value since the information about the viscosity effects is not

known. A constant value of f obtained from the published literature is used for simulations. The trapping effect is represented by the second to last term on the right side of equation 7.

The last mode of termination considered in this model is due of the presence of inhibitor molecules. Present oxygen and other inhibitor molecules combine with initiated radicals and convert them to nonradical species or radicals with very low reactivity not able to undergo propagation. The concentration of inhibitor present in the resin mixture can change the threshold for polymerization as the polymerization reaction will not propagate until the inhibitor molecules are significantly reduced. The concentration of inhibitor also changes as the reaction progresses and is defined by equation 8, where $[Z]$ is the distribution of inhibitor molecules and $[k_z]$ is the kinetic parameter that defines the rate of combination of inhibitor with radicals.

$$\frac{\partial Z}{\partial t} = [d]\left(\frac{\partial^2}{\partial x^2} + \frac{\partial^2}{\partial y^2} + \frac{\partial^2}{\partial z^2}\right)Z - [k_z][Z][R] \tag{8}$$

Termination by radical trapping and quenching is more significant at the initial stage of polymerization because of the low monomer molecular weight and the presence of inhibitor molecules. Radical trapping is significant at higher conversion rates as the radicals get entangled or trapped between dead polymer chains. The amount of available active radicals at the various stages of polymerization combines with the monomer molecules and converts them into reactive centers. The chain propagates from these reactive centers that result in high molecular polymer until trapping takes place.

3.4 Monomer Concentration Distribution

The active radical combine with monomer molecules to propagate the polymerization reaction takes place during the dark reaction phase or the off laser pulse time. The polymerization propagation changes the monomer concentration as the monomer converts into high molecular weight polymer as presented by equation 9. The rate at which the active radicals and monomer molecules combine defines the monomer conversion. Diffusion of monomer

molecules is also present because of the spatial gradients in monomer concentration. However, the effect of monomer diffusion is limited because of higher concentration and much larger size of monomer molecules that leads to smaller diffusion coefficient. The first and second terms in equation 9 represent the effect of monomer diffusion and reaction propagation respectively. The propagation of the polymerization reaction significantly depends on the propagation rate constant that defines the rate at which monomer molecules combine with active radicals. Also, the rate constants, k_p, k_t and k_z have an Arrhenius relationship with temperature similar to diffusion constant. The temperature dependence of k_p, k_t and k_z is depicted by equations 10 where k_{io} is the respective pre-exponential factors for different processes, and E_{ia} represents the activation energies for the processes of propagation, termination and inhibition.

$$\frac{\partial M}{\partial t} = [d]\left(\frac{\partial^2}{\partial x^2} + \frac{\partial^2}{\partial y^2} + \frac{\partial^2}{\partial z^2}\right)M - [k_p][R][M] \tag{9}$$

$$[k] = k_{io} \exp\left(\frac{-E_{ia}}{R_g[T]}\right) \quad \text{where } i = \{p,\ k,\ t\} \tag{10}$$

As the number of pulses increases and at higher conversion ratios, significant temperature rise may take place that changes the reaction and diffusion kinetics. By capturing the temperature profile at various time scales, the relative kinetic parameters could be evaluated and used for subsequent analysis. The model tries to represent the 2PP process in a mathematical form which can be effectively used to simulate different process conditions by modulating the various process and material dependent parameters. The governing PDE for each species concentration depend on the kinetic parameters, diffusion constant and also on other species concentrations. The governing equations are all coupled together and have to be solved with each time step and representative system state is carried on to the subsequent step. A finite difference approach is used to solve these equations numerically to understand the role of various mechanisms on polymerization dynamics and how they affect the size and

shape of polymerized voxel. The methodology followed to solve and simulate the coupled governing equations is presented in chapter 4. Also, the results obtained from the mathematical simulations and a detailed discussion on the interesting observed phenomenon are presented in that chapter.

CHAPTER 4

SIMULATION RESULTS AND DISCUSSION

Most of the published research in the area of 2PP is based on experiments. 2PP involves a delicate balance between various process and material related parameters that influences the polymerization dynamics and the resolution of the process [10, 13]. Various research groups have postulated theories in an effort to explain some of the phenomena very typical to 2PP process [7, 21, 32, 38, 40]. But, because of the experimental nature of their research, the role of these mechanisms could not be fully understood. A mathematical framework was needed to assist with the understanding of the role of nonlinear polymerization kinetics and transport phenomena that are confined in a very small volume. The developed model was analyzed to understand the role of various input process and material dependent parameters and their effect on the polymerization dynamics and the resolution of 2PP process. The proposed model includes radical diffusion, along with radical quenching and trapping, providing a mean to study their effect on the spatial resolution and the voxel size and shape as well.

The governing equations presented in chapter 3 were numerically solved to understand the dynamics of polymerization process and the reaction dynamics. In this chapter, the simulation results to understand the species gradients in radial and axial directions at various time steps are presented. The PDEs were solved simultaneously, since they are coupled and the condition of the system changes at each time step. The temperature gradient and the change in photoinitiator, radical, inhibitor and monomer concentration have similar boundary conditions and were defined by setting the first spatial derivative to zero because of the bigger spatial domain compared to the focal volume. The initial concentrations of various species and

relative physical and chemical parameters used for the analysis and simulations are presented in table 4.1.

Table 4.1 Values of Process Parameters used for Numerical Analysis

Parameter	**Value-Units**
Applied energy per pulse	30 nJ (1 kHz), 0.0625 nJ (80 MHz)
Beam radius – ω	$5x10^{-6}$ m (1 kHz), $1x10^{-6}$ m (80 MHz)
Pulse width – τ	150 fs
Two-photon cross-section – δ	10^{-58} m^4 sec [48]
Diffusion constant – d_o	10^{-7} m^2 sec^{-1} [56, 61]
Pre-exponential Termination constant - k_{to}	$6x10^3$ m^3 mol^{-1} sec^{-1} [52, 60]
Pre-exponential Propagation constant - k_{po}	$5x10^3$ m^3 mol^{-1} sec^{-1} [52, 60]
Pre-exponential Inhibition constant – k_{zo}	10^5 m^3 mol^{-1} sec^{-1} [16, 41]
Initial monomer concentration	$3.3x10^3$ mol m^{-3}
Initial photoinitiator concentration	$1.32x10^2$ mol m^{-3}
Initial inhibitor concentration	$2.88x10^{-3}$ mol m^{-3} [41]
Pulse repetition rate	1 kHz, 80 MHz
Specific heat-monomer - c_p	1.89 J K^{-1} g^{-1} [16]
Density-monomer – ρ	$1.107x10^6$ g m^{-3} [16]
Thermal conductivity-monomer – k	0.142 W m^{-1} K^{-1} [16]
Activation energy for termination - E_{ta}	$2.94x10^3$ J mol^{-1} [52]
Activation energy for propagation - E_{pa}	$18.23x10^3$ J mol^{-1} [52]
Activation energy for inhibition - E_{Za}	$3.0x10^3$ J mol^{-1} [52]
Activation energy for diffusion - E_{da}	$2.94x10^3$ J mol^{-1} [52]
Gas constant – R_g	8.314 J K^{-1} mol^{-1} [16]
Trapping factor –f	0.9817 [54]
Quantum yield – ψ	0.99 [48]

The Finite Difference Method (FDM) is used to numerically solve the presented parabolic partial differential equations [57]. The FDM solves a PDE by discretizing the continuous physical domain into a finite grid and approximates the PDE by a set of algebraic

equations. For this analysis, the Forward-Time Centered-Space (FTCS) method is used that substitute the time derivative term by the first-order forward-time approximation and the spatial derivative term by a second order centered-space approximation [57]. The approximated expressions for first order time derivative and the second order space derivative are presented in equation 1 and 2 respectively, where u is variable changing in both space and time, Δt represents sub-step for time, Δx represents sub-step for space and i and j are the increments in time and space respectively.

$$\frac{\partial u}{\partial t} = \frac{u_i^{n+1} - u_i^n}{\Delta t} \tag{1}$$

$$\frac{\partial^2 u}{\partial x^2} = \frac{u_{i+1}^n - 2u_i^n + u_{i-1}^n}{(\Delta x)^2} \tag{2}$$

The approximation represented by equation 1 and 2 can be expanded to convert the governing PDE's for 2PP process into algebraic equations. Also, while working in Cartesian coordinates, the radial direction is represented by the x-direction and the axial is represented by the z-direction. The x-z plane defines the cross-section of the polymerization system and provides the information about the system state in both radial and axial directions. An example of the algebraic approximation of the photoinitiator concentration change is represented by equations 3 and the forward time expression for the photoinitiator concentration is represented by equation 4 where n, i, and j are the increments for t, x, and z respectively. The estimation of the photoinitiator concentration at time $n+1$ is estimated by the concentration value from the previous time step n and respective spatial increments. The forward Time Centered Space (FTCS) methodology to calculate the species concentration is represented by figure 4.1. The spatial species concentration at the forward time step is evaluated from the knowledge of spatial concentration values in the previous time step. Each discrete increment in the grid presented by figure 4.1 is calculated using this methodology and the procedure is repeated for subsequent

time increments. It should be noted that the species concentration for the initial grid 'n' is defined by the information about the initial conditions of the system. Also, the discrete data points on the boundary of the grid are evaluated from the knowledge of the boundary conditions. In the presented analysis, the initial conditions of the various species (temperature, photoinitiator, radical, inhibitor, and monomer) are presented in table 1. For the boundary conditions, the first derivative of the species concentration at the boundaries is represented by zero and the information is used to evaluate the discrete points at the boundary of the grid.

$$\frac{P_{i,j}^{n+1} - P_{i,j}^{n}}{\Delta t} = d_{i,j}^{n}\left(\frac{P_{i+1,j}^{n} - 2P_{i,j}^{n} + P_{i-1,j}^{n}}{(\Delta x)^2} + \frac{P_{i,j+1}^{n} - 2P_{i,j}^{n} + P_{i,j-1}^{n}}{(\Delta z)^2}\right) - \frac{\delta (I_{i,j}^{n})^2 P_{i,j}^{n}}{\hbar^2 \nu^2} \qquad (3)$$

$$P_{i,j}^{n+1} = A(P_{i+1,j}^{n} + P_{i-1,j}^{n}) + B(P_{i,j+1}^{n} + P_{i,j-1}^{n}) + (1 - 2A - 2B)P_{i,j}^{n} - C(I_{i,j}^{n})^2 P_{i,j}^{n} \qquad (4)$$

Where, $A = \frac{(d_{i,j}^{n})\Delta t}{(\Delta x)^2}$, $B = \frac{(d_{i,j}^{n})\Delta t}{(\Delta z)^2}$, $C = \frac{\delta.\Delta t}{(\hbar \nu)^2}$

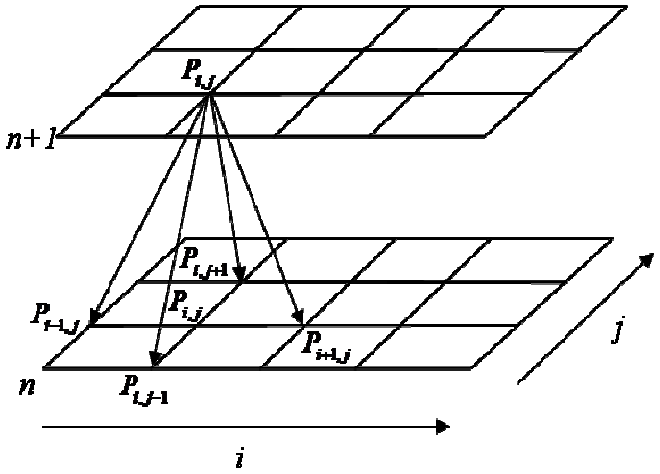

Figure 4.1 FTCS grid for numerical analysis

The system state changes with each time step, the concentration of various species changes with the irradiation of laser pulse. The temperature of the system increases as the polymerization reaction progresses with each time step and causes a change in polymerization

kinetics and diffusion constants. Though, the temperature change is relative to the instantaneous rate of monomer conversion and amount of monomer molecules in the resin system. As the concentration of monomer changes as the reaction progresses, the relative effect on the temperature distribution also changes. Similar to temperature distribution, the rate of polymerization also depends on the instantaneous concentrations of various species. Hence, all the governing PDE's and the derived algebraic equations are coupled together and have to be solved simultaneously with each time step to evaluate the temporal and spatial species concentration and correctly capture the dynamics of the polymerization process.

Because of the pulsed nature of laser source, the time period used to evaluate the temperature distribution and change in concentration of various species was separated in two parts: 1) the time period during laser irradiation referred to as irradiation period, and 2) the time period from the end of the pulse width until the second pulse arrives based on the pulse repetition rate referred to as dark period. This was essential as the laser pulse that changes the initial state of the system and causes the decomposition of photoinitiator is only active during the pulse width or irradiation period. It is also essential to understand the polymerization dynamics during the dark period as the effect of reaction kinetics and diffusion is significant during this period based on longer characteristic time. Thus, during the irradiation period, the laser intensity dependent terms are considered in the analysis, where for the dark period the intensity dependent terms are neglected. The system state at the end of dark period becomes the initial condition for the dark period, and the system state at the end of the dark period is considered to be the initial conditions for the subsequent pulse. The loop was run over and over until the desired number of pulses or desired conversion ratios are reached. The procedure followed to evaluate temporal and spatial distribution of various species concentrations is presented by figure 4.2.

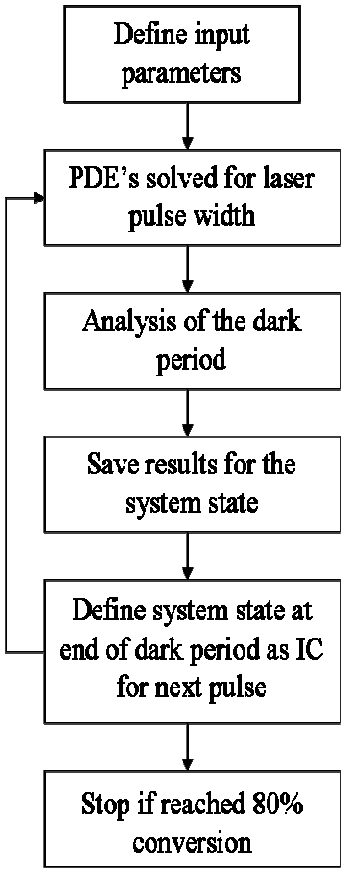

Figure 4.2 Procedure employed to simulate 2PP process

With the irradiation of laser pulses, the temperature of the resin in and around the irradiated volume increases because of the absorption of laser energy and the heat generated by the exothermic polymerization reaction. The increase in temperature affects the polymerization dynamics since the polymerization kinetics and diffusion have Arrhenius relationship with temperature. To illustrate the effect of temperature on the kinetic parameters, the changes in propagation and termination constants as a function of temperature are presented in figure 4.3. The rate of change in propagation and termination kinetics parameters is significantly different as the activation energy required for propagation is higher than termination. Though the pre-exponential factors for both propagation and termination constants are of similar magnitude (k_{po}= 5 x 10^3 and k_{to} = 6 x 10^3), but due to higher activation energy at 300 K the actual k_p value is a couple of orders in magnitude smaller. Similarly, the other kinetic

and diffusion parameters change with temperature and directly affect the dynamics of 2PP process. Hence, it becomes essential to properly capture the time varying spatial temperature distribution to correctly model the polymerization process.

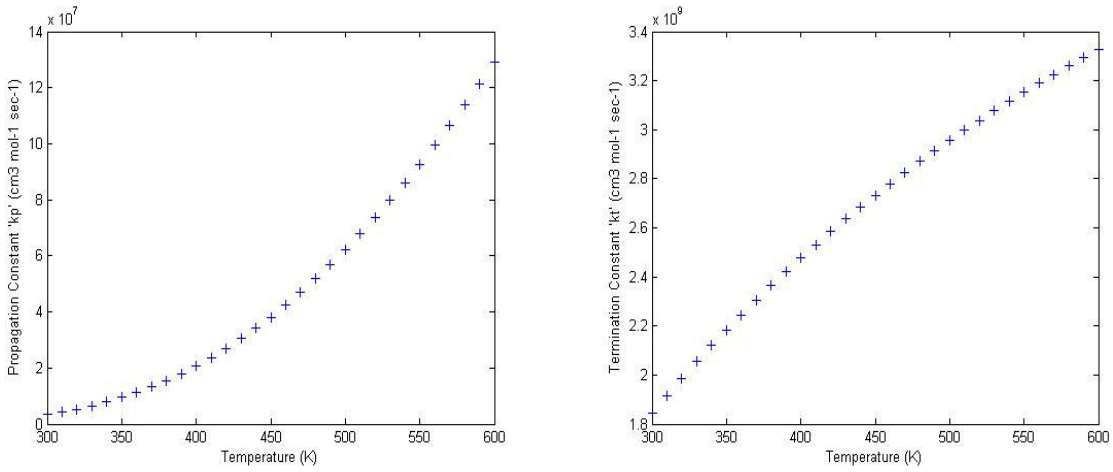

(a) (b)

Figure 4.3 Effect of temperature on kinetic constants (a) Propagation rate constant, (b) Termination rate constant

4.1 2PP using low repetition rate (1 kHz) laser system

An amplified laser system working at 1 kHz is often employed for subtractive micromachining applications as the pulses have enough energy to ablate the material [42, 43]. Most of the 2PP research is performed with high repetition rate laser systems some work has been reported for the micro/nano feature fabrication using amplified laser systems [62]. The amplified laser systems compared to have much higher energy per pulse which often causes burning of polymer. The pulse energy for 1 kHz system is a couple of orders in magnitude higher than the high repetition rate system and additional optical elements are required to reduce the energy at a usable level for polymerization without any detrimental effects. But, the high energy pulses from an amplified system can be utilized for multi-fabrication/parallel processing that can increase the throughput of 2PP process. Also, the polymerization dynamics of 1 kHz system are different compared to high repetition rate laser system attributed to a much longer dark period. The simulation also helps in analyzing the characteristic time scales at

which the polymerization kinetics become dominant and change the system state. First, single pulse analysis is employed for the 1 kHz laser system in an effort to understand the role of polymerization kinetics and how they affect the various polymerization phases. A multipulse analysis is also performed to further evaluate the monomer conversion ratio and voxel size based on the employed chemical and process parameters.

4.1.1 System state during the laser pulse width

A single pulse analysis is performed to evaluate the dynamics of polymerization process during the laser pulse width. The incident laser irradiation is active only during the pulse width period that changes the system initial conditions. The concentration changes in species gradients are analyzed to understand the role of process parameters and chemical kinetics. The temporal and spatial changes in temperature, photoinitiator, radical and monomer distributions are captured and related to the polymerization process.

4.1.1.1 Temperature distribution

The temperature of the irradiated volume changes with the irradiation by a laser pulse. Though, the temperature increase is very small because of low energies due to single pulse irradiation. The temperature profile in radial and axial directions is presented in figure 4.4(a). The temperature distribution is more spread out along the axial direction because of the intensity distribution mismatch related to the Gaussian beam or energy profile. The mismatch results in the spread of laser intensity along the optical axis with enough energy away from the focal center to change the system state. The radial and axial Gaussian intensity distribution of a laser pulse is presented in figure 4.4(b). Thermal diffusion is not observed during this time period because of the much shorter time scale (150 fs) compared to the characteristic diffusion time which is generally between few microseconds to milliseconds.

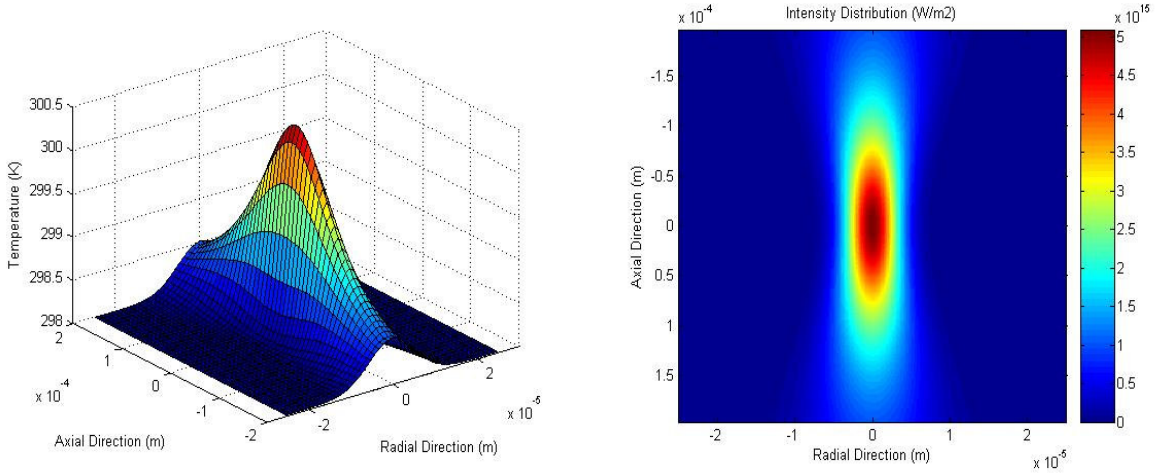

(a) (b)

Figure 4.4 Temperature and input laser intensity distribution after the pulse width for 1 kHz system (a) Temperature distribution, and (b) Gaussian intensity distribution

4.1.1.2 Photoinitiator, radical and monomer concentration

The governing PDE's for the polymerization substeps were also solved to further understand the spatial and temporal concentration of various species. The photoinitiator concentration decreases at the irradiated volume, and the severity of photoinitiator depletion depends on applied irradiation intensities and the two photon absorption cross-section of the photoinitiator. The spatial distribution of photoinitiator at the end of the dark period is presented in figure 4.5. Similar to thermal analysis, the diffusion of photoinitiator to the depleted region is not evident during the pulse duration because of the very short time interval.

The radical concentration increases with the decomposition of photoinitiator. The amount of generated radicals depends on the figure of merit (FOM) of photoinitiator [7]. The figure of merit is represented by the quantum yield, two photon absorption cross-section and the concentration of photoinitiator in the resin system. Photoinitiators with high figure of merit are desirable as they introduce flexibility in choosing the process parameters. But, most of the commercially available photoinitiators that can be used for 2PP have low figure of merit due to smaller two-photon absorption cross-section. Some groups have synthesized photoinitiator

molecules that have high figure of merit but these photoinitiator systems are not commercially available and are proprietary to the respective research groups [7, 36, 38].

So, the concentration of radicals changes with the decomposition of photoinitiator molecules into active radicals. The variation in radical concentration follows the spatial and temporal distribution of photoinitiator and its distribution at the end of dark period is presented in figure 4.5(b). Diffusion and radical termination is not observed during the pulse width period. Similar to diffusion, effect of polymerization kinetics appear at much longer time scales. Also, no variation in the monomer concentration was observed since the reaction kinetics is in dormant stage.

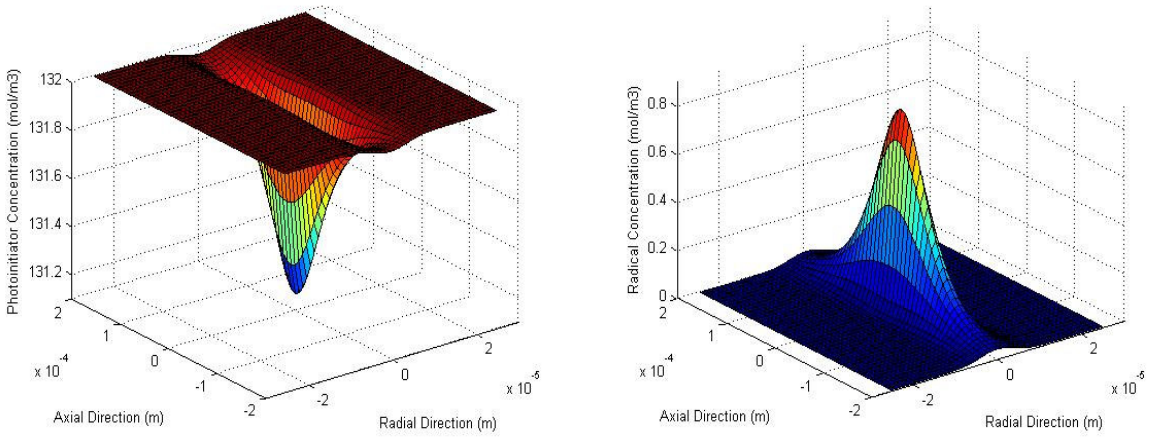

(a) (b)

Figure 4.5 Photoinitiator and radical distribution at the end of laser pulse width for 1 KHz system (a) Photoinitiator concentration distribution, (b) Radical concentration distribution

The presented analysis for the pulse width period assumes a highly responsive photoinitiator system where initiation and dissociation take place during the pulse width. In the case that the photoinitiator is not highly responsive, the presented procedure could still be employed to only calculate the number of radicals generated at the end of the pulse width but not to evaluate the radical concentration profile during the pulse width. The number of radicals at the end of the pulse width is assumed to remain constant until the photopolymerization

kinetics and molecular diffusion start affecting the system dynamics at time scales of 10^{-6} sec or longer, $t > 10^{-6}$ sec.

4.1.2 System state during the dark period

The system state at the end of the irradiation period is used to define the initial conditions for the subsequent analysis at the beginning of the dark period. The polymerization reaction and monomer conversion take place in the dark period because of the much longer time duration (1 kHz repetition rate laser system) required for the reaction kinetics to become dominant. Also, effect of diffusion is observed that tries to stabilize the concentration gradients produced during the laser irradiation and due to polymerization kinetics. In this section, the results from the dark period analysis are presented with a discussion of the polymerization kinetics on system state.

The radial and axial concentration gradients at the end of dark period are studied from the simulations by generating distribution plots. The spatial temperature distribution at the end of dark period is presented in figure 4.6(a). The temperature increase in the focal volume due to the laser irradiation tries to stabilize because of thermal diffusion. The thermal diffusion causes the dissipation of heat around the irradiated volume. Minimal accumulation of heat is observed as thermal diffusion is very active because of the longer time scales. Similar to the temperature distribution, the spatial gradients in photoinitiator, radical and monomer concentration were also analyzed. The diffusion of molecular species and polymerization kinetics changes the system state during the dark period. The photoinitiator molecules try to replenish the depleted volume caused due to laser irradiation.

The radical concentration in the focal volume changes due to molecular diffusion and termination kinetics. The spatial distribution and subsequent diffusion of radicals define the volume where monomer conversion takes place after the single pulse irradiation. The radicals combine with monomer molecules to propagate the polymerization reaction and increase the conversion ratio. The monomer conversion profile at the end of dark period is presented in

figure 4.6(b). Note that the small monomer conversion value obtained by the single pulse irradiation will translate into higher conversion ratios with increasing number of pulses. The information about the monomer conversion in and around the focal volume can be used to evaluate or predict the voxel size. The contour plot (figure 4.5(b)) depicts the spatial gradient in monomer concentration and illustrates the mismatch in axial and radial dimensions attributed to the Gaussian intensity distribution mismatch. This mismatch gives the voxel its ellipsoidal shape that is experimentally demonstrated by various research groups [21, 36, 37, 40]. Though, the mismatch is more pronounced while working with low N.A. lenses, it can be controlled by working at threshold conditions and high N.A. objectives [7, 41].

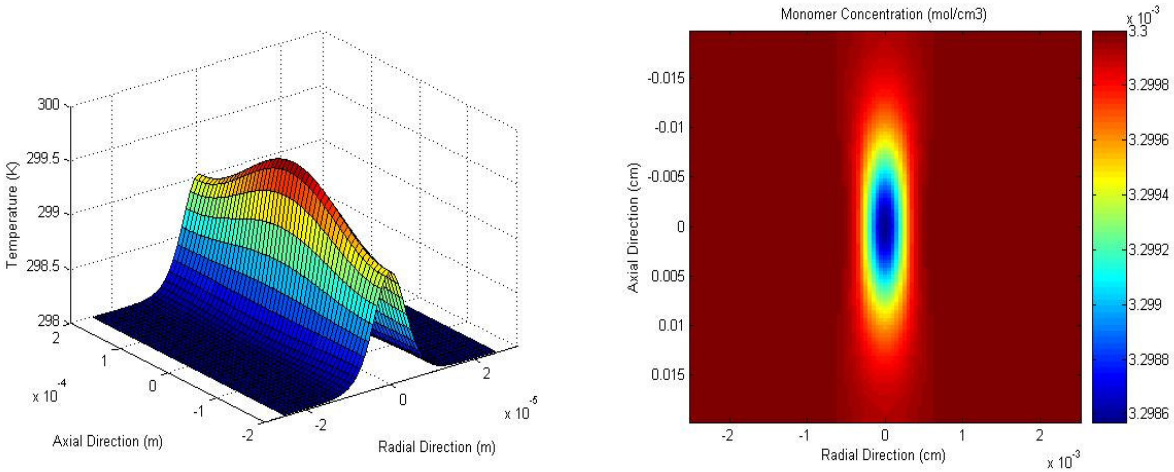

(a) (b)

Figure 4.6 Temperature and monomer concentration distribution at the end of dark period (a) Temperature distribution, and (b) Monomer concentration variation

The information from spatial species concentration distribution is helpful in defining the volume where polymerization reaction has initiated. The conversion profile of monomer can be used to predict the initial volume where voxel growth initiates as it captures the system state at the end of the dark time period. The limitation of spatial distribution plots is their inability to capture the polymerization dynamics and kinetics in the defined time period as these plots represent the system state at the end of dark period. To further analyze the polymerization process, temporal distribution plots were generated that capture the species of interest at

desired spatial distances. The temporal distribution of temperature and other species are presented in the following sub-section to understand the polymerization process during the dark period.

4.1.2.1 Temperature distribution

Thermal diffusion tries to dissipate heat from the focal volume, and in order to capture the thermal diffusion effects, temporal profile plots were studied from the analysis at various radial directions as presented in figure 4.7. The temperature along the focal center decreases and reaches a steady state value at the end of dark period. The temperature of the region away from the focal volume (r = 10µm > 5 µm spot radius) increases as the thermal energy from the irradiated volume is diffused to the surroundings. The temperature of the resin system surrounding the focal volume (5 times the spot radius) increases slightly with maximum rise at the focal volume (~ 0.5 K) after the single pulse irradiation.

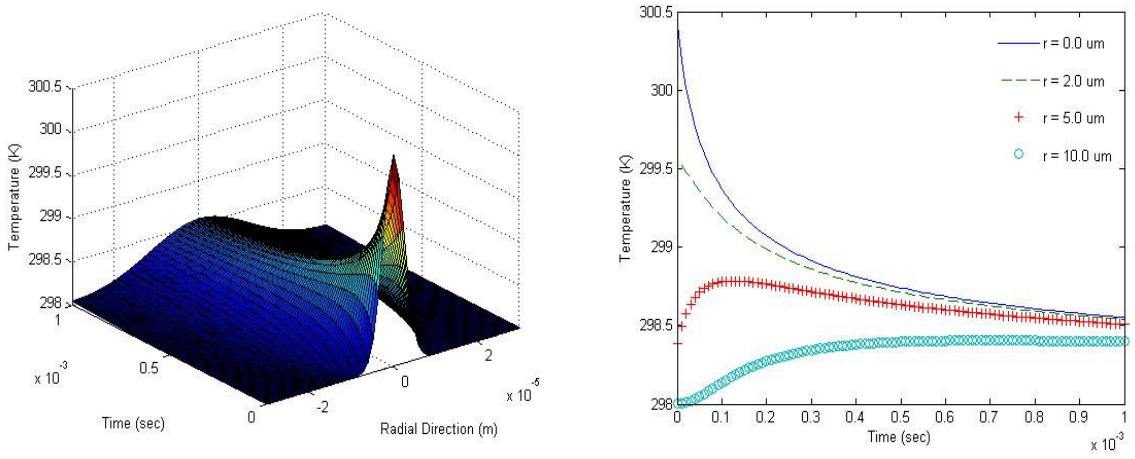

(a) (b)

Figure 4.7 Species concentration variation during dark period for 1 kHz system (a) Temporal and spatial temperature distribution, and (b) Temperature distribution at various radial distances

4.1.2.2 Photoinitiator distribution

Since, with the irradiation of laser pulses the photoinitiator molecules gets depleted from the focal volume. During the dark period, the replenishment of photoinitiator molecules at the irradiated volume takes place, governed by the diffusion from the surrounding higher

concentration areas. Also, 1 kHz pulse repetition rate provide enough time interval for diffusion to be significant and mitigate the concentration gradient. The temporal variation of replenishment dynamics was analyzed using the line plots in radial direction. The plot depicting the temporal concentration gradient of photoinitiator concentration at various radial distances is presented in figure 4.8. The maximum depletion of photoinitiator molecules takes place at the center of focal volume because of high intensity of laser pulse. The effect of molecular diffusion during the dark period is captured and is also presented in figure 4.8. Because of diffusion, the photoinitiator concentration again increases at the center as the diffusion of photoinitiator molecules from the surrounding volume tries to mitigate any variation in concentration gradient. Hence, replenishment of photoinitiator molecules is observed at the focal volume but a reduced concentration is observed away from the optical axis. The reduced photoinitiator concentration after the first pulse will become the initial condition for the next pulse and will affect the number of generated radicals and hence the polymerization dynamics.

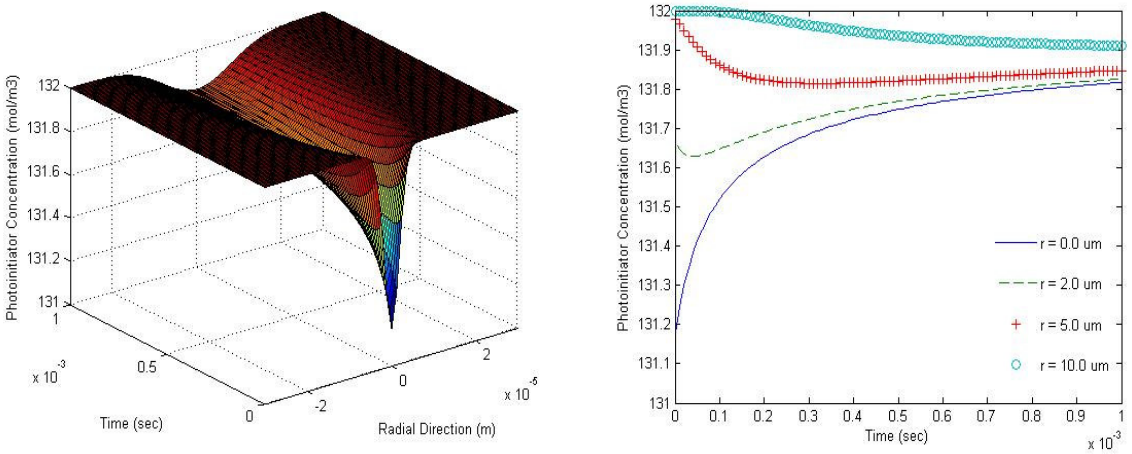

(a) (b)

Figure 4.8 Photoinitiator concentration gradient for 1 KHz system (a) Temporal and spatial photoinitiator concentration distribution, and (b) Photoinitiator distribution at various radial distances

4.1.2.3 Radical distribution

The generated radicals during laser irradiation (end of irradiation period) start to deplete during the dark period because of termination kinetics of free radical polymerization reaction. In addition, some diffusion is observed that causes the radicals to propagate away from the focal volume. The diffusion of radicals may lead to a bigger voxel size as the diffused radicals could combine with monomer molecules and initiate the chain polymerization reaction. However, the diffusion alone does not define the radical dynamics. The termination of radicals defines the volume where actual polymerization takes place and affects the size of voxel. Without radical termination, the radicals will diffuse and polymerize the whole photoresponsive resin system, but fortunately this does not happen because of the strong termination of radicals. Hence, it becomes important to correctly understand the radical dynamics, as their time integral spatial distribution will define the volume where polymerization reaction will take place and generate the voxel.

The temporal distribution of radical concentration and its variation at different spatial distances during the dark time period are presented in figure 4.9. The plots illustrate the effect of both diffusion and termination and the variation in radical concentration during the dark period. The radical termination is strong along the optical axis because of the presence of higher concentration of radicals and causes a rapid decrease in their concentration during the dark period. It is also observed that the concentration of radicals increases away from the irradiated volume. The interesting behavior captured from the analysis is the termination rate that depends upon the concentration of radicals at a specific location. Higher termination rate is observed for high concentration areas but lower concentration areas do not experience any significant radical termination. This behavior is explained in the following section where a complete discussion on the termination kinetics is presented. The radical diffusion and termination kinetics define the concentration gradients and the volume where polymerization initiates leading to a polymerized voxel.

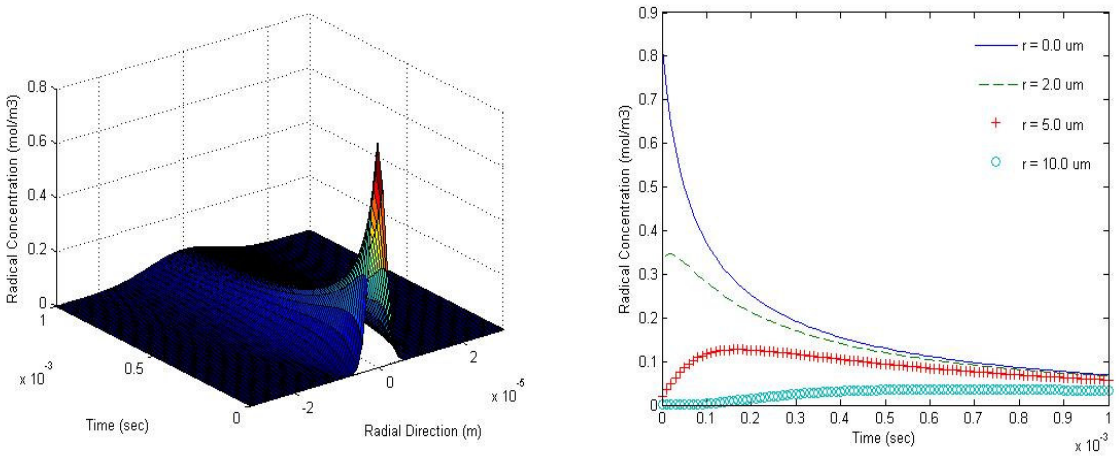

(a) (b)

Figure 4.9 Spatial distribution of radical concentration for 1 kHz system (a) Temporal and radial distribution of radicals, and (b) Temporal radical distribution

4.1.2.4 Radical termination kinetics

The termination of radicals plays a significant role in limiting the polymerized volume and affects the resolution of 2PP process. As presented in equation 7, the generated radicals terminate by combination, trapping and encountering inhibitor molecules. Hence, the distribution of radicals in and around the focal volume varies and the distribution defines the size of polymerized voxel. The termination of radicals by combination depends on the termination constant-k_t, and the active number of radicals in the area. A higher termination constant and a stronger concentration of radicals lead to a rapid decease in radical concentration as there is a strong probability for two radicals to interact and terminate. At higher concentration areas, the probability of a radical to encounter another active radical or an inhibitor molecule is high. This leads to rapid decrease in radical concentration at the center and the surrounding high concentration areas. This behavior is also observed in figure 4.9(b) where the radical concentration at the center reduces rapidly compared to the surrounding volume. Also, even though the radical concentration decreases around the center of focal volume, there is a small increase around the edges. This increase is caused by the diffusion of radicals away from the high concentration regions and is presented in figure 4.9(b) for the radial direction. Radical

termination is not observed at the radial distance of 10 μm which is twice the size of the actual beam radius and has relatively much low radical concentration. Because of these much smaller concentrations, the termination kinetics is very weak and no noticeable termination is observed. Hence, termination plays a critical role in defining the number of active radicals that can actually take part in the polymerization reaction and the subsequent growth of voxel. It is important to consider the effect of the termination modes and their relative dominance periods as they affect the rate of polymerization and the size of final feature.

The role of termination by combination and trapping is more dependent on the type of photoinitiator and monomer used for polymerization. On the other hand, termination by quenching of radicals by inhibitor molecules varies as it depends on the initial concentration of inhibitor molecules present in the monomer system or the diffusion of oxygen molecules from the surrounding that also creates a very strong inhibition effect. Inhibitor molecules are always present in the monomer system as they are added by the manufacturer to avoid any unwanted polymerization reaction and increase their shelf-life. Therefore, the termination kinetics depends upon the relative concentration of dissolved inhibitor molecules and the rate of their combination with active radicals. The concentration of inhibitor decreases from the irradiated volume upon laser pulse irradiation as the quenching process takes place. The temporal concentration distribution of inhibitor molecules at various radial distances is presented figure 4.10. The presence of inhibitor defines the threshold for polymerization as the rate of polymerization also depends upon the concentration of inhibitor molecules and how strongly they terminate the active radicals [7, 16, 41, 52]. This mechanism can be effectively used to control the size of the polymerized volume by varying the concentration of inhibitor molecules in the resin and will be discussed in the following section. Upon laser irradiation, a rapid decrease in inhibitor concentration from the center of irradiated volume is evident from figure 4.10. The rate of change in inhibitor concentration depends on the available concentration of both inhibitor and active radicals along with the inhibition kinetic parameter k_z. Higher radical concentration

regions show a rapid decease in inhibitor concentration. Note that, the inhibition kinetic parameter is a couple of orders in magnitude greater than the termination by combination constant - k_t. This along with the relative concentration of inhibitor and radical molecules defines the rate of inhibition kinetics as presented by equation 8.

The presence of inhibitor molecule affects the polymerization dynamics as it decreases the actual available radicals that can initiate polymerization and hence presents a thresholding behavior. Most of the inhibitor molecules deplete early during the dark period and control the initial polymerization kinetics. Diffusion of inhibitor molecules is also noticed from the surrounding volume that changes their spatial concentration. The coupled effect of inhibitor diffusion and termination kinetics changes the 2PP process dynamics and eventually affects the resolution of polymerization process or the voxel size. The inhibition effect along with photoinitiator's FOM is effectively employed for the fabrication of voxels with a diameter of 80 nm [41]. Hence, a precise control on the inhibition kinetics can be effectively employed to achieve a high resolution 2PP process.

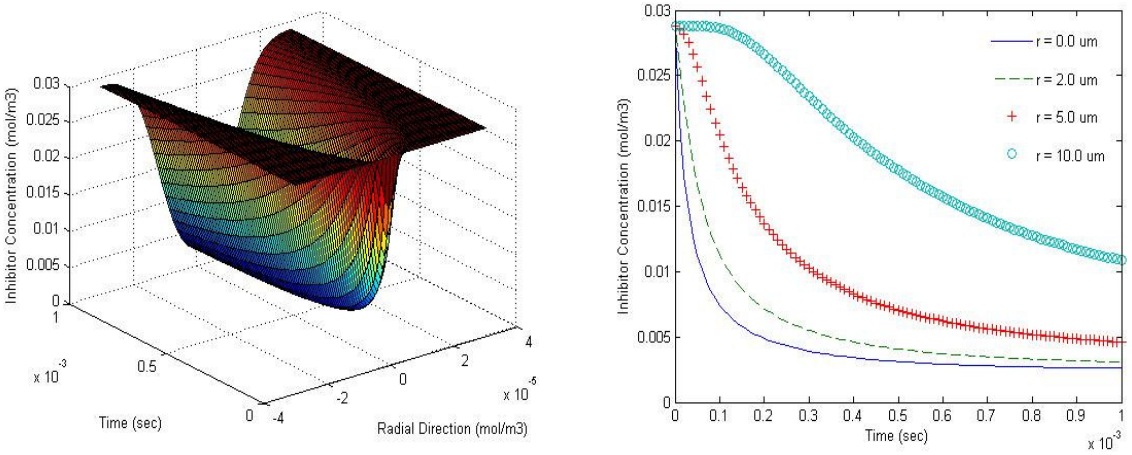

(a) (b)

Figure 4.10 Spatial distribution of inhibitor concentration for 1 kHz system (a) Temporal and radial distribution of inhibitor, and (b) Temporal distribution of inhibitor at various radial distances

4.1.2.5 Monomer conversion with increasing number of pulses

The conversion of monomer molecules into high molecular weight polymer depends on the propagation of chain polymerization reaction. As already discussed, the available active radicals combine with monomer molecules to create reactive centers. These reactive molecules propagate the polymerization reaction until they terminate by various termination processes. As the polymerization progresses, the monomer converts into high molecular weight polymer. The final size of polymerized voxel is defined by the areas that exceed a critical conversion value and have enough molecular weight and structural rigidity to withstand the developing process. The conversion of monomer into high molecular weight polymer is a gradual process as the percentage conversion increases with subsequent pulses until the monomer concentration depletes and the volume saturates. It is analyzed that at high energies photobleaching can take place causing stagnation in conversion ratios. The applied energies for polymerization reaction should be chosen depending upon the initial photoinitiator concentration and its two photon absorption cross-section to avoid photobleaching and to reach high conversion ratios. The percentage conversion also depends on the surviving radicals and the propagation rate constant for the reaction. The conversion ratio of the monomer along the radial and axial directions is presented in figure 4.11. The maximum conversion takes place at the center of focal volume and drops considerably going away from it. The conversion profile along the axial direction is much wider compared to the radial direction and can be attributed to the Gaussian intensity distribution mismatch. The wider axial intensity distribution has enough energy to initiate the polymerization reaction and eventually leads to longer voxel size along the optical axis. The information obtained from the conversion profile can be used to predict the voxel dimension for various applied process and chemical parameters.

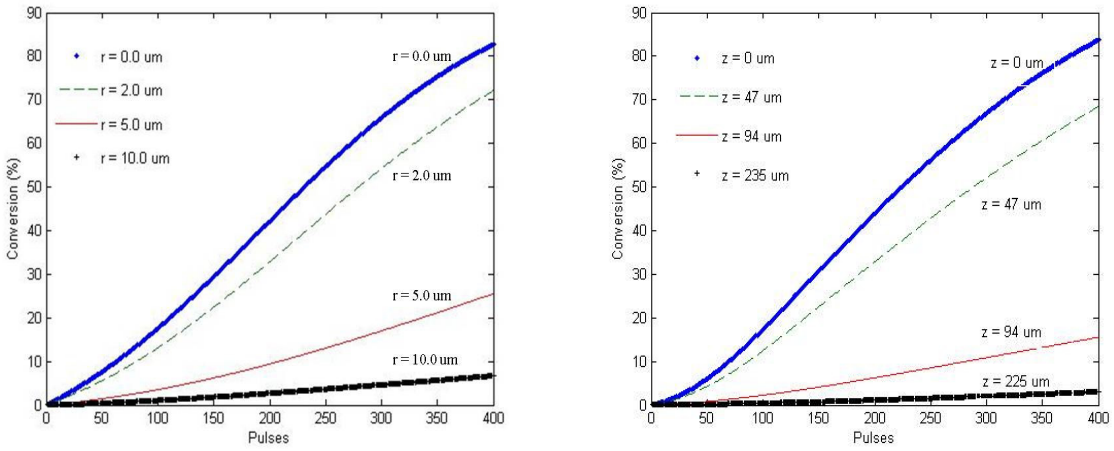

(a) (b)

Figure 4.11 Monomer conversion along radial and axial directions (a) Conversion in radial direction, and (b) Conversion in axial direction

The mathematical analysis of 1 kHz system presents interesting insights into the 2PP process. Single pulse analysis helps in understanding the role of thermal/molecular diffusion and polymerization kinetics on the 2PP process. The understanding on the variation in species concentration during the irradiation and dark period lays the foundation to evaluate the affect of various chemical and physical process parameters on the 2PP process. Similar analysis is extended to high repetition rate laser systems that are commonly used for 2PP process. The simulation results and discussed in the following section.

4.2 2PP using high repetition rate (80 MHz) laser system

An analysis was also performed to understand the polymerization dynamics for high repetition rate femtosecond laser systems commonly used for 2PP process. The polymerization dynamics for low and high repetition rate laser systems can be significantly different because of the shorter dark period for the latter. The same mathematical model is used to simulate the polymerization process by only changing the end time for the dark period. The dark period duration is approximately 12.5 nsec for high repetition rate laser system working at 80 MHz compared to 1 msec for 1 kHz system. A beam spot radius of 1 μm and average laser power of 5 mW were used that corresponds to commonly used parameter values with high repetition rate

laser systems found in the literature. The energy of each pulse is much lower (< 1 nJ) because of high repetition rate (80 MHz) and may not cause significant system state change as compared to an amplified laser system with single pulse irradiation. The photoinitiator decomposes from the irradiated volume with the generation of radicals during the irradiation period. Reaction kinetics and molecular diffusion are dormant without any conversion of monomer taking place similar to the 1 kHz repetition rate system. The radial temperature distribution and photoinitiator concentration during the single pulse irradiation state are presented in figure 4.12. Though, the dynamics of the system is similar to the amplified laser system, it is observed that the temperature rise and depletion of photoinitiator concentration are very small because of the much lower pulse energy. Also, the generated radical concentration is much lower (couple of orders in magnitude) with single pulse irradiation attributed to lower photoinitiator decomposition.

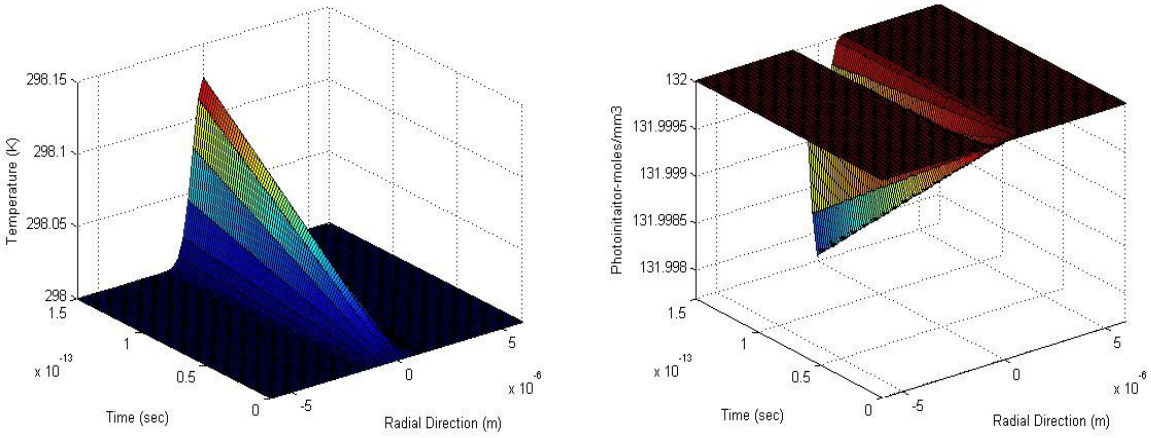

(a) (b)

Figure 4.12 Spatial distribution of temperature and photoinitiator for 80 MHz system for single pulse irradiation (a) Temperature distribution, and (b) Photoinitiator concentration distribution

The polymerization dynamics of the high repetition rate system during the dark period is quite different from the amplified laser system. The longer dark period duration for the 1 kHz system provides more information on polymerization kinetics compared to an 80 MHz system. As presented in section 4.1.2, the reaction kinetics and diffusion affect the system state and the

polymerization process. In high repetition rate laser systems, the effects of diffusion and termination are not noticed during the dark period because of the much smaller time interval (12.5 ns) with the single pulse irradiation. This time period is much smaller than the characteristic time for diffusion and polymerization kinetics to be dominant and cause a change in the system state. The time in which the polymerization kinetics and molecular diffusion dominate can be estimated by L^2/d, where L is the characteristic diffusion length and d is diffusion constant [56]. The characteristic time for the photoinitiator concentration to start replenishing the depleted region is in the order of 10 μsec, causing the diffusion and polymerization kinetics in and around the irradiated volume to have no visible effects within the time between pulses of 12.5 nsec. The radial and temporal distribution of photoinitiator and radical concentrations used to further understand the polymerization dynamics for 80 MHz system during the dark period are presented in figure 4.13.

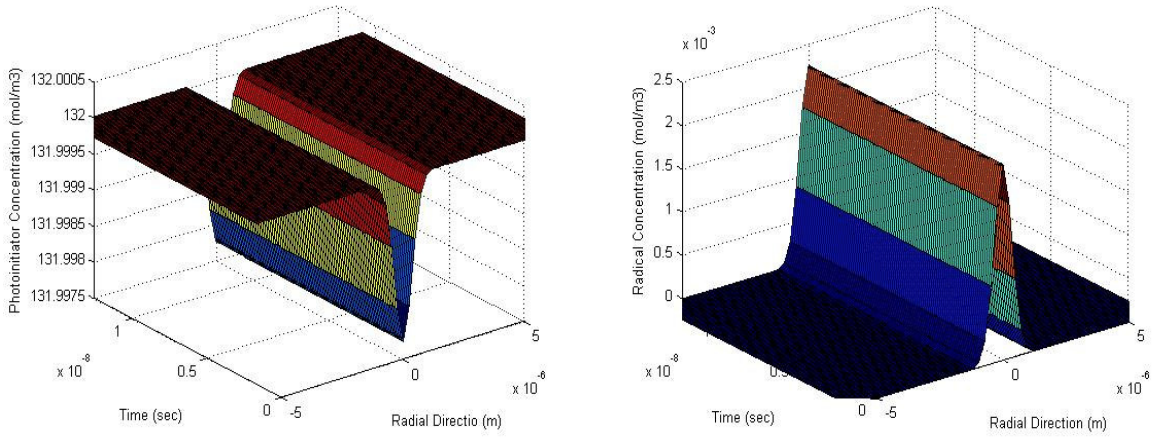

(a) (b)

Figure 4.13 Radial and temporal distribution for high repetition rate system during dark period for 80 MHz system (a) Photoinitiator concentration distribution, and (b) Radical concentration distribution

The single pulse analysis of the 80 MHz system during the dark period illustrates no change in the system state from the irradiation period. The temperature of the irradiated volume remains the same without any thermal diffusion. The concentrations of photoinitiator and

radicals do not change during the dark period. Also, the effects of molecular diffusion and radical termination are not evident from the plots in figure 4.13. The photoinitiator concentration depleted from the irradiated volume after the single pulse irradiation is not replenished in this period. In addition, radical termination kinetics, that can change the radical concentration, are not noticed. Hence, the irradiation with the next pulse, the number of newly generated radicals will be added to the existing radical concentration from the previous pulse, and will keep accumulating until the termination kinetics become active. Also, there is no change in the inhibitor concentration and monomer conversion as their kinetics depends upon the characteristic time. Monomer conversion starts at much longer time scales (few microseconds) and continues until millisecond time duration as presented for 1 kHz analysis. Therefore the single pulse analysis of high repetition rate system does not provide any useful information about the polymerization dynamics because of the much shorter time interval. Thus, in order to understand how the polymerization progresses with irradiation from high repetition rate laser system, a multi-pulse analysis must be performed.

4.2.1 Multipulse analysis for high repetition rate (80 MHz) laser system.

The irradiation with multiple pulses from a high repetition rate laser system has interesting effects on the polymerization process. Simulations were performed to further enhance our understanding about the 2PP process while employing high repetition rate laser system. Irradiation with a high repetition rate laser system causes heat accumulation in and around the irradiated spot or focal volume. The resin system absorbs the input laser energy and causes an increase in temperature. Also, the exothermic nature of polymerization reaction generates heat that further raises the system temperature. A temperature distribution plot was created at different spatial distances to correctly understand the temperature profile with increasing number of pulses. For the analysis, the irradiated spot diameter of 2 μm and the spatial distance of 12 μm were analyzed. The temperature rises steadily during the initial reaction phase because of the higher concentration of photoiniator molecules. Heat is

dissipated away from the irradiated spot through thermal diffusion causing the temperature of the whole simulated system to increase. The rate of increase in temperature reduces significantly and approaches a steady state after the reduction in monomer concentration at high conversion ratios as is presented in figure 4.14(a). The induced temperature gradient has significant effect on the polymerization dynamics as explained previously in the 1 kHz system analysis. The information of the temperature distribution is carried out through out the simulations as it directly affects the kinetic and diffusion parameters.

The simulations were also used to evaluate the percentage conversion of monomer into high molecular weight polymer. The monomer conversion approximately follows the Gaussian intensity distribution, and the maximum conversion takes place at the center of irradiated spot as presented in figure 4.14(b). It is also evident that the conversion ratio drops rapidly moving away from the center leaving low molecular weight polymer around the irradiated spot. This low molecular weight polymer gets washed away during the development phase and only regions with high conversion ratios survive this process.

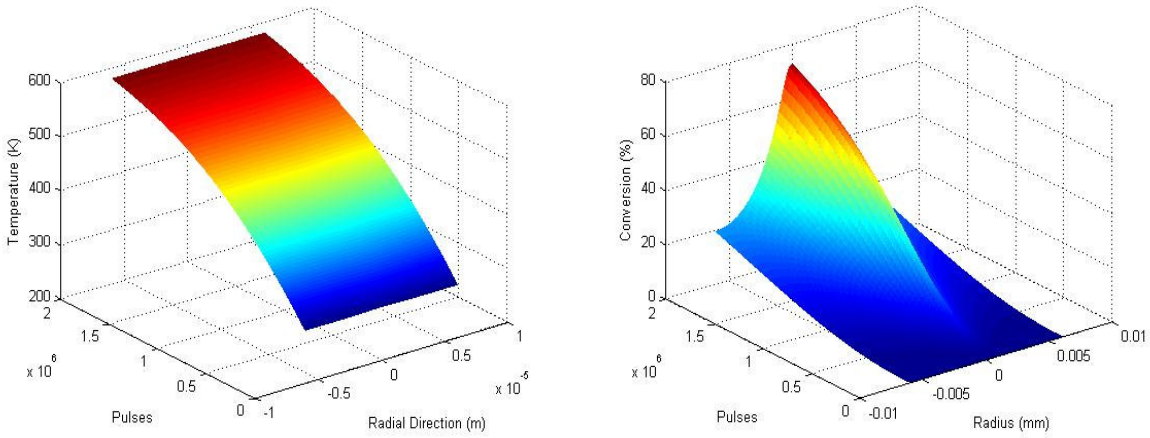

(a) (b)

Figure 4.14 Temporal and spatial temperature and conversion ratio for multi-pulse analysis of 80 MHz system (a) Temperature profile, and (b) Percentage conversion of monomer

Detailed analysis is also performed to further understand the effect of multipulse irradiation of ultrashort laser pulses from the high repetition rate laser system on the spatial and

temporal concentration distribution of various species. The multipulse analysis will provide an insight on the dynamics of the polymerization process and how it may get affected by the change in temperature and the concentration of various species of interest (photoinitiator, radicals and inhibitor). The following subsections presents the simulated results and discussion on the concentration change in the species of interest with increasing number of pulses.

4.2.1.1 Photoinitiator concentration with increasing pulses

The simulations were used to understand the species decomposition/generation which is the integral part of polymerization process. Results from the analysis were first plotted to evaluate how the photoinitiator concentration changes with the irradiation of laser pulses at high repetition rate as presented in figure 4.15. As expected, the results illustrate that the photoinitiator concentration decreases with increasing number of pulses. But, the interesting behavior observed was the replenishment of the photoinitiator molecules in the irradiated volume or focal volume through diffusion from the surrounding regions. This diffusion causes the photoinitiator concentration to change significantly and causes a significant decrease in photoinitiator concentration from the regions away from the irradiated volume. It is noticed that the regions which are five times the irradiated volume have significant drop in photoinitiator concentration, primarily because of active diffusion. This indicates that photoinitiator molecules have high mobility that affects the actual volume where their concentration significantly changes. This is an interesting result which was not anticipated as it was assumed that the photoinitiator concentration changes only at the focal volume. But because of the increased temperature conditions with multipulse irradiation, the mobility of molecules is increased causing this behavior. Also, effect of diffusion is also significant because of the much smaller spatial distances produced by the tight focusing conditions.

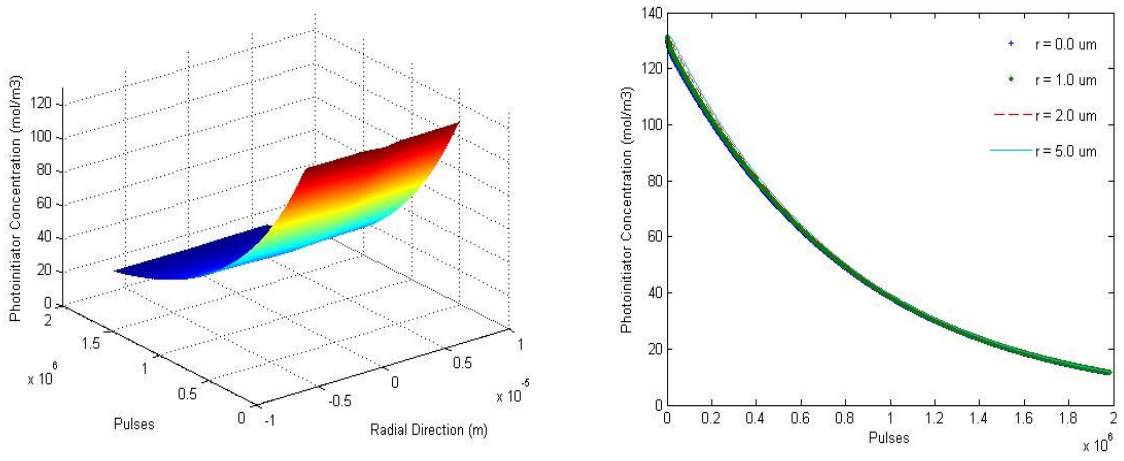

(a) (b)

Figure 4.15 Photoinitiator concentration distribution for multi-pulse analysis of 80 MHz system (a) Temporal and radial distribution, and (b) Temporal distribution of photoinitiator

4.2.1.2 Radical concentration with increasing pulses

The decomposition of photoinitiator molecules causes an increase in radical concentration. The radical concentration distribution plot with increasing number of pulses is presented in figure 4.16. The concentration of radicals increases during the irradiation with laser pulses. The maximum increase in the concentration of radicals takes place at the center of irradiation spot. The initial accumulation is followed by a rapid termination that takes place after a few thousand pulses. From the presented plot, it is concluded that there is a characteristic time limit before which the polymerization kinetics and molecular diffusion effects are in a dormant stage. However, once the characteristic time is reached, the polymerization kinetics and diffusion effects become active and considerably change the radical concentration and hence the dynamics of polymerization reaction.

As discussed during the 1 kHz analysis, the generated radicals terminate by the modes of quenching, trapping and combination. Though, the effect of each mode is dominant at different time scales. Termination by quenching is stronger during the initial termination phase because of the high available concentration of inhibitor in the resin system. The inhibitor molecules are consumed rapidly because of their higher reactivity defined by stronger kinetic

rate constant. Though, radical trapping is usually stronger at higher conversion ratios as the amount of dead polymer significantly increases creating a stronger probability to confine the radical molecules by dead polymer. In between these two limits, radical termination occurs mostly by combination. Note that, there is no clear demarcation when one termination mode becomes really dominant. Also, the termination rate is stronger at regions having higher concentration of radicals that provide higher probability of combination with other similar active molecules or the present inhibitor molecules in the resin system. The same behavior was also observed and discussed for the single pulse analysis of 1 kHz system. It is important to correctly capture the radical distribution as it defines an envelope where polymerization reaction progresses and leads to the formation of voxel.

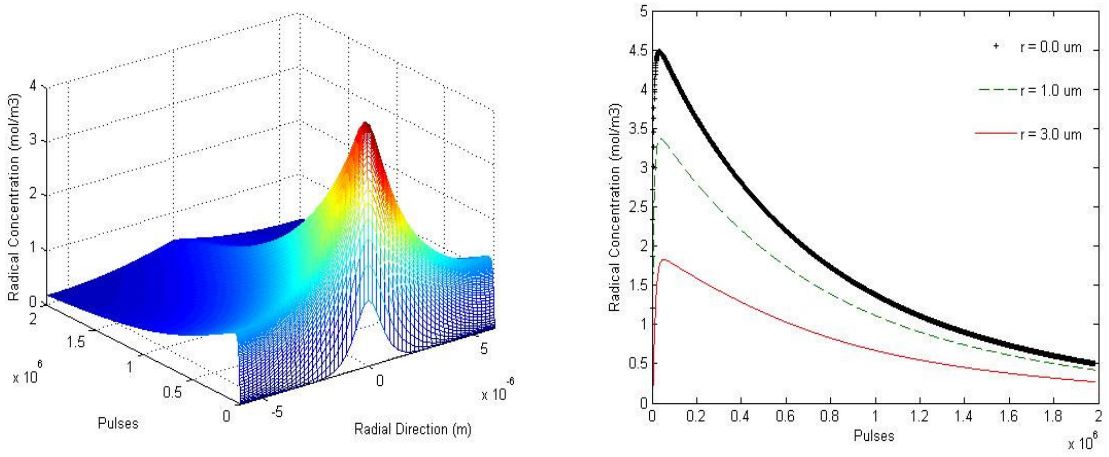

(a) Temporal and radial distribution (b) Temporal distribution of radicals

Figure 4.16 Radical concentration distribution for multi-pulse analysis of 80 MHz system (a) Temporal and radial distribution, and (b) Temporal distribution of radicals

4.2.1.3 Monomer concentration with increasing pulses

The radicals are generated on photoinitiator decomposition and their termination occurs after a characteristic time defined by the kinetic constants of polymerization. Even though the radicals terminate, they also initiate the polymerization reaction by combining with monomer molecules to form reactive centers. The termination and propagation of polymerization reaction occurs simultaneously and leads to a change in monomer concentration. A significant change in

monomer concentration occurs mostly in the volume where there are high numbers of active radicals. The monomer distribution plots for the radial direction are plotted in figure 4.17. The maximum concentration drop takes place at the center of the focal volume and decreases going away from it. Eventually, the volume with significant monomer conversion defines the generated polymerized voxel after significant conversion ratios are achieved.

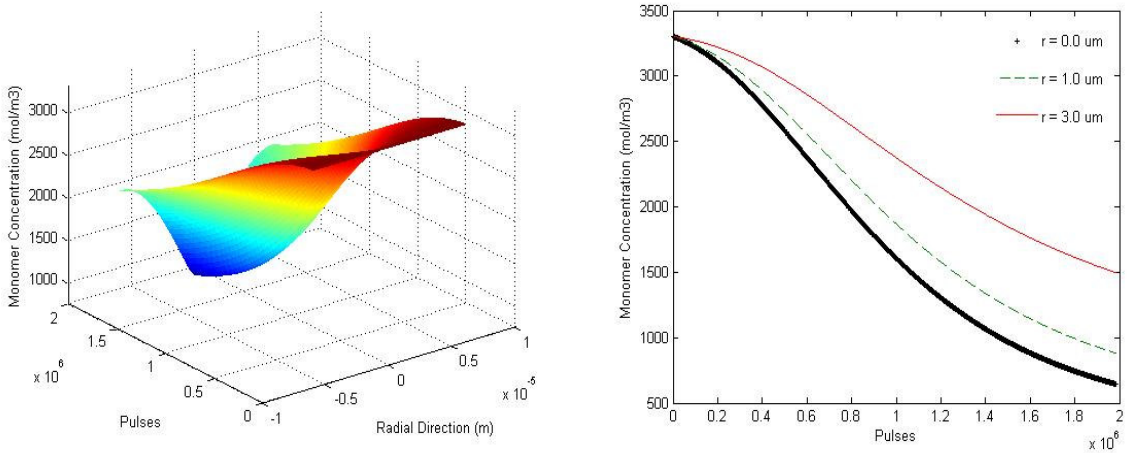

(a) (b)

Figure 4.17 Monomer concentration distribution for multi-pulse analysis of 80 MHz system (a) Temporal and radial distribution, and (b) Temporal monomer distribution

The size of voxel can be easily captured by defining the volume that exceeds certain conversion ratios. Generally, a conversion ratio of 70% and higher provides structurally integral polymerized features that can withstand the developing process [16]. Monomer conversion plots were generated to further understand how the conversion ratio varies with increasing number of pulses in both the radial and axial dimensions as shown in figure 4.18. The polymer conversion at three different radii (0 µm, 1µm and 3 µm) is presented in figure 4.18(a), and three different axial distances (1.6 µm, 6.3 µm, and 7.9 µm) are presented in figure 4.18(b). The maximum conversion of approximately 80% is achieved at the center of the focal volume and it decreases rapidly (~70% and ~50%) while going away in the radial direction. As polymerization is a gradual process, the low conversion regions do not have structural integrity and are washed of during development phase. The conversion of monomer into high molecular weight polymer

along the axial direction takes place to a much wider region. Around 70% conversion ratio is achieved at a distance of 6.3 µm away from the center along the axial direction compared to ~1 µm along radial direction as presented in figure 4.18.

Another interesting feature is the change in polymerization dynamics with increasing number of pulses. The reaction exhibits a slow start during the initial few thousand pulses but a sudden increase in the rate of reaction is noticed thereafter. The reaction rate drops towards the end and exhibits a monotonic behavior. Increase in the rate of reaction at the mid stage is normally not expected as it is assumed that the reaction rate will reduce with time or increase in the percentage conversion of monomer because of the depletion in photoinitiator and monomer concentration. But the rise observed in the reaction rate is characterized by the presence of an auto-acceleration phase that changes the polymerization dynamics [10, 41]. The auto-acceleration is attributed to the increase in temperature of the irradiated volume because of the heat accumulation from laser pulses and exothermic nature of polymerization reaction. The dependence of polymerization kinetics on the temperature is governed by an Arrhenius relationship as presented in equation 6. The temperature increases causes the propagation and termination rate constants to increase causing a change in reaction rate. This relative increase in polymerization kinetic constants leads to the auto-acceleration phase thus resulting in an increased reaction rate.

The size of polymerized voxel can be estimated by capturing an isoline with a certain conversion ratio that leads to a high molecular weight polymer with high structural integrity. Using the result of the presented analysis, it is evaluated that the polymerized voxel has a width of 2 µm and height of 12.6 µm for 80% conversion ratio after the irradiation with 2 million pulses as presented in figure 4.18. This significant difference in width and height of the voxel is mostly attributed to the Gaussian intensity distribution mismatch as explained in the 1 kHz analysis. The simulated results presents a voxel with an aspect ratio of ~6, which can be significantly reduced by simulating tight focusing conditions normally employed for 2PP.

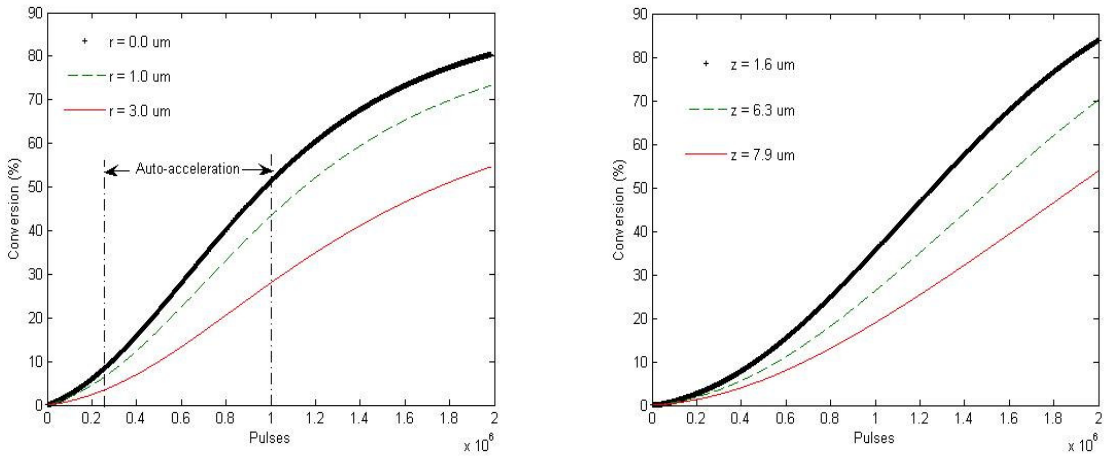

(a) (b)

Figure 4.18 Radial and axial conversion ratios for 80 MHz system (a) Radial conversion ratio, and (b) Axial conversion ratio

4.2.2 Effect of applied input power on polymerization dynamics

Another critical aspect of 2PP process is the range of input average powers that can be used for polymerization. Similar to time thresholding, there is power thresholding and a range of average power values that can be used called the *Dynamic Power Range* (DPR) [40]. The lower band of DPR is represented by power threshold value below which insignificant polymerization takes place. But the interesting aspect of DPR is that at the higher end it produces interesting results. Generally, exceeding DPR causes burning of monomer because of very high intensities and subsequent high temperatures produced by high powers and tight focusing conditions. The burning is not desirable and should be avoided and this defines the maximum power that can be used for polymerization. But burning is not the only problem that occurs at high power levels. The other behavior noticed is the extensive growth in the axial dimension of polymer voxel while working at higher power levels. This growth cannot be simply explained by the polymerization mechanisms considered for the 2PP process indicating that some other nonlinear phenomenon occurs only at high powers and affects the size of voxel. This phenomenon will be discussed in the following chapter along with experimental data obtained from in-house experiments.

Another important consideration of the useable power levels is the effects of photobleaching that occurs especially at higher input powers. Photobleaching is a common problem in fluorescence microscopy where it leads to the destruction of fluorophore. Similar problem can take place in 2PP while working at higher power levels. While employing higher powers, the polymerization reaction starts at a rapid rate but does not reach high conversion ratios. This causes a stagnated region where conversion ratio stays mostly constant even with increasing number of pulses. The effect of various power levels on the achievable conversion ratios is presented in figure 4.19. At lower power levels close to the threshold limit, conversion ratio increases very slowly because of much slower reaction rates. Though at higher power levels, the stagnation occurs because of the depletion of photoinitiator molecules from the irradiated volume as presented in figure 4.1(b). This causes a stagnation of achievable conversion ratio as radicals are not generated that can propagate the polymerization reaction. Hence, it becomes important to correctly employ power levels that efficiently leads to higher conversion ratios and do not create photobleaching situations. Generally it is desirable to have a wider DPR that provides much more flexibility in choosing power levels. DPR is dependent on the figure of merit of photoinitiator that highly depends upon the two-photon absorption cross-section and the quantum yield. Photoinitiators with high figure of merit provide researcher to tune the applied power levels and photoinitiator concentration that might be critical for certain applications. For example, working with biological material, it is required to have lower applied powers levels along with small concentration of toxic photoinitiators as they may have an adverse effect on the biological organisms.

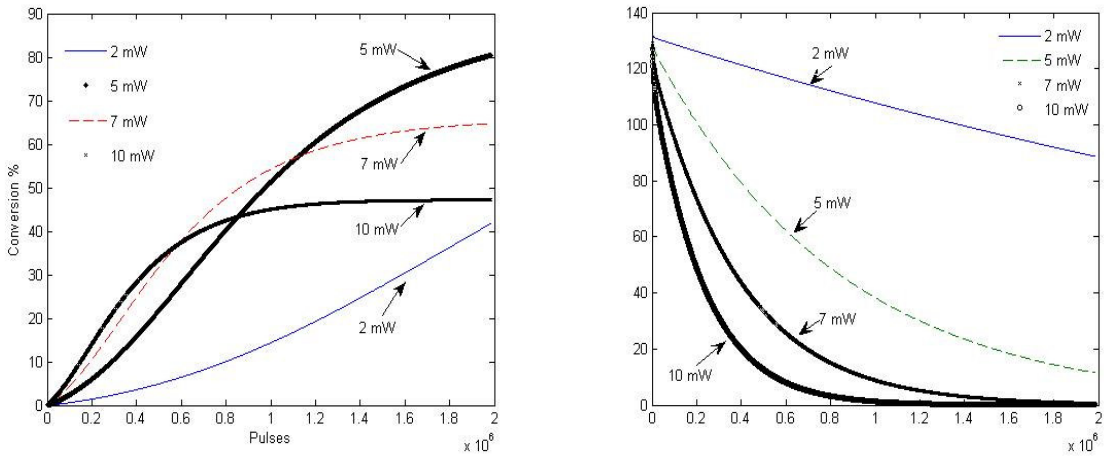

(a) (b)

Figure 4.19 Effect of power on conversion ratio (a) Conversion ratio, and (b) Photoinitiator concentration

4.2.3 Controlling the spatial distribution of radicals

From the analysis, it is understood that the voxel grows with increasing power levels (between the DPR) and increasing exposure time. As the technologies are moving to smaller and smaller features, it is essential to reduce the size of fabricated feature that can enable a high resolution process. There are a couple of ways to achieve smaller voxel size: 1) using high numerical aperture lenses, 2) working at threshold conditions. Small features sizes can be obtained by the combination of these methods, but to further reduce the size can be challenging. One way to further enhance the resolution of 2PP process is by controlling the amount of radicals that take part in the polymerization process. We know from the analysis that generated radicals combine with monomer molecules to initiate polymerization reaction. These radicals also diffuse spatially that increase the volume where polymerization takes place. One way to reduce the size of voxel is by controlling the volume where these radicals initiate polymerization. One way to achieve that is by increasing the radical termination kinetics. As discussed earlier, the termination is governed by three modes: termination by combination, trapping and inhibitor effect. We do not have much control over termination by combination and trapping but termination by quenching can be controlled by modulating the inhibitor

concentration in the resin system. Increasing the inhibitor leads to higher thresholding conditions and higher number of radicals have to be generated to overcome the increased inhibition effect. The increased thresholding effect has been reported to enable feature size much smaller than the diffraction limit [32, 38, 41].

To correctly understand the effect of increased inhibitor concentration on the polymerization dynamics, simulations were performed by choosing different inhibitor concentration values. The results from modulating inhibition concentration are presented in figure 4.20. The increased inhibitor concentration severely retards the conversion ratios and limits the regions where polymerization progresses. This is caused because of much lower radicals take part in polymerization reaction that limits the shrinks their spatial distribution as presented in figure 4.20(b). This leads to smaller polymerized voxels primarily attributed to high thresholding conditions created by increased inhibitor concentration. Modulating inhibitor concentration is an effective method that can enable high resolution 2PP process.

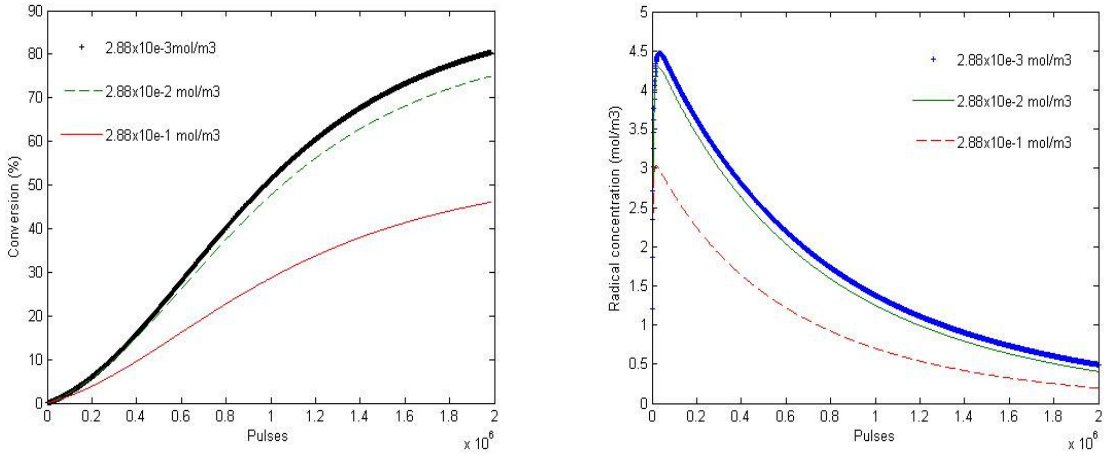

(a) (b)

Figure 4.20 Inhibitor effect on conversion ratio (a) Conversion ratio at focal center, and (b) Radical concentration

4.2.4 Validation of the developed model

To further understand how the voxel grows and to verify if the model depicts the actual 2PP process, a comparison was performed with experimental results from the published

literature. Contrast plots were developed that presented the growth of voxel with increasing exposure time (number of pulses) but at a constant applied average power (5 mW). The simulated contrast plots for both the width and height of voxel were compared to the experimental plots obtained from literature as presented as an inset in figure 4.21 and individually in figure 4.22 [21]. The simulated contrast plots exhibits the same trend by which voxel grows and verify that the model correctly depicts the actual 2PP process with all its inherent non-linearity and 3D confinement. The time exposure contrast plots also present a time thresholding effect which causes no significant monomer conversion below certain exposure conditions. Once, the exposure time increases, the voxel starts to grow in both radial and axial directions. The simulated results and the obtained contrast plots verifies that the developed model depicts the actual 2PP process and incorporates the nonlinear photophysical and photochemical changes that take place in a 3D volume. The model also represents correctly the growth of voxel in both radial and axial direction and is verified by the contrast plots obtained from the published literature.

Experimental verification of the developed model was also performed by polymerizing walls in a resin system consisting 97% by wt. of monomer (SR499) and 3% by wt. of photoinitiator (Lucirin TPO-L). The walls were fabricated using the 80 MHz system and a 0.4 NA microscope objective. An applied power of 10 mW and a scanning speed of 3 mm/min were chosen for fabrication. Five set of walls were fabricated in the liquid resin and the width and height were measured using optical microscopy. The width and height of the fabricated walls represent the radial and axial resolution of the 2PP process respectively. The average width and height of the polymerized walls obtained from the measurements were 1.9 ± 0.22 μm and 20 ± 0.85 μm respectively. Again the mismatch between the radial and axial dimension is attributed to the low NA lens used for the polymerization process.

The simulations were performed to numerically evaluate the width and height of the polymerized voxel based on the experimental process parameters. The simulations present a

width of 2.4 µm and a height of 18.4 µm respectively. The simulated and experimental measurements are reasonably accurate, keeping in mind that the exact values of various material dependent properties are not know. Also, the model does not include the effect of density change and reducing free volume that may have an effect on the simulated results. The model can be used for more accurate prediction by the knowledge of actual values for the material kinetic parameters.

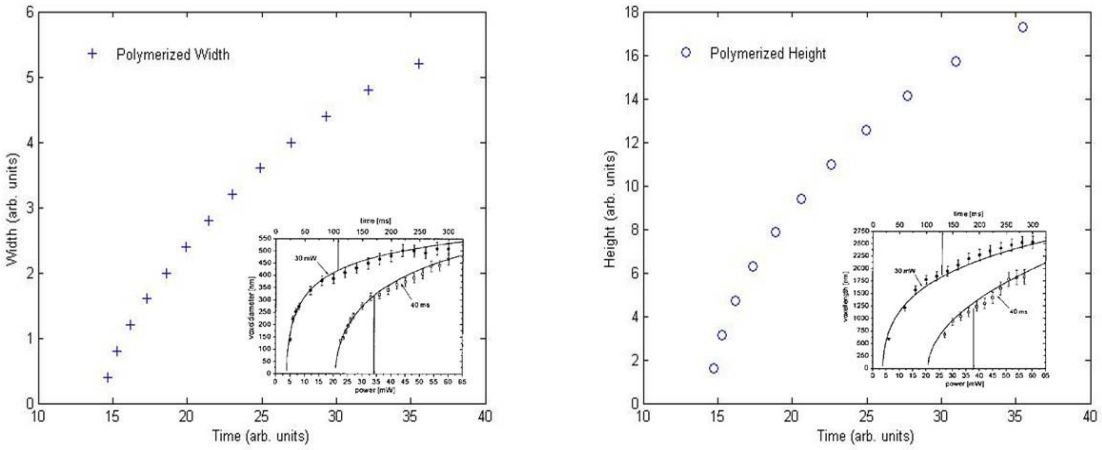

(a) (b)

Figure 4.21 Simulated contrast plots of voxel growth (a) Width contrast plot, and (b) Height contrast plot

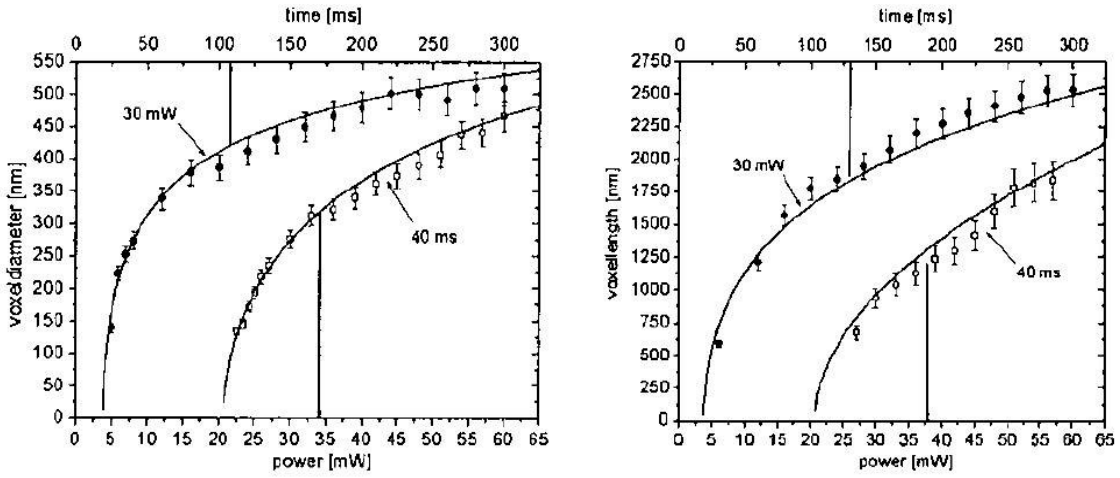

(a) (b)

Figure 4.22 Contrast plots for comparison (a) Width, and (b) Height [21]

4.3 Discussion

The developed model is numerically analyzed to study and understand the role of various mechanisms associated with the 2PP process. The model was effectively used to analyze the role of polymerization kinetics and molecular diffusion along with the effect of their characteristic time scales. The radicals are generated upon photoinitiator decomposition and the temperature of the irradiated volume increases during the irradiation period. No diffusion or polymerization is observed as their onset takes place much later in the dark period. The generated radicals combine with monomer molecules and initiate the chain propagation reaction. The conversion of monomer into high molecular weight polymer takes place with increasing number of pulses. The analysis of 1 kHz repetition rate provides information about the characteristic time scales of diffusion and how the polymerization takes place in the dark period. Diffusion plays a significant role in the replenishment of the decomposed photoinitiator at the focal volume that affect the generation of radicals on subsequent pulses. Surviving radical diffusion also affects the resolution of 2PP process as the propagation of radicals outwards from the focal volume increases the actual polymerized volume. Though, the change in radical concentration also depends upon the termination kinetics and is attributed to three different termination processes: termination by combination, inhibition and trapping. The role of combination and inhibition takes place during the initial polymerization phase where as trapping generally becomes significant after certain degree of polymerization has occurred. The higher conversion ratios result in entangled polymer species and increase the chances of radical trapping. Though, there is no clear time demarcation between the different termination processes.

The role of polymerization kinetics is presented through a comparison between high and low repetition rate systems. The polymerization dynamics of high repetition rate system are different due to the much smaller dark period duration. The effects of diffusion and radical termination are not observed in the dark period because their onset occurs at the microsecond

time duration which is much longer than the dark period time duration. The single pulse analysis of 1 kHz system provides more insight on the polymerization process dynamics not observed with high repetition rate systems due to smaller dark period duration. The presented mathematical model discusses the ultrashort pulsed laser induced polymerization by analyzing the initiation, propagation and termination kinetics as they relate to 2PP. The developed model provides insight to the polymerization process and the understanding of the dynamics at various time scales. The information obtained from the model and subsequent analysis can be used to enhance the understanding about 2PP process and puts a mathematical framework to an experimentally demonstrated and analyzed technique. The model can also be employed for 2PP resolution prediction and evaluating the affect of various applied process parameters.

Single pulse analysis was first employed to understand the dynamics of polymerization reaction for both the 1 kHz and 80 MHz laser system. The radicals are generated by photoinitiator decomposition during irradiation and remain at the focal volume without diffusing away during the irradiation period. Most of the monomer conversion for the 1 kHz laser system occurs in the dark period due to the longer time between pulses compared to MHz pulsing systems. The longer time for the dark period of 1 kHz system provides reaction kinetics to be dominant and lead to a change in system state. Effect of diffusion is also analyzed and it becomes more dominating for smaller spot sizes normally achieved by high N.A. objectives. The resolution of the 2PP process is controlled by the focusing lens, diffusion of molecular species and the termination of radicals in the resin system. The diffusion effect is also important for the replenishment of decomposed photoinitiator, since the generation of radicals with subsequent pulses depends on the available photoinitiator concentration at the irradiated focal volume. The simulation results of 1 kHz laser system provide interesting information about the effect of diffusion and polymerization kinetics mainly due to the longer dark periods. This information is lost while simulating a high repetition rate system because of the much smaller time duration between laser pulses. But multi-pulse simulation of high repetition rate laser

system illustrates the effect of photoinitiator diffusion as the molecules surrounding the irradiated volume try to replenish the lower concentration areas. It was also presented that the spatial concentration gradient in photoinitiator concentration is not significant with increasing number of pulses primarily because of diffusion effects.

The role of temperature on the polymerization process was also captured from the analysis. The temperature of the polymerization system increases during the polymerization process causing an increase in the relative magnitude of diffusion, propagation and termination constants. The temperature sensitivity of the fabrication spatial resolution for 2PP was experimentally demonstrated by Kawata et al [59] where they noticed that a temperature increase causes a decrease contrary to the expected increase of voxel size. This phenomenon can be explained by various radical termination kinetics. The propagation, termination and diffusion constants have an Arrhenius relationship with the temperature and their values increase with temperature. In some monomers like acrylates, the radical termination constant is a couple of orders in magnitude higher than the propagation constant [16, 52]. Also, the temperature effect on propagation constant is smaller compared to the termination constant because of higher activation energy requirement for the former [52]. Thus, with the temperature increase, radical termination dominates the propagation and diffusion kinetics as most of the generated radicals are rapidly terminated. This leads to the achievable smaller spatial resolution or smaller voxel size with increase in temperature as observed by Kawata et al [59].

Multi-pulse analysis of high repetition rate laser system has also provided some interesting insight on the role of various input parameters. The effect of photobleaching was discussed as it leads to the stagnation in conversion ratios. Also, the depletion in photoinitiator at higher power levels can lead to a spatial variation in conversion ratio that can induce nonlinear optical effects. Also the role of inhibitor concentration was discussed as it leads to a higher thresholding effect and subsequent reduction in voxel size. This can be effectively employed to achieve high resolution 2PP process with voxel size much smaller than the

diffraction limit. A comparison was also presented between the simulated results and experimental results obtained from the published literature. The model correctly depicts the growth of voxel and adheres to the inherent nonlinearities and 3D confinement of 2PP process. The accurate depiction of 2PP process by mathematical simulation allows the users to evaluate the role of various process and material dependent parameters on the polymerization process which can not be extracted from the experimental analysis.

CHAPTER 5

SENSITIVITY ANALYSIS AND RESOLUTION PREDICTION

The mathematical analysis presented in chapter 4 aimed at providing an understanding of 2PP dynamics and the effects of various process and material dependent parameters on 2PP process. The developed mathematical model provides the means to understand the role and influence of various process and material dependent parameters on the achievable resolution of 2PP process. However, to further enhance our understanding of 2PP process and to compare the experimental results with the simulations, experiments were performed using the FLM system in our laboratory. The objective of experimental analysis was to evaluate the significance of commonly employed process parameters on the resolution of 2PP process. Fabrication throughput and dimensional control can be significantly improved by having a good understanding on the synergistic effect of common controlled process parameters and their effect on the sensitivity of the process resolution.

The radial and axial sizes of voxel are the critical parameters that affect the resolution of 2PP process. Good control on the radial and axial sizes could be achieved but a thorough understanding of their growth at various process parameter combinations is required. The resolution of 2PP process partially depends on N.A. of objective lens, applied laser power, concentration of photoinitiator and scanning speed of laser pulses; parameters for which the user has complete control. It is generally demonstrated that high resolution 2PP process can be achieved by working with high N.A. lenses and at thresholding conditions. But still, it is not completely understood how the various factors interact with each other in defining the size of polymerized voxel. Experiments were performed to understand how the voxel grows in both radial and axial directions and a discussion on some of the phenomena observed during the

experimental analysis is also presented. Explanations to the observed phenomena are also presented based on the information gained from the mathematical analysis.

All the experiments were performed using the Ti:Sapphire femtosecond laser system discussed in detail in chapter 2. For the experimental analysis, the high repetition rate (80 MHz) laser pulses were used. Three parameters, applied laser power, scanning speed and photoinitiator concentration were chosen and their effect on the size of voxel was analyzed. Applied laser power was considered at six levels (12.5 mW, 16 mW, 20 mW, 25 mW, 35 mW and 50 mW), scanning speed was considered at three levels (1 mm/min, 3 mm/min and 5 mm/min) and photoinitiator concentration was considered at three levels (2.56%, 3.78% and 4.96%). A 0.4 N.A. microscope objective was used for all the experiments. A low N.A. objective has an advantage of much higher available working distance (2-9 mm) and much simpler fabrication process. The choice of objective lens is application specific and it is known that smaller focal volumes can be achieved with higher a N.A. lens [32, 36, 38]. But, the effects of laser power, scanning speed and photoinitiator concentration on the polymerization process require good understanding as different levels of their values may produce entirely different than expected results and make process prediction and control a difficult task. Experiments were performed using SR499 monomer (Sartomer Inc.) and Lucirin TPO L as photoinitiator that undergoes free radical chain polymerization reaction as discussed in chapter 2. Polymerized walls were fabricated in liquid resin by scanning the laser pulses in a predefined pattern and measurements of wall width (thickness) and height were taken using optical microcopy. The width measurement was taken from the walls which were fabricated close to the substrate to avoid any kind of structural deformation that may lead to inaccurate width measurement. For the height measurement, freely floating walls were used that represented the full achievable height based on the process parameter combinations and to avoid any substrate truncation effects. The measured width and height of the polymerized walls represent the radial and axial resolution of the process. Five sets of polymerized walls were fabricated for each process

parameter combination. An example of polymerized wall fabricated at 20 mW average power, 3 mm/min scanning speed and 3.78% photoinitiator concentration that was used for analysis is presented in figure 5.1.

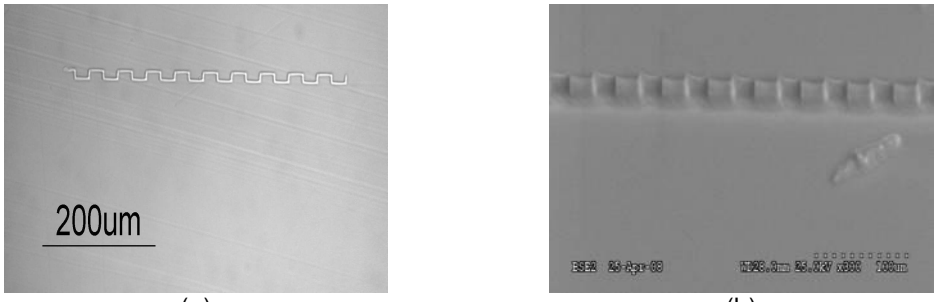

(a) (b)

Figure 5.1 Example of polymerized pattern used for measurements (a) Wall pattern-top view, and (b) SEM image of pattern – scale 100 µm

Lateral and axial polymerization sizes change as functions of various levels of process parameters were measured and are presented in figure 5.2 in the form of contrast plots. Similar contrast plots have been reported by other research groups that depict the effect of laser scanning speed and applied laser power on radial and axial resolution of the process [21, 36, 40]. The radial and axial polymerized size increases with an increase in applied power and decreases with an increase in scanning speed. It has been discussed in the literature that smaller polymerized dimensions can be achieved by a combination of low laser powers, low photoinitiator concentration and high speeds/low exposure time that leads to thresholding conditions [36, 38, 40]. But there is no discussion on how the process resolution changes at various levels of these process parameters and/or with their interactions. Also, these plots do not consider the variance in measurements and are not an efficient way to infer the effect of process parameters. The contrast plots are ideal for understanding the combined general behavior of process parameters on the process resolution but they do not answer all the questions that an experimenter would like to evaluate. Answers to questions that we wanted to extract from the experimental analysis are: How do the speed, power and concentration affect the radial and axial resolution and is their effect at various levels the same? Is there is any

significant interaction between the process parameters and how it affects the process resolution? Which of the analyzed process parameters have the strongest affect and influence on the voxel size? How does the sensitivity of process resolution changes with process parameter combinations and levels? How the lateral and axial resolution of 2PP process can be effectively controlled leading to an efficient fabrication process?

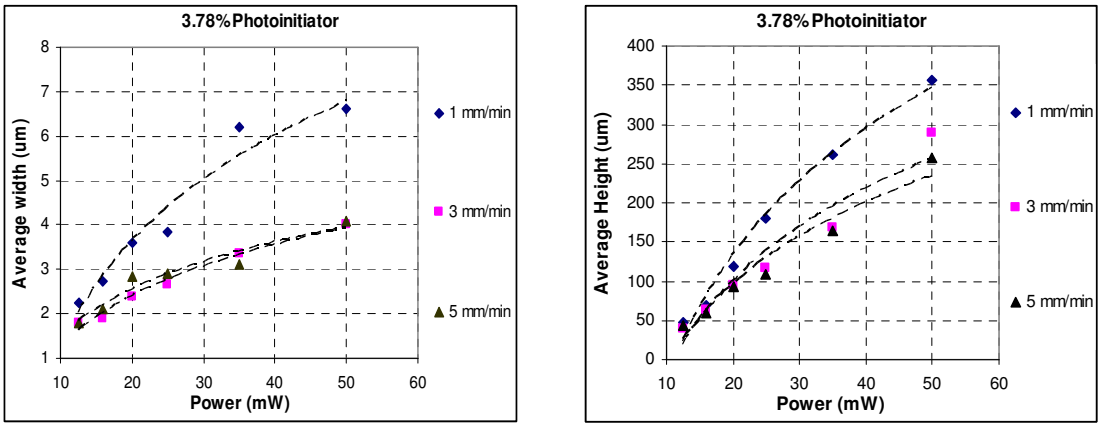

(a) (b)

Figure 5.2 Change in 2PP resolution as a function of Power and Scanning Speed (a) Polymerized width, and (b) Polymerized height

Statistical analysis was performed to understand the effect of the common process parameters in order to achieve good control for the fabrication of micro/nano structures using 2PP process. The statistical approach accommodates for the variance in measurements and unravels hidden information that remains unnoticed from contrast plots like the ones presented in figure 5.2. A design of experiments methodology is adapted to statistically analyze the role of chosen process parameters on the 2PP process resolution. Also, a multiple linear regression approach is used to develop a statistical model that can be employed to predict the radial and axial resolution of 2PP process. The statistical analysis should allow an enhance understanding on the effects of process parameters on the 2PP resolution and should also assist in answering the questions that remain unanswered from the contrast plots.

5.1 Design of Experiments Methodology

A design of experiments approach was utilized to evaluate the effects of process parameters and to identify any significant interactions among these process parameters that have a strong effect on both the radial and axial resolution of 2PP process. A three way complete model was used to evaluate the effect of controlled process parameters on the average width and height values based on the experimentally measured data. The considered statistical model that includes the main effects along with their interactions is presented in equation 1.

$$Y_{ijkt} = \mu + \beta_i + \gamma_j + \omega_k + (\beta\gamma)_{ij} + (\beta\omega)_{ik} + (\gamma\omega)_{jk} + (\beta\gamma\omega)_{ijk} + \varepsilon_{ijkt} \quad (1)$$

Where, Y is the dependent variable (height or width), β is the photoinitiator concentration main effect, γ is the speed main effect, ω is the power main effect, $(\beta\gamma)$, $(\beta\omega)$, $(\gamma\omega)$ and $(\beta\gamma\omega)$ are their interaction terms, and ε is the error term. The levels of these factors and observation number are i, j, k and t respectively. The model has certain assumptions that have to be met in order to provide correct analysis and subsequent estimates. The common model assumptions that have to be verified are fit of the model, test for outliers, normally distributed errors, constant error variance and uncorrelated errors. The proposed model is only valid if there is no deviation from the model assumptions [63, 64]. These assumptions have to be verified before the model can be used for ANOVA and the subsequent analysis. The methodology used to verify these assumptions is presented in section 5.1.1.

5.1.1 Verification of model assumptions:

The verification of model assumptions was performed for the polymerized width and height models. All the assumptions are checked and remedial measures are taken in case of serious departures. The verification and remedial measures in case of departures are an important step in accurate statistical analysis. The model assumes that the errors 'ε_{ijkt}' are independent and normally distributed N(0, σ^2) with zero mean and a constant but unknown

variance σ^2. In some cases, these assumptions do not hold and it is recommended not to infer from the analysis of variance until the validity of all the assumptions have been checked. To verify this, a detailed assumption verification analysis is performed in this section that assures the validity of proposed statistical model for subsequent statistical analysis.

5.1.1.1 Fit of the model and constant error variance assumption

To check the fit of the model and the constant error variance, the standardized residuals were estimated and plotted against the estimated value of the response variable (width and height). The width residuals plots used for the analysis are presented in figure 5.3. The plots from the residual analysis of width model indicated that the fit of model and constant error variance assumptions are satisfied. The plots show no evident pattern and have a random scatter around zero indicating that the fit of model and constant error variance assumption holds for the width model. To remove any subjectivity in residual analysis, modified Levene test was employed to verify the constant error variance assumption. The output of modified Levene test obtained from SPSS is presented in table 5.1 [65]. The modified Levene test accepts the null hypothesis that the errors have constant variance with significance value $\alpha = 0.05$.

Table 5.1 Modified Levene test for width model

Dependent variable: Height			
F-Statistic	Degrees of freedom 1	Degrees of freedom 2	Significance
1.304	53	216	0.097

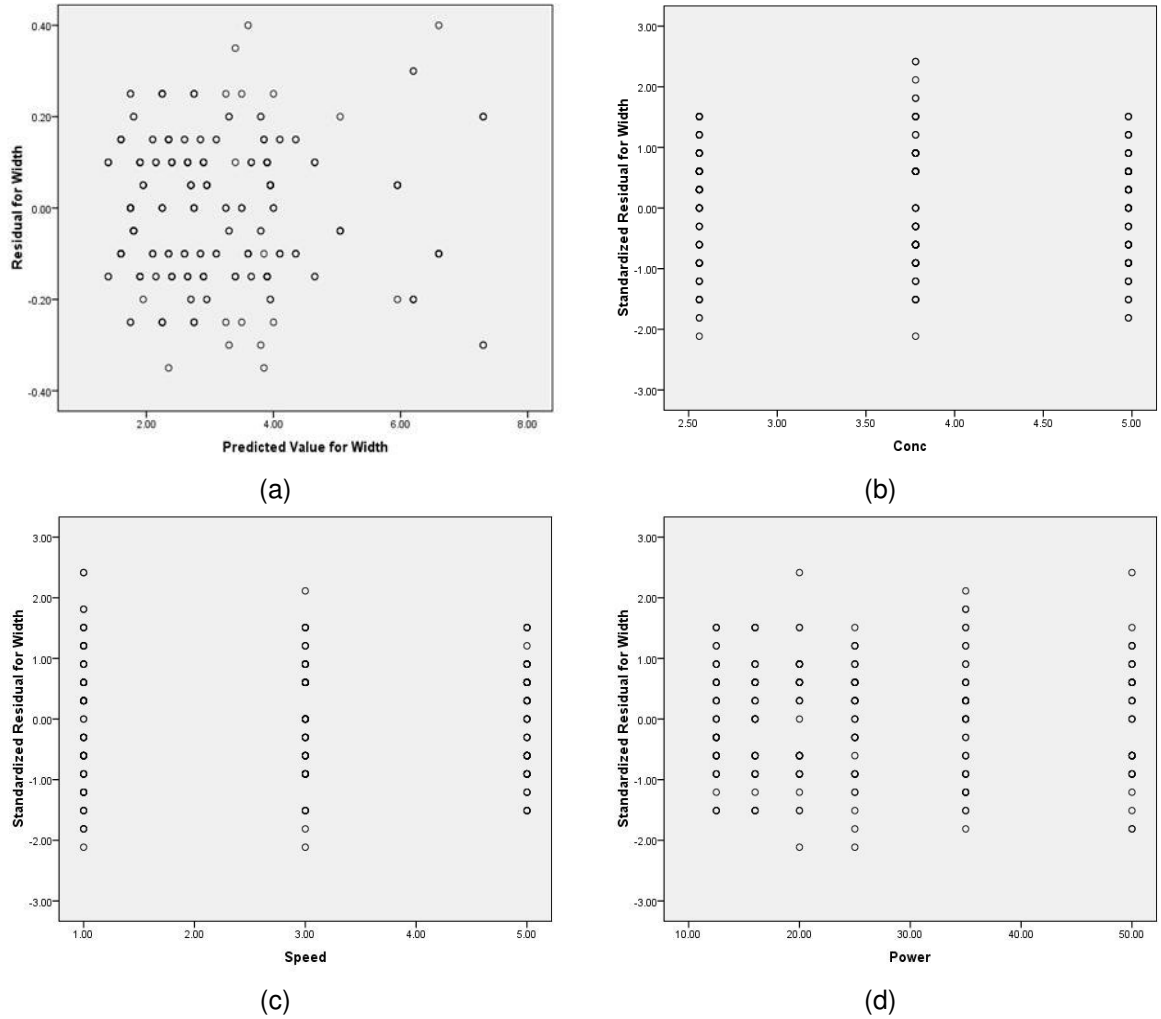

Figure 5.3 Width residual plots for model fit and constant error assumption analysis (a) Residual vs estimated response variable, (b) Photoinitiator residual plot, (c) Speed residual plot, and (d) Power residual plot

Similar residual analysis was also performed for the height model. On exploring the residual plots for height, it was observed that the error variance is not equal across the power and speed dependent variables. The residual plot for power and speed presented in figure 5.4 shows the unequal variance at different factor levels. To verify the results from residual plots and negate any errors due to subjectivity, a test for equality of error variance was formally conducted using the modified Levene test similar to the width model analysis. The null hypothesis (H_o) was checked for the equality of error variance at $\alpha = 0.05$. The modified Levene analysis was obtained from the SPSS output and the p-value is checked at the specified α-level.

The Levene test rejects the null hypothesis and proves that the constant error assumption does not hold for the height model. The SPSS output of the modified Levene test is presented in table 5.2. The modified Levene test along with the residual analysis indicates a departure of error variance for the height model. The ANOVA can not be used for hypothesis testing and subsequent statistical inferences for the height model unless remedial measures are taken.

Table 5.2. Modified Levene test for height model

Dependent variable: Height			
F-Statistic	Degrees of freedom 1	Degrees of freedom 2	Significance
2.038	53	216	0.000

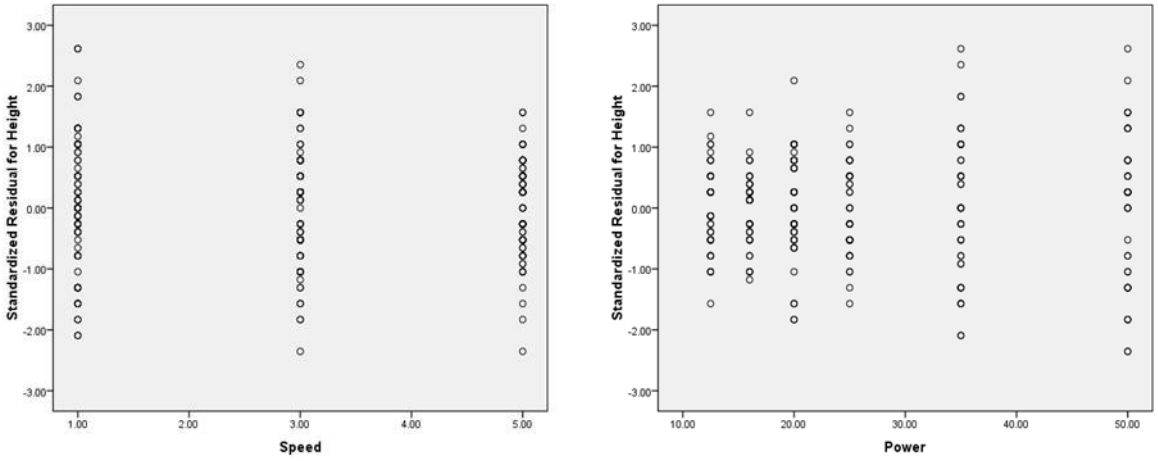

(a) (b)

Figure 5.4 Residual plots for height model (a) Speed, and (b) Power

5.1.1.2 Normally distributed errors

The next assumption verified was the normal distribution of errors. The model assumes that errors have a normal distribution with a zero mean and variance σ^2, N(0, σ^2). The ANOVA and subsequent analysis are based on this assumption and any deviation from it may lead to incorrect analysis. Normal probability plots were employed to check the normally distributed errors assumption for both the width and height models with the results are presented in figure 5.5. The plots do not show any deviation and verify that the errors are normally distributed for both the width and height models.

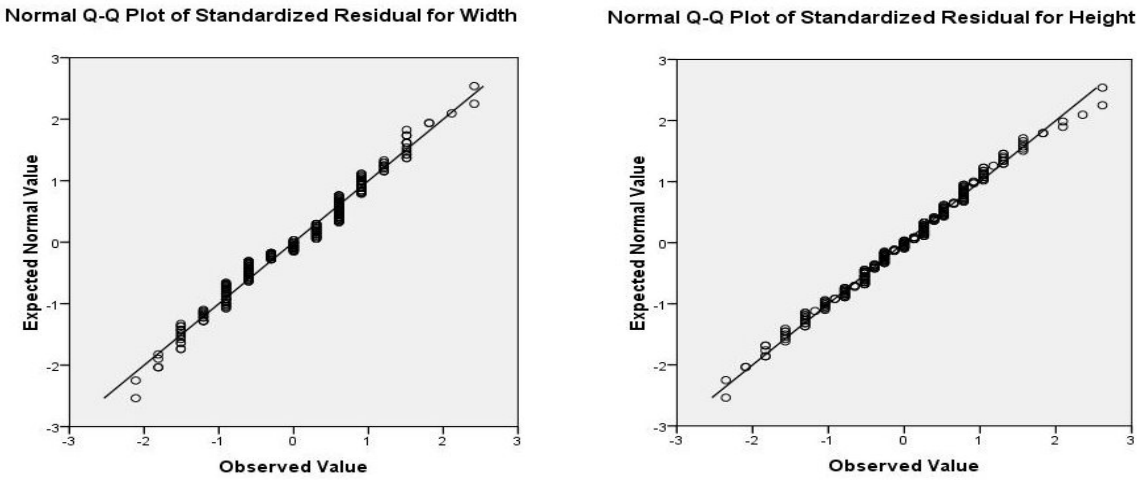

(a) (b)

Figure 5.5 Normal probability plots (a) Width, and (b) Height

5.1.1.3 Outliers detection and uncorrelated errors

The outlier detection was performed by checking the studentized residuals obtained from statistical analysis. The outliers can be easily identified by considering the studentized residuals which are greater than 3. It is generally accepted that 99.7% of the data should fall into ± 3 and residuals which falls outside this band should be considered as outliers [63, 64]. A formal outlier diagnostic test was also performed using the Bonferroni outlier detection scheme [64]. A formal test is conducted by comparing the studentized residuals with the Bonferroni test statistics at an $\alpha = 0.05$. From the analysis, it was verified that there are no outliers for both the width and height data.

The next assumption verified was the uncorrelated errors that checks for any correlation between the collected data. Correlation is not desirable as it violates the independence assumption of error and normally indicates multicollinearity. This is a potentially serious problem and has to be checked as it also leads to incorrect analysis [63, 64]. One way to check for uncorrelated errors is to use time order plots. The residuals and time sequence of collected data are plotted and if a pattern exists, it indicates uncorrelated errors. The time order plots for both the width and height data are presented in figure 5.6. The time order plots indicate that the

residuals do not have any pattern and are randomly scattered around zero. This validates the uncorrelated error assumption for both the width and the height model.

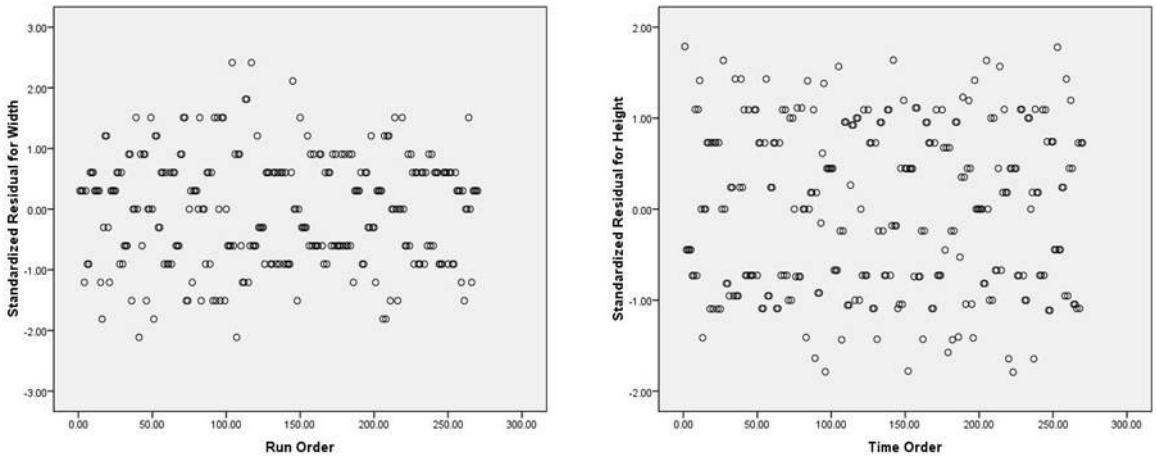

(a) (b)

Figure 5.6 Time order plots for verifying uncorrelated errors (a) Width model, and (b) Height model

The assumptions for the models were verified by the various techniques discussed above. It is concluded that the width model adheres to all the model assumptions and can be used directly for ANOVA interpretation and the subsequent analysis. However, for the height model, all the assumptions are met but for the constant error variance. The non constant error variance is corrected by applying remedial measures to be discussed in section 5.1.3. Once the height model is corrected for constant errors variance, the ANOVA and subsequent analysis can be performed to analyze the effects of process parameters on the polymerized height.

5.1.2 Analysis of polymerized width

Analysis was first performed to understand how the width of a polymerized feature varies with the process parameters combinations. The complete model presented in equation 1 is used to evaluate the significance of interactions between process parameters by using ANOVA analysis. The null hypothesis H_o:{all the treatments have same means} was identified and tested at $\alpha = 0.05$. The effect of chosen process parameters on the width of polymerized structure is analyzed using the calculated ANOVA and is shown in table 5.3. All the interactions

and main effects are statistically significant based on the calculated p-values from the test. Hence, the interactions among various process parameters become important and should be carefully analyzed. The significant interactions among the process parameters make the main effect analysis redundant and it will not be discussed in the presented analysis.

Table 5.3. The ANOVA table for Width

Source	Type III Sum of Squares	Df	Mean Square	F	Sig.
Model	3135.763	54	58.070	2.117E3	.000
Conc	18.867	2	9.433	343.899	.000
Speed	98.185	2	49.092	1.790E3	.000
Power	272.097	5	54.419	1.984E3	.000
Conc * Speed	10.140	4	2.535	92.418	.000
Conc * Power	4.339	10	.434	15.818	.000
Speed * Power	24.754	10	2.475	90.243	.000
Conc * Speed * Power	14.113	20	.706	25.724	.000
Error	5.925	216	.027		
Total	3141.688	270			

It is important to correctly understand the interactions among process parameters and how they affect the process resolution. It is evident from the analysis of variance that there are strong interactions among different process parameters. With the presence of interactions, the effect of a process parameter on the 2PP resolution may change significantly with the variation in the levels of other parameters. The contrast plots presented in figure 5.2 cannot effectively depict the role of interactions and specific interaction plots are required to understand the effect of interactions among process parameters on the 2PP resolution. The variation in average polymerization width for different treatments obtained from the complete model was analyzed with the help of interaction plots and multiple comparisons approach. The interaction plots were first used to visualize and understand the significant trends for various treatments. The interaction plots for the polymerized width for all the levels of speed, power and photoinitiator concentration are presented in figure 5.7.

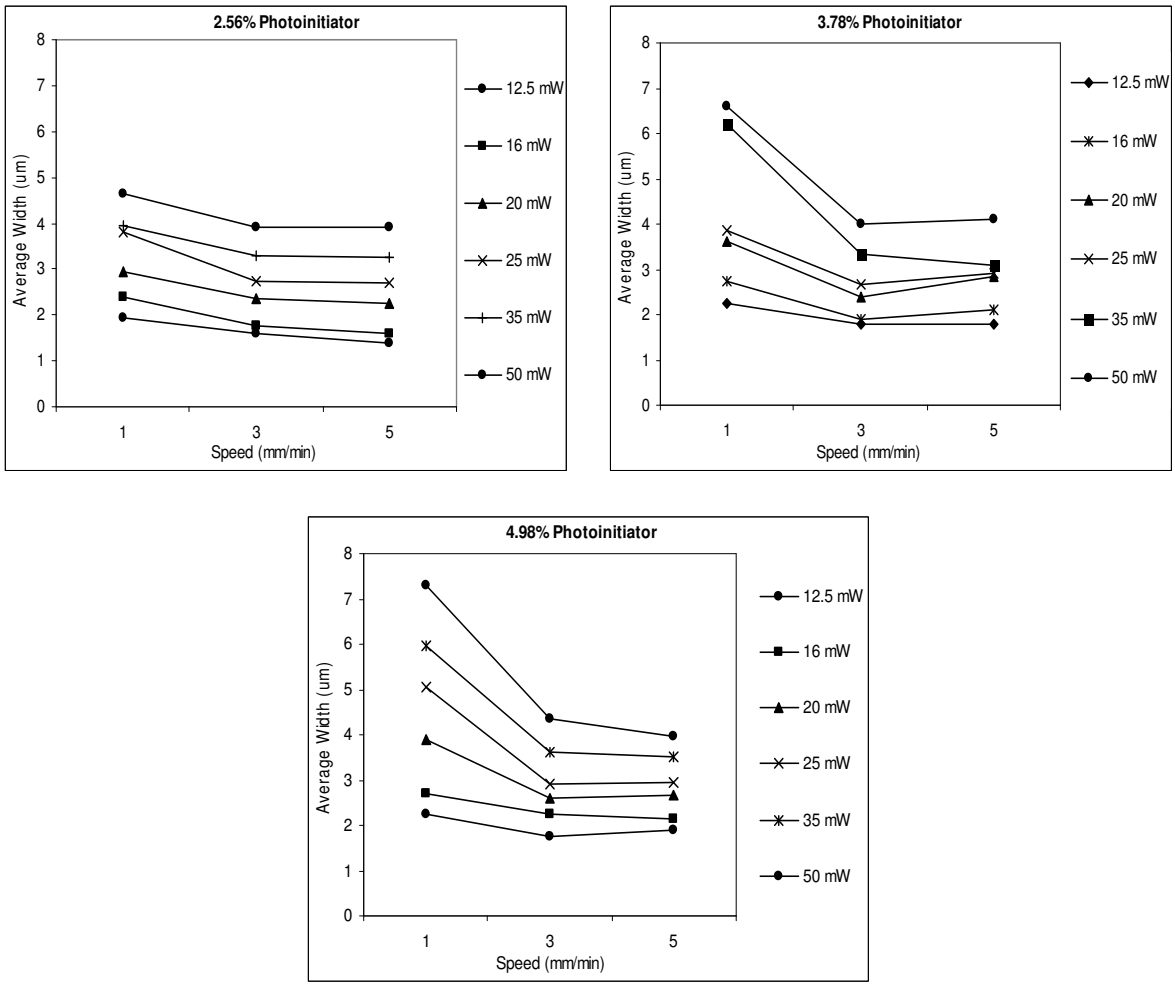

Figure 5.7 Interaction plots for polymerized width

The non-parallelity between the lines indicates interaction among various levels of process parameters. The interaction plots indicate that there is a significant decrease in polymerization width when the speed increases from 1 mm/min to 3 mm/min but the polymerized width does not change significantly when the speed increases from 3 mm/min to 5 mm/min. It is also observed that the polymerized width decreases when the speed increases from 1 mm/min to 3 mm/min while working at high powers (35 mW and 50 mW). The reduction is more significant at these high powers when the photoinitiator concentration is at high levels (3.78% and 4.96%). This indicates that the polymerization reaction is more sensitive to change in speed/time of exposure for higher powers at higher photoinitiator concentration levels. Also,

on analyzing the effect of various power levels it was observed that an increase in power causes an increase in width size for most levels of speed and photoinitiator concentration. The amount of increase in polymerized width though varies for different levels of process parameters combinations. As discussed, the width of the polymerized structure increases significantly while working at higher power levels with slower speeds and high photoinitiator concentration. But, the effect of power on the average increase is gradual and consistent while working at higher speed levels (3 mm/min, 5 mm/min).

The interaction plots are extremely helpful for quick analysis and interpretation of the effects of various parameters on the response, but they do not provide any indication on the size of experimental error or data variance. Depending upon the magnitude of error variance, the evident interactions might become statistically insignificant. A detailed analysis on the difference of treatment means should also be obtained through multiple comparisons. The obtained confidence intervals through multiple comparisons consider the standard error in treatment means and provide the intervals with defined confidence level.

The multiple comparisons for treatment means are obtained using the Tukey method for all multiple comparisons between different treatments and the confidence intervals are estimated by equation 2 [63].

$$\sum\sum\sum c_{ijk}\tau_{ijk} \in \left(\sum\sum\sum c_{ijk}\,\bar{y}_{ijk.} \pm w_t\sqrt{msE\left(\sum\sum\sum c_{ijk}^2 / r\right)}\right) \qquad (2)$$

Where w_t is the Tukey coefficient ($w_t = \frac{1}{\sqrt{2}} q_{v,n-v,\alpha}$), c is the contrast coefficients, τ is the treatment mean, $\bar{y}$ is treatment estimated mean, *msE* is mean square error, and *r* is the number of replications. Tukey method is ideal when the number of multiple comparisons is large. Multiple comparisons can also be obtained using the Scheffé method but the confidence intervals are wider because of large number of comparisons [63]. The wider confidence interval might not capture some statistically significant differences. A quick way of analyzing the

difference in treatment means is comparing the minimum significant difference (*msd*) with the least square estimators. The *msd* is calculated by multiplying the Tukey coefficient and the estimated standard error ($msd = w_s \sqrt{msE\left(\sum\sum\sum c_{ijk}^2 / r\right)}$). If $\left|\sum\sum\sum c_{ijk}\, \bar{y}_{ijk.}\right|$ is smaller than *msd* or the confidence intervals includes zero, then the difference in treatment means is insignificant. Multiple comparisons for all the treatments were evaluated at α = 0.05 with some of the comparisons presented in table 5.4. The remaining comparisons are not shown because of space limitation but rest assured they were carefully studied and analyzed for treatment effects on the polymerized width.

Table 5.4 Multiple comparison for treatment differences using Tukey method

Treatment mean τ_{ijk}: where *i* = three levels of speed, *j* = six levels of power and *k* = three levels of concentration				
Difference in Treatments	Msd	Least Square Estimator	95% Confidence Interval from Tukey comparison	Significant
$\tau_{111} - \tau_{211}$	0.4251	0.35	(-0.07, 0.77)	No
$\tau_{211} - \tau_{311}$	0.4251	0.20	(-0.22, 0.62)	No
$\tau_{232} - \tau_{332}$	0.4251	0.45	(0.03, 0.87)	Yes
$\tau_{321} - \tau_{323}$	0.4251	-0.55	(-0.97, -0.12)	Yes
$\tau_{113} - \tau_{133}$	0.4251	-1.55	(-1.97, -1.12)	Yes

The important results from the multiple comparisons for difference in treatment provide an insight into the effect of process parameters and their levels on the polymerized width. The increase in speed from 1 mm/min to 3 mm/min at all the power levels for high (3.78% and 4.98%) photoinitiator concentration causes a drop in polymerized width. A similar behavior was also evaluated at 2.56% photoinitiator concentration but with one insignificant difference, where no change in width size was evaluated for 12.5 mW at 2.56% photoinitiator concentration ($\tau_{111} - \tau_{211}$) as presented in table 5.4. Increase in speed from 3mm/min to 5 mm/min for all photoinitiator concentrations and almost all power levels indicate no statistically significant change in polymerized width. Only one treatment combination ($\tau_{232} - \tau_{332}$) out of 18 total combinations shows a deviation from the trend, as the 95% Tukey confidence interval indicates statistically significant difference as presented in table 5.4. However, the *msd* value is close to

least square estimate indicating that the deviation may be attributed to experimental error in measurement.

The effect of various levels of power on the size of polymerized width is also analyzed using the multiple comparisons approach. The interaction plots indicate that the size of polymerized width increases with an increase in power but they do not indicate if the increase is statistically significant. From the Tukey multiple comparison analysis, it is evaluated that the low powers (12.5 mW and 16 mW) at high speed levels (3 mm/min and 5mm/min) have no significant effect on the average change in polymerized width size for all the levels of photoinitiator concentration. Hence, the power levels in this range can be used at high speeds and any studied levels of photoinitiator concentration without affecting the lateral resolution of the process. However, the difference in the size of polymerization width is statistically significant for all the power levels greater than 20 mW and their combination with different levels of speed and photoinitiator concentration.

The multiple comparison on the difference in photoinitiator concentration levels and their combination with other factor levels also produced interesting results. In general, at slower speeds and power levels greater than 16 mW, the polymerized width size increases with an increase in photoinitiator concentration from 2.56% to 3.78%. The same trend was also observed for the photoinitiator concentration increase from 3.78% to 4.98%. But, increasing the photoinitiator concentration does not necessarily translate into larger polymerized width sizes. As previously indicated from interaction plots, the change in average width with an increase in photoinitiator concentration at speed levels of 3 mm/min and 5 mm/min for all power levels is statistically insignificant. This again confirms that at high speeds/less exposure time does not cause any significant increase in polymerized width at all the studied power and photoinitiator concentration levels. But, the difference in treatment means of polymerized width was evident at the slower speed of 1mm/min.

From the analysis it is evaluated that the lateral resolution is more sensitive to the applied laser power as compared to speed and photoinitiator concentration. Also, speed/exposure time has a stronger affect on the lateral resolution when compared to photoinitiator concentration. Better improved lateral resolution can be achieved at low power levels with high scanning speeds and at any studied photoinitiator concentration levels. Slower speeds do cause an increase in polymerized width but working at higher speeds with any photoinitiator concentration does not have any adverse affect on the process resolution. This provides flexibility in the choice of photoinitiator concentration for higher speed levels and provides for one less parameter to worry about while designing the fabrication process.

5.1.3 Analysis of polymerized height

As evaluated from the model assumption verification analysis, the model for the polymerized height does not have a constant error variance and is more likely to make a type I error. Therefore, a remedial measure has to be performed for the departure from ANOVA model. As the error terms are normally distributed (Figure 5.4), the standard remedial measure is to evaluate transformations that can lead to equality of error variance. The common transformations that can be used based on the relationship between the estimated means and variance are presented in table 5.5 [64].

Table 5.5 Transformation to rectify unequal error variance

$\mu \approx \sigma^2$	$y' = \sqrt{y}$
$\mu \approx \sigma$	$y' = \log(y)$
$\mu^2 \approx \sigma$	$y' = 1/y$

The transformations were evaluated but proved ineffective in treating the non-constant error variance. The model still cannot be employed for ANOVA analysis indicating that some other remedial measure has to be performed as the errors have serious departures. The other treatment is to use the Weighted Least Squares (WLS) for ANOVA analysis and use an approximate method for multiple comparisons. For WLS, the sample variance (s^2_{ijk}) was first

estimated for all the treatments before defining the weights. The weight for the *ijk* treatment and *t* case was defined as: $w_{ijkt} = 1/s^2_{ijk}$. The analysis was performed on the WLS data and residual plots were generated to again verify the error variance conditions as shown in figure 5.8. The residual plots verify that WLS was effective in treating non-constant error variance. To further verify and avoid any errors due to subjectivity, the modified Levene test was performed to verify the constant error variance and its SPSS output is presented in table 5.6. The modified Levene test accepts the null hypothesis and proves that the constant error assumption holds. Similar to polymerized width analysis, the ANOVA from the weighted data was evaluated and concluded that the treatment means are different and all the interactions are statistically significant.

Similar to the width model, the interaction plots were formed to understand the effect of various process parameter combinations on the polymerized height and are presented in figure 5.9. The interaction plots suggest that unlike width, the height is very sensitive to changes in process parameters. It was also concluded that the polymerized height changes very significantly with all increasing power levels. Unlike width, the polymerized height is affected by the change in photoinitiator concentration and also by high scanning speed conditions. To further analyze and extract more information from the analysis, Satterthwaite's approximation method is employed to conduct multiple comparisons.

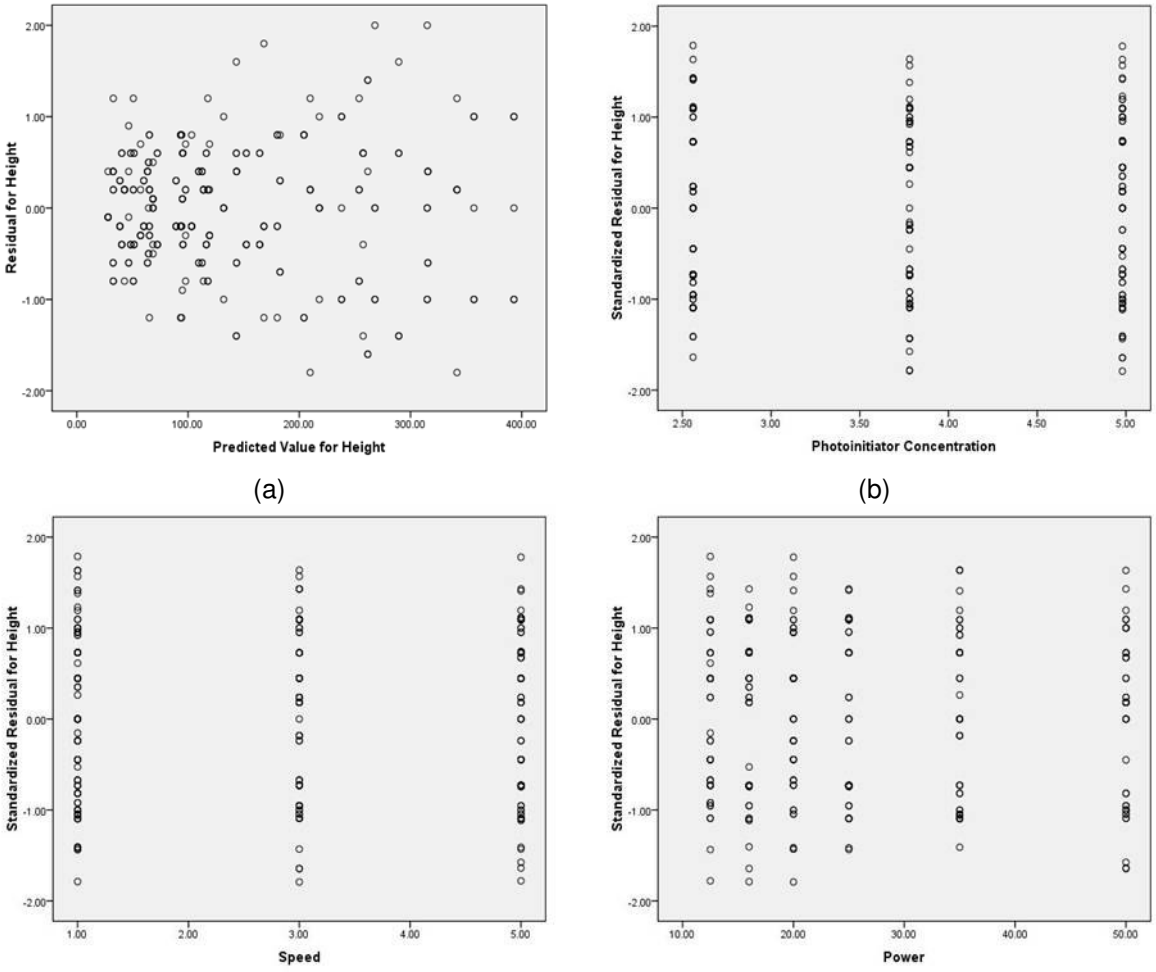

Figure 5.8 Residuals plots for WLS height data (a) Predicted vs residuals for height, (b) residual plot for photoinitiator concentration, (c) residual plot for scanning speed, and (d) residual plot for applied power

Table 5.6 Modified Levene test on WLS height data

Dependent variable: Height			
F-Statistic	Degrees of freedom 1	Degrees of freedom 2	Significance
0.197	53	216	1.000

Table 5.7 ANOVA for height model using WLS data

Source	Type III Sum of Squares	Df	Mean Square	F	Sig.
Corrected Model	4.651E6	53	87763.829	8.794E4	.000
Conc	316902.324	2	158451.162	1.588E5	.000
Speed	171784.763	2	85892.382	8.606E4	.000
Power	2872143.250	5	574428.650	5.756E5	.000
Conc * Speed	30101.625	4	7525.406	7.540E3	.000
Conc * Power	53338.215	10	5333.822	5.344E3	.000
Speed * Power	115877.323	10	11587.732	1.161E4	.000
Conc * Speed * Power	16462.548	20	823.127	824.764	.000
Error	215.571	216	.998		
Total	1.335E7	270			
Corrected Total	4651698.499	269			

As the height model does not have constant error variance, common multiple comparison methods can not be directly employed for treatment comparisons. Satterthwaite's approximation method is employed to conduct multiple comparisons on the different process parameter effects on polymerized height. The statistically significant interactions were checked by forming the confidence intervals similar to the polymerized width analysis. But because of non constant variance, the intervals can not be formed directly from the *msE* and w_t. The confidence intervals were formed by using the Satterthwaite's approximation method to accommodate for the non constant error variance. The Satterthwaite's approximate confidence intervals were used for the multiple comparisons and for evaluating the statistically significant difference in treatments and some of the confidence intervals are presented in table 5.8.

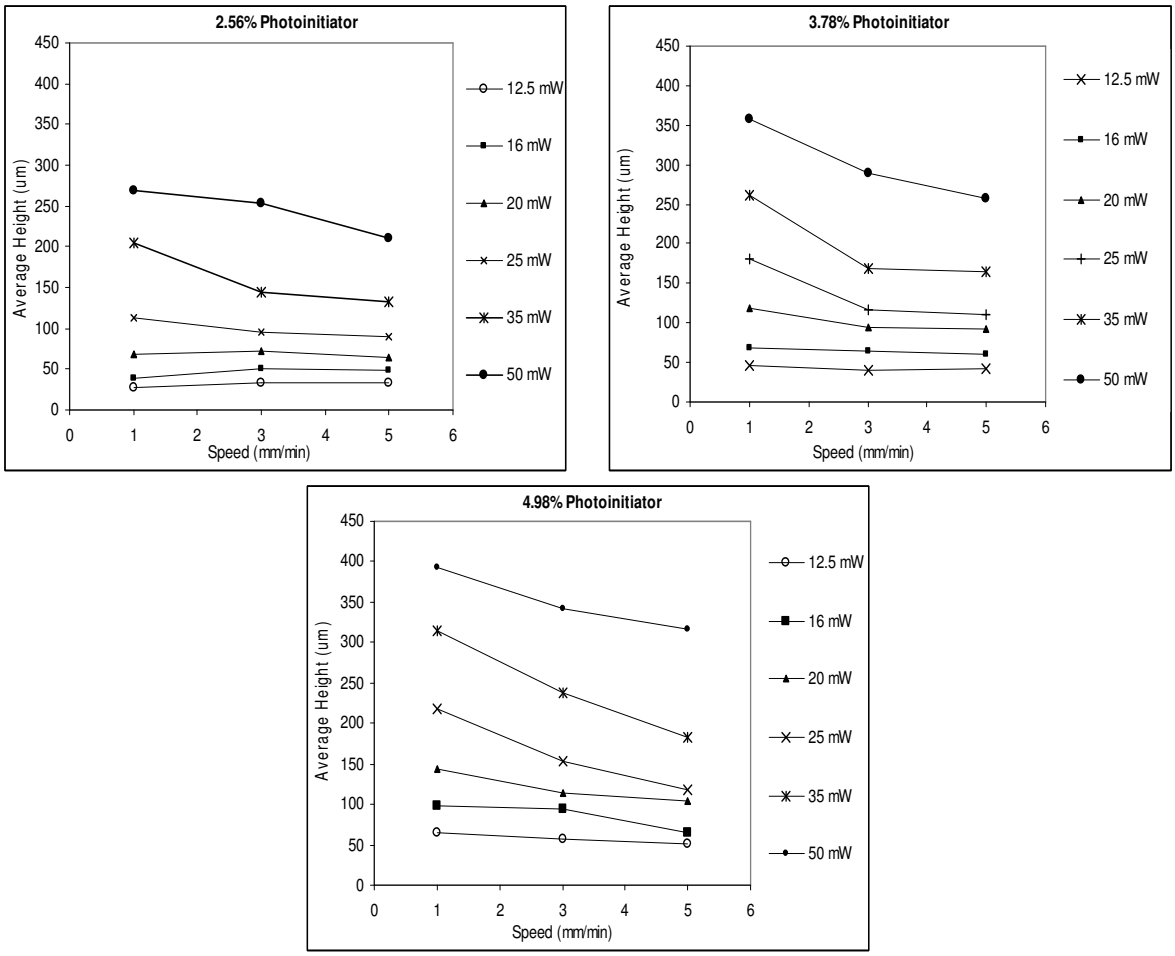

Figure 5.9 Interaction plots for polymerized height

Table 5.8 Satterthwaite's confidence intervals for height

Treatment mean τ_{ijk}: where i = three levels of speed, j = six levels of power and k = three levels of concentration				
Difference in Treatments	Msd	Least Square Estimator	95% Confidence Interval from Satterthwaite's Approximation	Significant
$\tau_{111} - \tau_{211}$	2.681	-4.70	(-7.38, -2.02)	Yes
$\tau_{211} - \tau_{311}$	2.687	0.20	(-2.49, 2.89)	No
$\tau_{221} - \tau_{321}$	2.687	2.40	(-0.29, 5.09)	No
$\tau_{121} - \tau_{131}$	1.148	-29.80	(-30.95, -28.65)	Yes
$\tau_{141} - \tau_{151}$	3.493	-91.60	(-95.09, -88.11)	Yes

The effect of various treatment combinations on the difference in treatment means for polymerized height is studied using the confidence intervals. It is evaluated that the axial resolution is very sensitive to changes in process parameter levels. The change in

concentration at constant speed and power levels has statistically significant difference on the polymerized height for all the combinations. The same is true for the change in power at constant speed and concentration levels. The smallest polymerized height can be achieved at high speeds and low power and concentration levels. The axial resolution of the process does not changes significantly only at high speeds (3 mm/min and 5 mm/min) with powers below 16 mW and 2.56% photoinitiator concentration. All other treatment differences are statistically significant and lead to a change in polymerized height at various factor level combinations. In general, the change in speed from 3 mm/min to 5 mm/min for powers less than 20 mW causes a smaller change in average polymerized height as compared to the change from 1 mm/min to 3 mm/min. The effect of speed on axial resolution is similar to that evaluated from lateral resolution analysis but only at low powers. However, unlike lateral resolution, the variation in process parameters does produce statistical significant changes on the axial resolution. Therefore, it is concluded that the height is more sensitive to variations in controlled process parameters as compared to polymerized width. Care should be taken in defining the process parameters for 2PP considering how these parameters effect polymerized width and height and hence the resolution of process and size of polymerized features.

5.2 Prediction model for 2PP resolution

Multiple linear regression analysis was performed to develop a predictive statistical model that includes the effect of considered process parameters on the polymerized width and height. The regression analysis was performed on the independent factors, their interactions and their higher order terms. The complete model considering all the possible interactions and second and third order terms was set to predict the response variable. The model was completely analyzed to exclude factors which are not statistically important based on the F-statistic from ANOVA model [63]. The logarithmic transformation of the response variable and applied power was performed to obtain a good fit of the model with smaller and independent residuals. The model assumptions were verified for the regression model and the procedure

was similar to that discussed for the three way complete model used for factorial analysis. The analysis of residuals was instrumental to verify the constant variance assumption and fit of model. Normal probability plots were employed to verify the normal distribution of errors. The analysis verified that all the model assumptions are met and the model includes only those terms which have a statistically significant effect on the response variable. The evaluated model for the prediction of polymerized width (W) and height (H) as a function of photoinitiator concentration (C), speed (S) and power (P) are presented in equation 3 and 4 respectively.

$$Ln(W) = -2.036 + 0.217 * C - 0.155 * S + 0.948 * Ln(P) - 0.013 * C * S....$$

$$....-0.001 * S * P + 0.00014P^2 - 0.002C^3 + 0.005S^3 \quad (3)$$

$$Ln(H) = -2.951 + 0.633 * C + 0.152 * S + 2.024 * Ln(P) - 0.053 * C * S....$$

$$....-0.005 * C * P - 0.005 * S * P - 0.027 * C^2 + 0.001 * S^3 + 0.001 * C * S * P \quad (4)$$

From the regression analysis, the effect of various process parameters on the response variable was also studied using the Added Variable Plots (AVP) [66]. In multiple regression, the coefficients do not always interpret the effect of a certain predictor on the response variable. But, AVP's provides an experimenter an efficient way to evaluate the effect of each predictor and how it changes or affects the response variable. It was evaluated from the AVP's that applied power has a stronger effect on polymerized width and height when compared with speed and photoinitiator concentration. The AVP's for the logarithm of width and height are shown in figure 5.10. These AVP's also verify the design of experiment analysis that showed the dominance of applied power over other process parameters on the change in polymerized width and height.

The developed regression model was used to predict the polymerized width and height by using process parameter values within the analysis domain. Experiments were performed to validate the regression model and to evaluate its predictive accuracy. Four different combinations of process parameters were selected and used to fabricate walls in the polymer

resin. The measurements for width and height were performed similar to the experiments for data analysis as discussed in section 2. The estimated values of width and height from the regression model and their comparison with the experimental values are presented in table 5.9. The statistical model is able to predict the lateral and axial resolution of polymerized structures with good accuracy. The maximum percentage difference between the predicted results for width and height are 5.14 % and 4.36% respectively. This small deviation can be easily accommodated in the actual fabrication process.

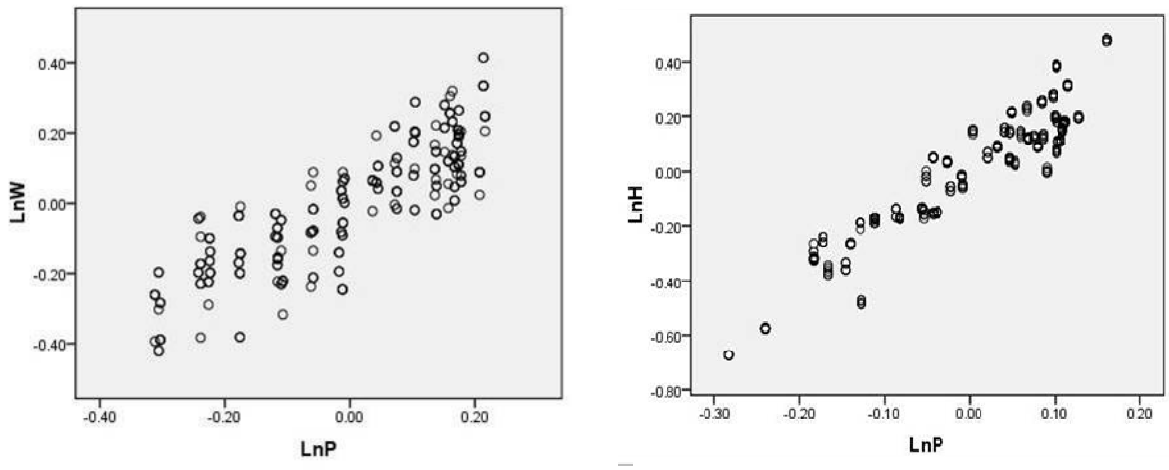

(a) (b)

Figure 5.10 Added variable plots (a) Polymerized width, and (b) Polymerized height

Table 5.9 Comparison between predicted and experimental process resolution

Width					
Conc. (% wt.)	Speed (mm/min)	Power (mW)	Estimated (µm)	Experimental (µm)	% Difference
3.78	2.0	17.0	2.72	2.80	2.86
2.56	2.5	15.0	1.92	1.95	1.54
2.56	3.0	13.5	1.66	1.75	5.14
3.78	4.0	22.0	2.97	2.85	-4.21
Height					
3.78	2.0	17.0	76.62	75.60	-1.35
2.56	2.5	15.0	42.37	40.60	-4.36
2.56	3.0	13.5	35.33	36.33	2.75
3.78	4.0	22.0	105.60	103.00	-2.52

5.3 Parameter identification and 3D microfabrication

The statistical analysis of the experimental data helped in evaluating the effect of applied laser power, scanning speed and photoinitiator concentration on the resolution of 2PP process. In general, increase in power causes an increase in lateral and axial polymerization size. But, the lateral resolution does not change significantly at low power levels with a combination of high scanning speeds and all studied photoinitiator concentration levels. As already discussed in chapters 3 and 4, the two photon polymerization is governed by free radical chain reaction where radicals are needed to initiate the reaction [16]. The generation of these active radicals depends on the square of applied laser power, scanning speed/exposure time and photoinitiator concentration. The insignificant change in the lateral resolution at low powers and high speeds irrespective of photoinitiator concentration is attributed to the generation of few radicals. The radicals terminate by combination or by reacting with present inhibitor molecules in the resin system before any significant polymerization or diffusion can occur. Hence the polymerization takes place only in and around the spot that has high energies capable of producing enough radicals that can withstand the termination mechanisms. Also, the applied laser intensity drops very quickly along the radial direction because of the Gaussian intensity distribution and thus limits the effect of lower powers on the change in radial resolution. On the other hand, the axial resolution is more sensitive to power variation because of the intensity distribution mismatch for a Gaussian beam and the guiding of laser pulses along the optical axis [37, 40, 67].

The variation in polymerized width and height at different power levels can also be attributed to the thresholding effect because of the Gaussian intensity distribution of laser pulses. Increase in power produces a larger volume that exceeds the power required to initiate the reaction and hence translating into a bigger lateral and axial dimensions. But at low photoinitiator concentrations with low powers and high scanning speeds, the change in axial resolution is statistically insignificant and is attributed to the thresholding effect and lower radical

generation. Also, high speed/low exposure levels do not produce high number of radicals thus limiting the polymerization reaction along the optical axis. But, increases in power and photoinitiator concentration levels while working at slower speeds generates enough radicals and radical diffusion can be significant thus causing the increase in polymerized volume and significant differences among various treatment levels.

The experimental analysis indicates that there is a rapid growth of polymerized height compared to the width. The size of polymerized features increases very strongly along the optical axis compared to the radial direction as it was also obtained from the mathematical analysis. The time exposure contrast plots obtained from the mathematical simulations are presented in figure 5.11(a). One reason of such behavior is the intensity distribution mismatch in the axial and lateral directions. A typical Gaussian intensity distribution is presented in figure 5.11(b). The axial intensity distribution of laser beam has wider heavy tailed profile causing the initiation of radicals in a much wider region at higher intensity values. This causes a rapid increase in polymerization reaction along the axial direction and leads to faster growth of polymerized height compared to the width. This behavior becomes more and more pronounced while working at higher powers or at a longer exposure setting which is evident from the figure 5.11(a).

Another interesting result from the experimental analysis is the significant change in polymerized height at higher power levels. The axial size of a polymerized feature increases significantly while working at 35 mW and 50 mW power levels for all the speed and photoinitiator concentrations. There are a couple of reasons that can explain this behavior. One explanation can be attributed to the heavy tailed Gaussian intensity distribution of the laser beam. Another reason is the depletion of photoinitiator that takes place at high power levels as it was also predicted by the mathematical model. Because of higher intensities produced at higher power, the photoinitiator decomposes very early into the reaction as presented in figure 5.12 (a). As the laser has a Gaussian intensity distribution, the depletion is more pronounced

along the optical center compared to the regions away from it. The depletion of photoinitiator produces a gradient in achievable conversion ratios as presented in figure 5.12(b). This gradient produces a variation in the refractive index of the polymerized volume, where higher conversion ratios produce higher contrast in the refractive index. The refractive index gradient acts as a low NA lens and trap the beam along the optical axis. Hence, the created voxel has a longer height compared to the width as was also evaluated from the experimental analysis.

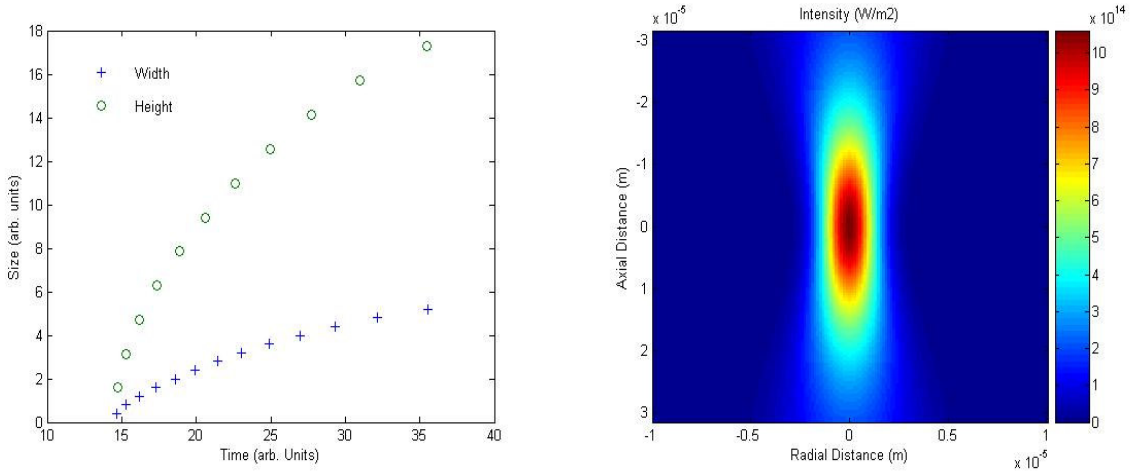

(a) (b)

Figure 5.11 Growth of polymerized width and height (a) Comparison between width and height, and (b) Gaussian intensity distribution

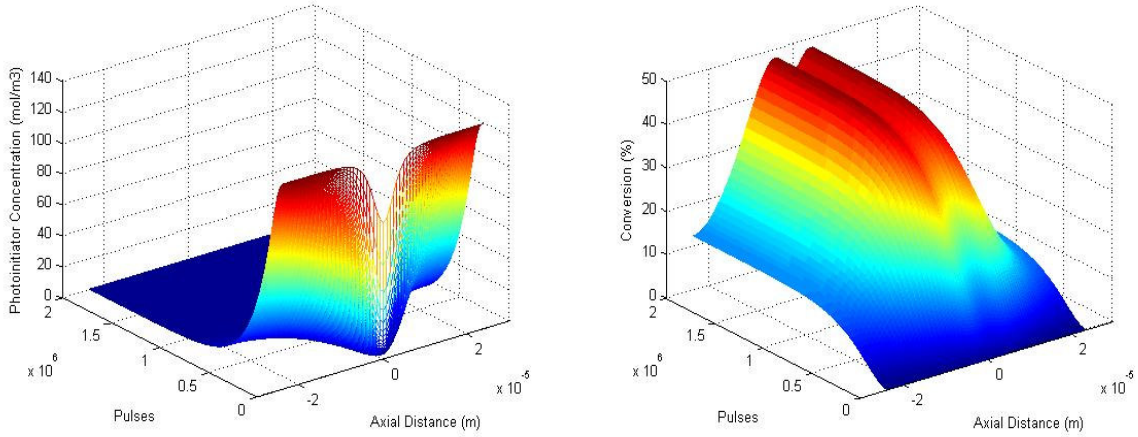

(a) (b)

Figure 5.12 Conversion ratio gradients due to photobleaching (a) Photoinitiator depletion, and (b) Conversion ratio

It is understood that the polymerization in axial direction controls the resolution of 2PP process. The radial resolution can be easily controlled by using combinations of low power levels and high speeds at any photoinitiator concentration level considered in the experimental domain. The process resolution is more sensitive to power variation than speed or photoinitiator concentration. Though slow speed (1mm/min) has strong effect, insignificant or small changes in polymerized resolution are obtained at higher speed levels. The effect of the process parameters studied on the 2PP process resolution cannot be easily predicted without the presented statistical analysis.

Another important aspect of this analysis is that it unravels the coupling effect between the process parameters on 2PP resolution. Increase in power alone has completely different effect at various speed and photoinitiator concentration levels. The same is true for speed and photoinitiator concentration. The significant interactions were first predicted by ANOVA analysis and later on carefully studied using the multiple comparison approach. Change in a process parameter level does not always result in the change of output. As discussed earlier, low power levels (12.5 mW – 16 mW) at slow speed with 3.78% and 4.96% photoinitiator concentration results in an increase in polymerized width. But the same power levels at the considered photoinitiator concentrations do not have a statistical significant effect at higher speeds. The interactions among various process parameter levels have a synergistic effect and should be well understood. The statistical analysis presents the role of each process parameter and how the interactions affect the lateral and axial resolution of 2PP process. The interaction effects can be advantageously employed to control the resolution and increasing the overall throughput for this process.

The presented analysis evaluates the combined effect of scanning speed, applied power and photoinitiator concentration levels on the process resolution. The control of lateral or axial resolution can also be application specific. In certain micro/nano fabrication requirements, controlling the lateral resolution might be more important than axial resolution. For example, in

fabricating a diffraction grating the spacing between the lines and the thickness of the lines has to be fully controlled and characterized. The produced diffraction patterns are very sensitive to the spacing between the lines. The axial resolution is not very important as truncation of axial dimension will be caused by substrate. Therefore, low power levels with high speeds at any of the analyzed photoinitiator concentration levels are recommended for the fabrication of diffraction grating. High speeds reduce the fabrication process time and lower power levels gives the smaller line widths. A diffraction grating presented in figure 5.13(a) was fabricated at 12.5 mW average power, 5 mm/min scanning speed and 3.78% photoinitiator concentration.

The axial resolution though is very important for true 3D micro/nano structures. A microbridge, an example of 3D microstructure, is presented in figure 5.13(b). This microbridge is build layer by layer, hence the knowledge of axial resolution is very important. Minimum resolution can be obtained by using low powers and high speeds but only at low photoinitiator concentrations. A prism grating array was also fabricated and is presented in figure 5.13(c) and 5.13(d). Higher power levels were used as high aspect ratio was needed to reduce the fabrication time. The processing parameters used for the microstructure fabrication are summarized in table 5.10. The understanding on how these common process parameters and their interactions behave at various levels can be advantageously employed in defining a robust and controlled 2PP process. The information obtained through statistical analysis and the regression model was used in defining the process parameters for the microstructures shown in figure 5.13. The fabricated structures have good dimensional control when compared to the originally designed dimensions and they demonstrate the achievable three dimensionality of the 2PP process.

Table 5.10 Process parameters employed for microfabrication

	Applied power (mW)	Scanning speed (mm/min)	Photoinitiator concentration (%)
Diffraction grating	12.5	5	3.78
Microbridge	15	3	2.56
Prism grating	30	3	3.78

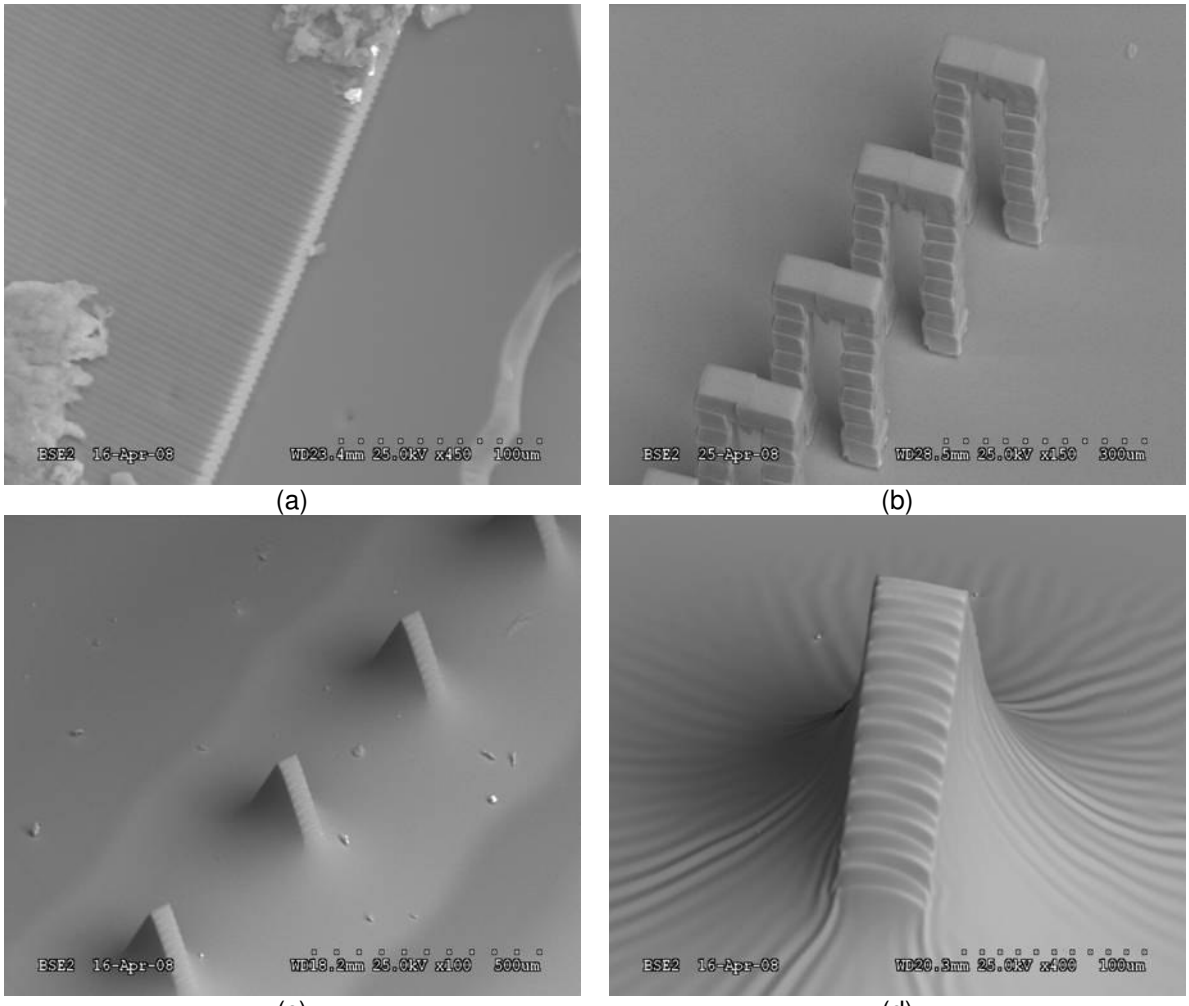

(a) (b)

(c) (d)

Figure 5.13 Two photon polymerized 3D microstructures (a) Diffraction grating, (b) Microbridge, (c) Prism grating array, and (d) Prism grating

In conclusion, the detailed statistical analysis using experimentally obtained data was performed to understand the effect of common process parameters on the 3D resolution of 2PP process. Design of experiments methodology effectively helped in understanding the role of speed, photoinitiator concentration and applied laser power on the 2PP resolution that can not be effectively extracted from the contrast plots. Differences in the average polymerized lateral and axial resolutions from various process parameter combinations were analyzed using the interaction plots and multiple comparison approach. It is concluded that the size of polymerized height is more sensitive to changes in considered process parameters. On the other hand, the

size of polymerized width can be easily controlled by using lower power levels along with higher scanning speeds. The effect of photoinitiator concentration does not have any significant effect on the lateral resolution at low power levels and high speeds. The statistical model developed based on regression analysis approach was validated with the experimental results being within ± 5% error. The statistical model along with the information obtained from process parameters analysis was successfully employed to define the fabrication process parameters for fabricated microstructures with good dimensional accuracy.

CHAPTER 6

HIGH ASPECT RATIO STRUCTURE FABRICATION IN A SINGLE LASER SCAN

The developments in the micro/nano technology offer numerous applications in various areas. However, the transformation of an idea into an actual product or prototype depends upon the availability of microfabrication technologies. Micro/nano structures with various degrees of complexities are routinely fabricated using available fabrication techniques. Common subtractive techniques routinely used for micro/nano fabrication include lithography, LIGA, etching and laser micromachining [46, 63-65]. But every technology has its advantages and limitations and its use is generally dependent on the user familiarity with the process, the workpiece material, process simplicity, cost and achievable process resolution and control.

As discussed in previous chapters, 2PP is an effective technique to fabricate complex 3D micro/nano polymeric structures by scanning the tightly focused ultrashort pulses in photoresponsive resin in a predefined pattern. In addition, the polymerization reaction is confined in the focal volume and true 3D structures can be easily fabricated by scanning the ultrashort laser pulses in a mixture of liquid resin consisting of a suitable monomer and photoinitiator. The micro/nano structure fabrication is inherently a layer by layer method where polymerized voxels are stacked in a defined pattern.

Traditionally, 2PP is performed using high repetition rate femtosecond laser systems (with pulsing rates of approximately 80 MHz) along with high numerical aperture microscope objectives [21, 36, 38-40]. Most of the work with 2PP is primarily performed using tight focusing of very low energy pulses from high repetition rate laser system. The tight focusing of laser pulses produces the required intensities to initiate the polymerization reaction. 2PP is very efficient for the fabrication at micro/nano scale with good dimensional control and has been

used to fabricate high aspect ratio structures. In our laboratory, we have also employed high repetition rate system for fabrication of various structures that shows the 3D fabrication capability of 2PP with some of the structures shown in figure 6.1.

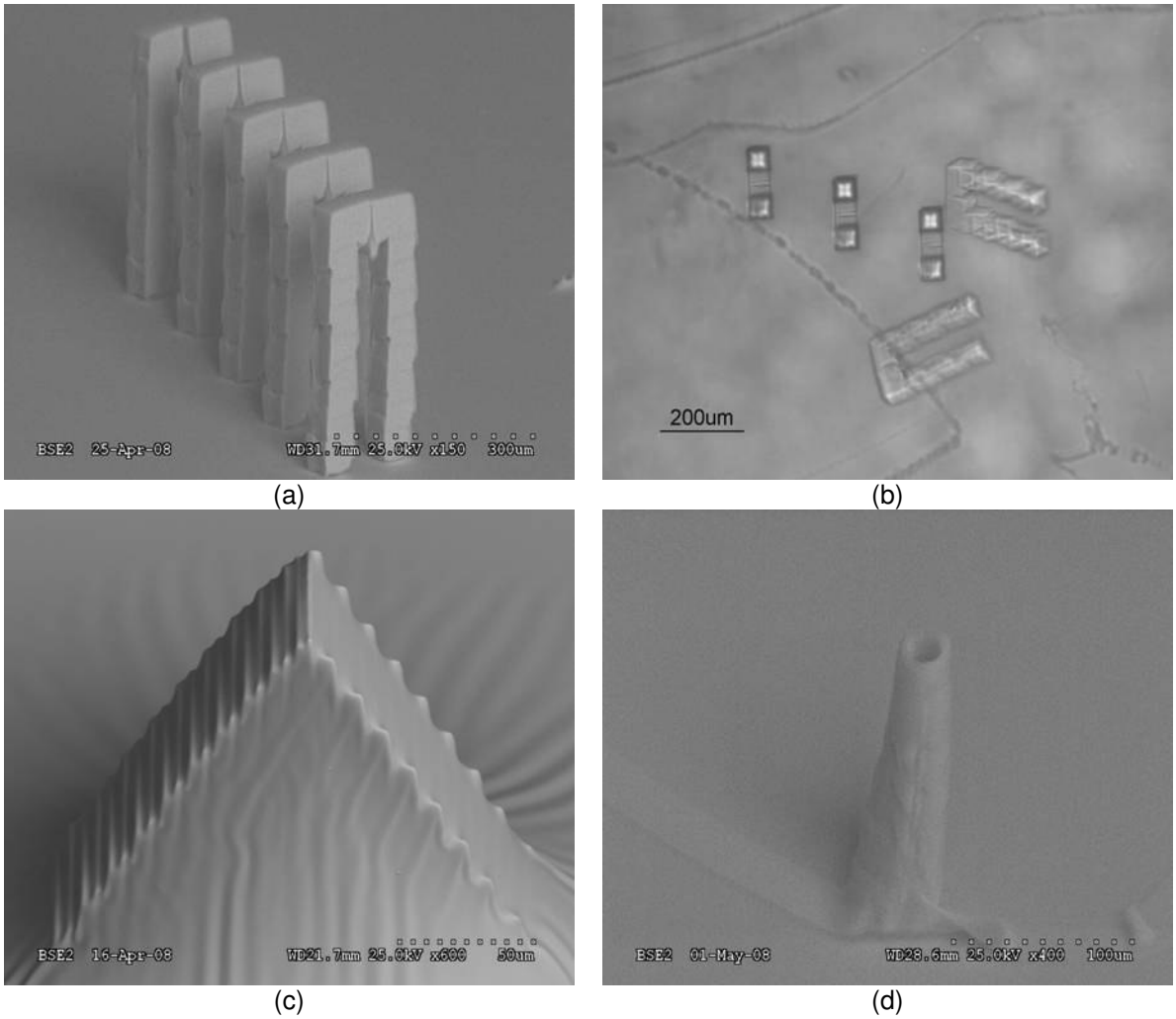

(a) (b)

(c) (d)

Figure 6.1 2PP fabricated microstructures (a) Microbridges, (b) Microbridges floating in resin, (c) Prism grating, and (d) Micronozzle

All the above features were fabricated in a layer by layer manner where the axial and lateral dimensions were chosen based on the desired geometry of the fabricated features. The fabrication was performed using low energy pulses from the oscillator and 0.4 N.A. microscope objective for focusing. These features are not of large geometries and the fabrication time was short for example, single microbridge and prism grating were fabricated in ~ 10 min and

micronozzle was fabricated in ~ 5 min. But if the overall dimension of the fabricated structures is in the order of few hundred microns, the layer by layer fabrication method requires a lot of time, even for simple structures.

In this chapter, we present a simple methodology for the fabrication of high aspect ratio microstructures using 2PP by employing low N.A. lens in a single laser scan thus avoiding the tedious and time consuming polymerized layer stacking process or methodology. Femtosecond laser systems working at 1 kHz and 80 MHz repetition rates are used for the microfabrication but with loose instead of tight focusing conditions created by low N.A. lens. The methodology of employing the off-focus laser pulses and self-trapping of the laser beam is discussed and experimentally demonstrated for the fabrication of high aspect ratio microstructures. The fabricated structures have good dimensional accuracy and are polymerized in a single laser scan thus substantially improving overall fabrication cycle time.

6.1 Off-focused and self trapped pulses for high aspect ratio structures

Most of the 2PP research is performed using the tight focusing of very low energy pulses from the high repetition rate femtosecond laser system. The tight focusing conditions generate high photon fluxes that increase the probability of two photon absorption in a quasi-simultaneous event [8]. The tight focusing condition and the thresholding effect are effective in achieving feature sizes much smaller than the diffraction limit imposed by the focusing optics. This achievable high resolution is ideal for fabricating 3D micro/nano components with complex geometry. But if the structure geometry is 2 ½ D in nature and has a larger footprint, the layer by layer fabrication takes a lot of time.

2PP has been used for the fabrication of sub-diffraction limit high aspect ratio structures [66-68]. Lee et al have used the 2PP process with a high repetition rate (80 MHz) ultrashort laser source for the fabrication of simple walls with an aspect ratio of 9 in epoxy based SU-8 material [67]. Working with SU-8 for the high aspect ratio structures is advantageous as it provides better mechanical strength. They also employed the reactive ion etching (RIE) method

for transferring the high aspect ratio polymerized pattern on to silicon. Another method employing the 2PP and UV light was used by Pan et al to fabricate structures in acrylate based liquid resin with an aspect ratio of ~7 [68]. Pan et al also employed a high repetition rate (80 MHz) ultrashort laser source for the fabrication but they used a focusing objective with moderate N.A. The UV light was used for pre-exposure to create short polymer chains that increase the viscosity of liquid resin and provides stable condition for high aspect ratio fabrication. Though, these methods are effective for fabricating sub-diffraction limit structures with aspect ratios smaller than 10 are mostly achieved by the Gaussian intensity distribution mismatch. Note that, both of these methods are multistep and again rely on layer-by-layer fabrication for larger structures thus increasing the fabrication time.

6.1.1 Amplified laser pulses for 2PP

Very little work has been performed and reported with a low repetition rate (1 kHz) laser system for 2PP because each pulse has energy of about three orders of magnitude higher than the high repetition rate system. The tight focusing of high energy pulses leads to the burning of monomer because of the high intensities produced as presented in figure 6.2. These high energy pulses have to be attenuated by using external optical setups such as a polarizer and half wave plate to make them suitable for polymerization [69]. The low energies and tight focusing conditions help in confining the region where polymerization reaction would take place and hence leading to a high resolution process. But because of a much slower pulse repetition rate (1 kHz), the scanning speed has to be much slower in order to achieve significant overlap between the consecutive voxels leading to a continuous structure. The slower scanning speed and layer by layer scanning fabrication methodology again increases the fabrication time and actually leads to an inefficient process compared to 80 MHz laser system.

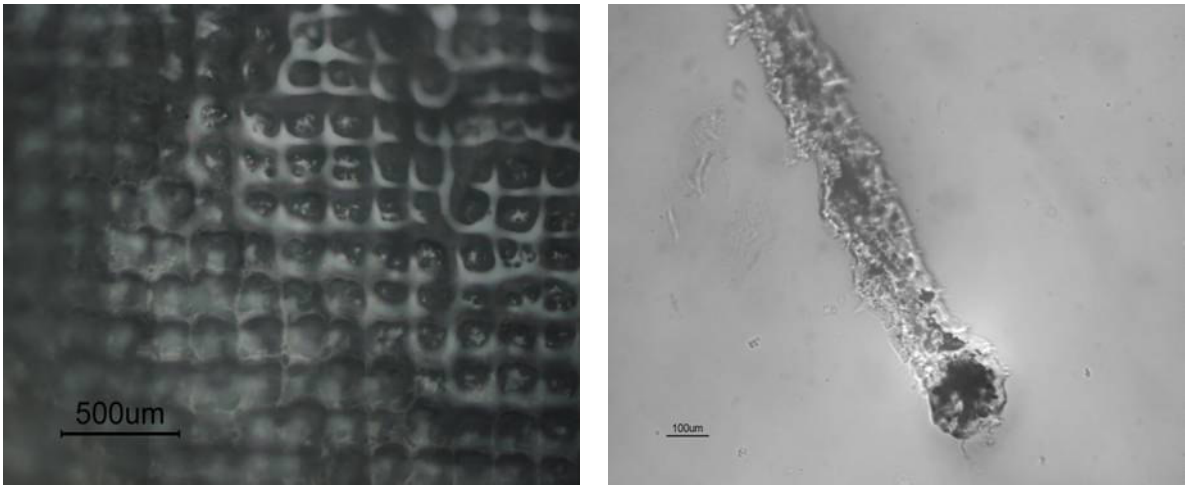

Figure 6.2 Burning of polymer by amplified laser pulses

6.1.2 Off-focusing condition for high aspect ratio fabrication

In tight focusing conditions, the amplified laser pulses (1 kHz) can generate excessive heat that can burn the monomer. But, these amplified laser pulses can be effectively used for 2PP of high aspect ratio 2 ½ D structures without causing the burning of monomer. To avoid excessive heating, the amplified pulses are loosely focused using a low N.A. lens (25.4 mm focal length) inside the liquid resin. The use of low N.A. lens provides a much wider intensity distribution in axial direction resulting in longer polymerization region along the optical axis. The high energy pulses from the amplifier were effectively used by focusing them just inside the substrate and the energy of the unfocused part subsequently used to initiate the polymerization reaction. The amplified laser pulses, even at moderate average powers of 2 to 3 mW, can cause polymer charring when focused in the liquid resin. However, the off-focus regions are away from the stronger intensities and do have sufficiently high energies to initiate the polymerization reaction by the two photon absorption process. The schematic of the laser system with off-focused condition is shown in figure 6.3.

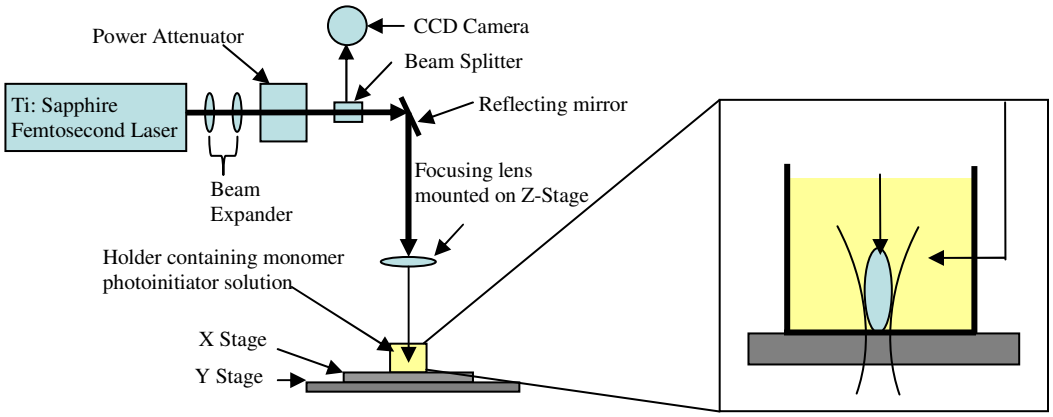

Figure 6.3 Schematic of fabrication process

Polymerization of microstructures is performed with 25.4 mm focusing lens which has a very low N.A and using a photoresponsive resin consisting of ethoxylated(6) trimethylolpropane triacrylate (SR499-Sartomer) and 3.78% by wt. acyl phosphine oxide (Lucirin TPO-L -BASF) photoinitiator. The advantage of using low N.A. lens is the achievable mismatch in radial and axial intensity distribution. This mismatch can be favorably exploited to fabricate polymerized structures with high aspect ratio. The mismatch is inherent to the intensity distribution of a Gaussian beam as shown in equation 1 [70] where I_o is the laser intensity at the center of the beam, ω_0 is the theoretical beam waist, z_o is the Rayleigh length, λ is the laser wavelength, r and z are radial and axial distances. The Rayleigh length, z_o, represents the axial distance where the intensity distribution does not change readily. The radial intensity distribution is confined in the beam spot but the axial intensity distribution depends on the Rayleigh length which is proportional to the square of diffraction limited spot radius. Hence, the mismatch greatly increases with low N.A. lenses as compared to high N.A. lenses generally used for two photon polymerization. The intensity distribution achieved from the high and low N.A. lens is presented in figure 6.4 (a) and (b) respectively.

$$I(r,z) = I_o\left(\frac{-\omega_o^{\,2}}{\omega^2(z)}\right)\exp\left(\frac{-2r^2}{\omega^2(z)}\right) \qquad (2)$$

$$\omega(z) = \omega_o \sqrt{1 + \left(\frac{z}{z_0}\right)^2} \quad \text{and} \quad z_o = \frac{\pi w_o^2}{\lambda} \tag{3}$$

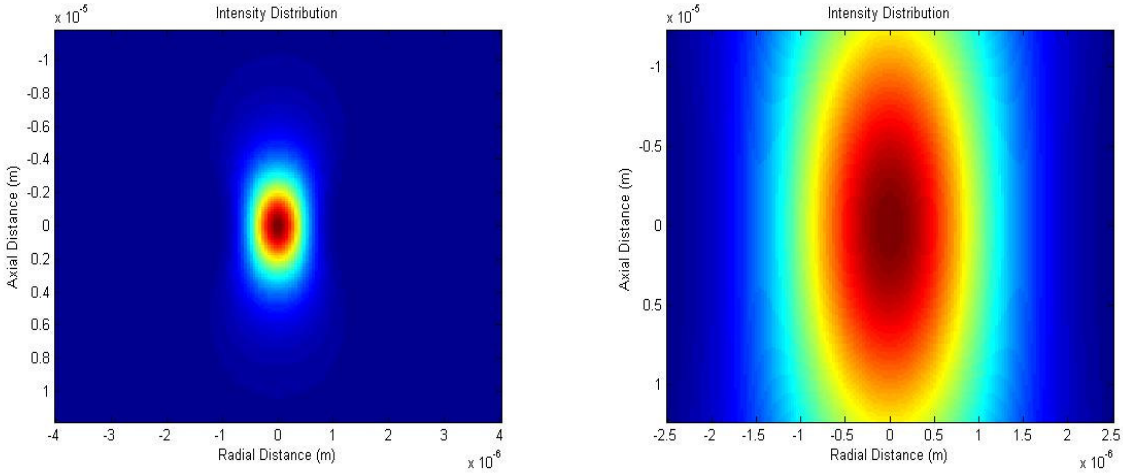

(a) (b)

Figure 6.4 The Gaussian beam intensity distribution comparison (a) Point spread function for high N.A., and (b) Point spread function for low N.A.

6.1.3 Self-trapping of laser pulses in photopolymerization

Another important factor that was advantageously exploited was the self-trapping of laser pulses that takes place during photopolymerization. The self-trapped laser pulses force the polymerization to propagate along the optical axis at much longer lengths. A self-trapped laser beam propagates along the optical axis with a constant diameter because of an exact balance between self-focusing and diffraction effects [71, 72]. Self trapped laser beams have been used to fabricate light induced self-written waveguides (LISW) and micro-optical structures based on single photon absorption from continuous wave UV laser beams where 2PP uses NIR pulsed femtosecond laser pulses. [73].

The effects of self-trapping and self-focusing of laser beam in photopolymerization are different from the Kerr-effect that takes place in optical non-linear media when irradiated with high intensity laser pulses. The self-focusing and trapping due to Kerr-effect take place in the order of femtoseconds and have been excessively studied and demonstrated in ultrashort laser

processing of transparent dielectrics [74]. Self-trapping of laser pulses in photopolymerization takes place at much longer time scales, generally in the order of few milliseconds to minutes.

The photopolymerization is a gradual process; the degree of polymerization increases with applied dosage of controlled energies and exposure time. The refractive index of the liquid resin changes as the irradiated area starts to polymerize. In 2PP, the radicals are generated during the pulse irradiation and the irradiation time depends upon the pulse width of laser source and generally lasts only a few hundred femtoseconds. But, the polymerization starts at a much longer time period, between few microseconds to milliseconds. The self-trapping effect was also discussed in chapter 5 where higher power levels were responsible for much longer polymerized heights. The use of higher powers leads to the depletion of photoinitiator molecules from the irradiated volume. The gradient produced by the depletion of photoiniator results in a difference in the degree of polymerization causing a local change in the refractive index of the irradiated spot. The change in refractive index acts as a low N.A. lens and produces waveguiding effect of laser pulses by trapping them along the optical axis and resulting in a much longer height of polymerization [69]. The depletion of photoinitiator and the resultant gradient in the degree of conversion are presented in figure 6.5 (a) and (b) respectively.

The self-trapping and self-writing effects were more pronounced for off-focus amplified laser pulses. Even though the focused amplified laser pulses lead to the burning of monomer, at certain energies the off-focus pulses have the right amount of energy to initiate the polymerization reaction and experience self-trapping. The energy of the off-focus amplified laser pulses is still much higher compared to the pulses from 80 MHz source, resulting in a much stronger depletion of photoinitiator and subsequent gradient in the refractive index. The induced gradient effectively guides the laser pulses to much longer distances compared to the 80 MHz system. These off-focus amplified laser pulses with the required low intensities are used to easily polymerize and fabricate structures with heights of ~ 2.5 mm in a single laser scan. The radial dimension of the polymerized features is very sensitive to the applied energies and

irradiation time, and it varies from 25 µm to 60 µm at moderate scanning speeds (1 mm/min to 3 mm/min) and average powers (6 mW to 12 mW) with 3.78% by wt of photoinitiator.

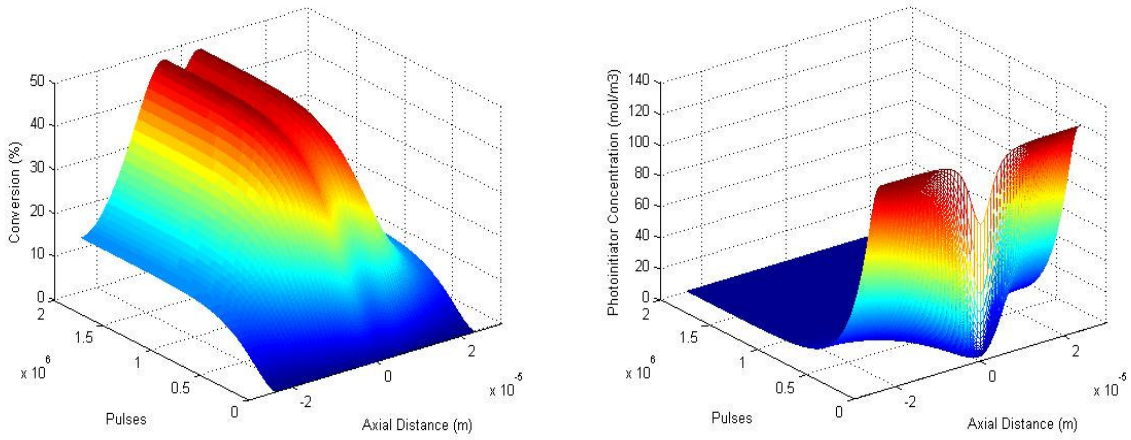

(a) (b)

Figure 6.5 Gradient in conversion ratio due to photoinitiator depletion (a) Gradient in conversion ratio, and (b) photoinitiator depletion

It was also observed that even the completely off-focus amplified pulses (10 mm away from focal point) have sufficient energy to initiate the polymerization reaction and produce free standing high aspect ratio structures. A *baseball bat* shaped free standing structure shown in figure 6.6 was fabricated by completely off focus pulses when the resin was exposed to the laser irradiation for 180 seconds and 10 mW irradiation power. Initially, the polymerization growth along the optical axis takes place due to initial refractive index change and guides the laser pulses along the axial direction. Once the polymerization saturates along the optical axis, the bulge on the top is attributed to transverse pulse leakage and radical diffusion.

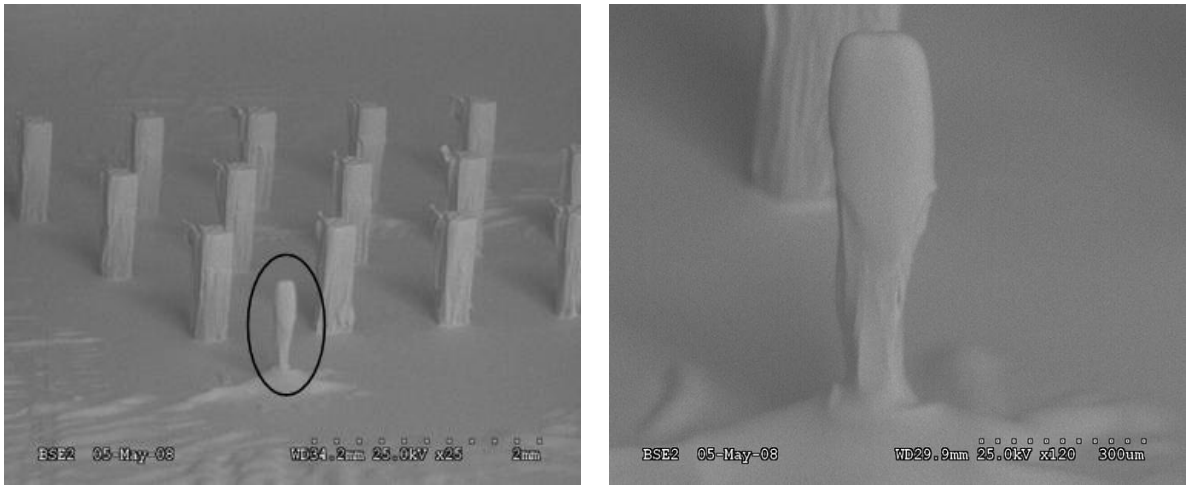

Figure 6.6 *Baseball bat* shaped feature fabricated by completely off-focus amplified laser irradiation; average power 10 mW, irradiation time 180 sec, (scale (a) 2 mm, (b) 300 µm)

The high repetition rate (80 MHz) laser pulses from the Mai-Tai oscillator were also used for fabrication. However, the achievable height of fabricated structures was smaller compared to those obtained from amplified pulses. With high repetition rate pulses, enough radicals are generated since a much higher number of pulses irradiate the monomer, and the polymerization takes place much uniformly with small variation in the changed refractive index distribution. This small refractive index change limits the self guiding effect of laser pulses and controls the achievable maximum polymerized height along the optical axis. By focusing the oscillator pulses through a 25.4 mm focusing lens, structures were fabricated with heights of ~800 µm and widths of ~15 µm in a single laser scan. Aspect ratios of ~50 were easily achieved by structuring polymerized wall patterns on the substrate.

Simple microstructures, columns, and rods were fabricated with both the amplified and high repetition rate pulses in a single laser scan to present the effectiveness of off-focus single scan fabrication and are shown in figure 6.7. The single scan fabrication process substantially improves fabrication cycle time as compared to layer-by-layer methodology. The columns and rods are fabricated by a trepanning operation and are analogous to rolled paper. The column width varies from 150 µm to 350 µm where the thickness of single wall layer is ~15 µm. The 800 µm tall and hollow columns are fabricated using the high repetition rate laser (80 MHz) pulses

with an average power of 200 mW and a scanning speed of 5 mm/min. The 1500 µm tall rods were fabricated using amplified laser pulses with an average power of 6 mW and a scanning speed of 2 mm/min. The fabrication time for single column varies between 30 sec to 2 min depending on the diameter and total traveling path of the laser pulses.

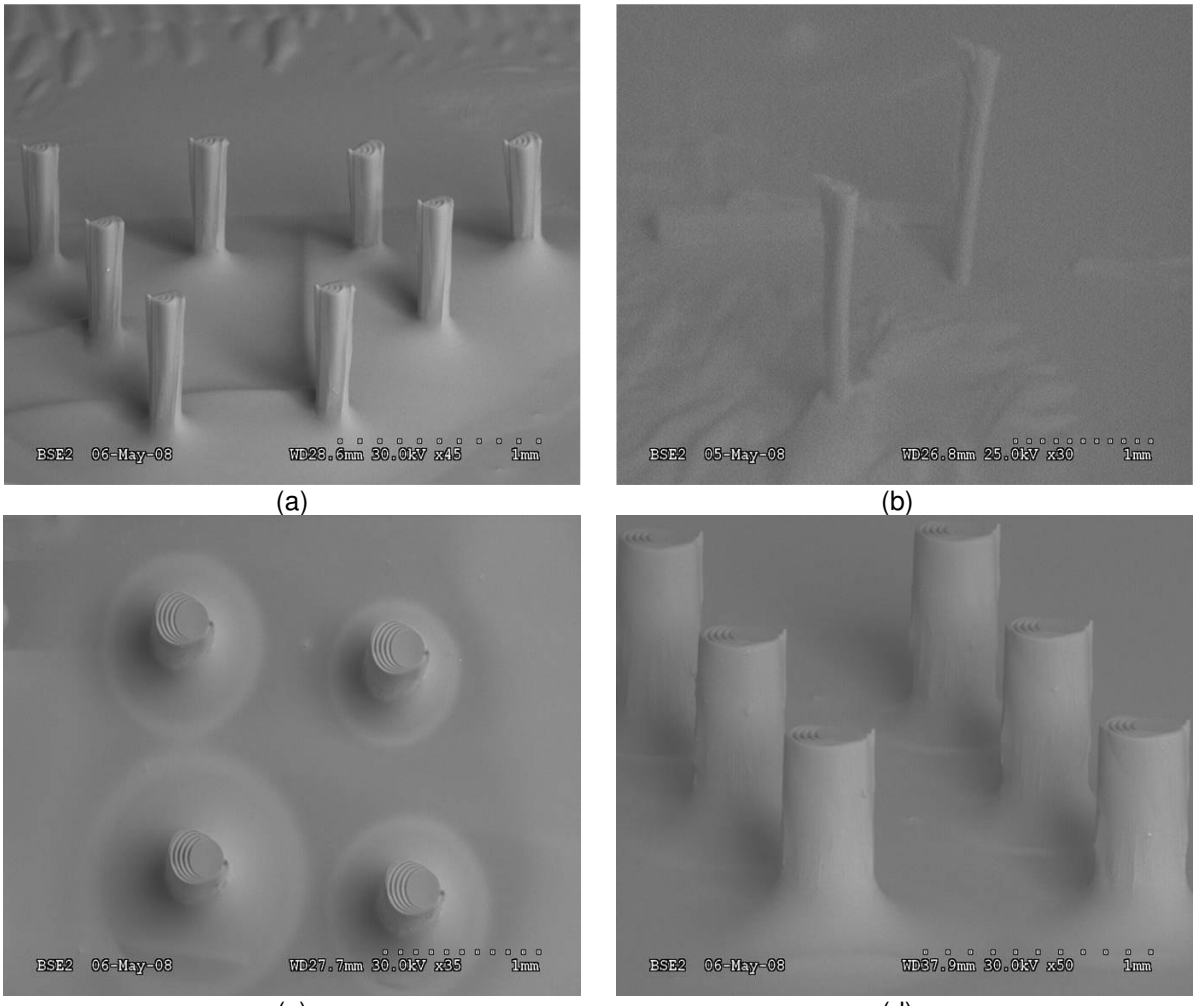

(a) (b)

(c) (d)

Figure 6.7 Fabricated microstructures using amplified and high repetition rate laser pulses (scale for all figures 1 mm) (a) 800 µm tall columns, (b) 1500 µm tall rods, (c) Hollow columns – top view, and (d) Hollow columns – side view

6.1.4 Scanning speed for fabrication

Another critical parameter in the single scan fabrication is the rate at which the laser pulses are delivered inside the liquid resin. The advantage of using 80 MHz system is that it speeds up the fabrication process because of very high pulse repetition rate. The pulses

irradiate the liquid resin once every 12.5 nsec (80 MHz pulse repetition rate) leading to a significant voxel overlap that results in a continuous structure. Speeds up to 5 mm/min were successfully employed for wall fabrication using the 80 MHz system as presented in chapter 5. While working with 1 kHz laser source, the time period between consecutive pulses is much longer (1 msec) requiring slower scanning speeds for significant overlap between voxels. The polymerized walls with 1 kHz and 80 MHz laser system at a scanning speed of 5 mm/min respectively are presented in figure 6.8. While the 80 MHz laser source leads to continuous polymerization, the 1 kHz laser source causes polymerization in a bridge like pattern. To achieve continuous polymerization with 1 kHz system, the scanning speed has to be reduced and that increases the fabrication time by a certain extent. Though, 1 kHz system is capable in achieving polymerization heights much taller compared to 80 MHz source, the scanning speed has to be lower to achieve continuous polymerization. There is a trade off and in selecting to use low or high repetition rate laser system depends on the application and feature geometry.

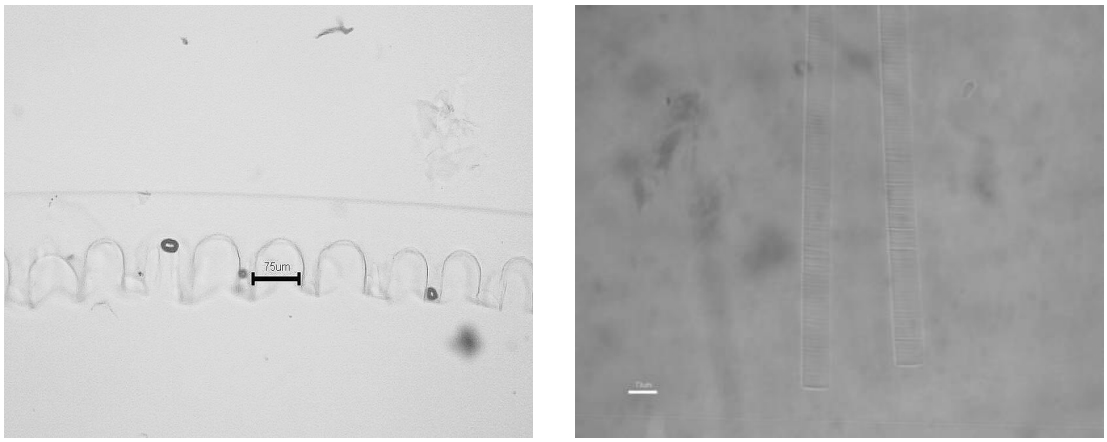

(a) (b)

Figure 6.8 Polymerized wall geometry using 1 kHz and 80 MHz laser system (scale bar - 75µm) (a) 1 kHz system, and (b) 80 MHz system

6.2 Deformation of polymerized structures

Loosely focused laser pulses along with low N.A. lens can be effectively used for 2PP of high aspect ratio structures. But because of high aspect ratio, the deformation of polymerized structures becomes a critical issue and should be addressed accordingly. The two common

deformation mechanisms that were observed during experimentation are waviness of polymerized walls, and deformation caused by the surface tension effects. In this section, a discussion and proposed solution to these problems is presented.

6.2.1 Waviness of polymerized walls

As the 2PP takes place in the liquid environment, the combined effect of liquid motion because of inertial effects produced by scanning stage motion along with mechanical properties of polymerized feature may lead to structural deformation. The stiffness of the polymerized feature decreases with an increase in the aspect ratio. Because of the liquid motion, the polymerized walls become wavy resulting in structural deformation. The waviness of polymerized walls is also reported by Qi et al who related it to the height of voxel [69]. The waviness of the polymerized walls observed in our experiments is presented in figure 6.9.

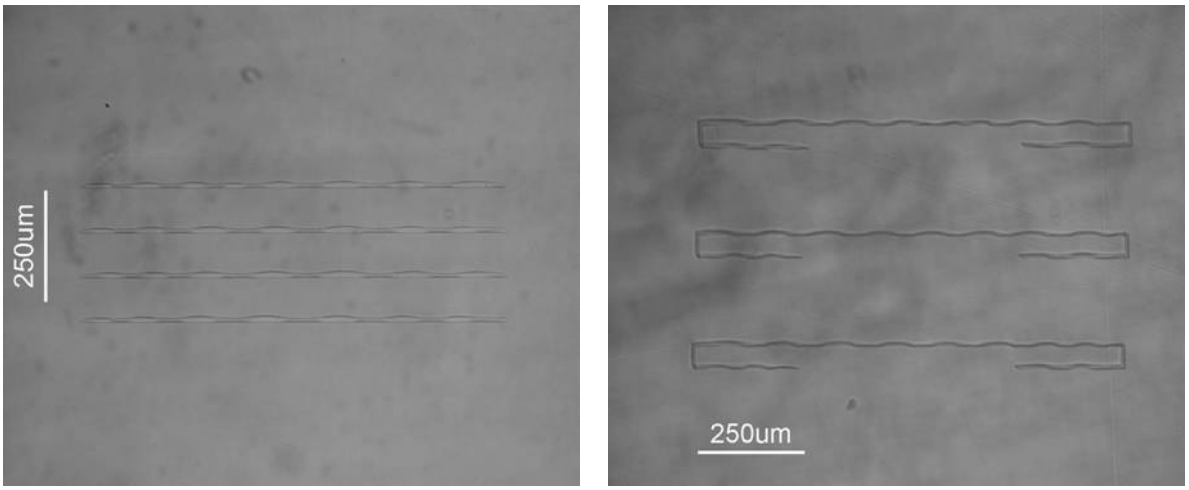

Figure 6.9 Waviness of polymerized walls because of inertial effects

The waviness is not desirable as it affects the quality and usability of the polymerized structures. The detrimental effect of wall waviness is presented in figure 6.10 where walls of a polymerized grating become wavy and resulting in the structural deformation of grating. One approach to maintain the structural integrity is to minimize the inertial effects either by decreasing the scanning speed or by increasing the viscosity of the liquid resin. The viscosity of the liquid resin can be increased by mixing a binder material with the monomer and

photoinitiator or by treating the liquid resin with UV light [68]. The UV light pre-exposure initiates polymerization reaction that results in shorter chains that increase the overall viscosity of the liquid resin. Another method is by adjusting the scanning speed to minimize the sudden acceleration and deceleration that leads to structural deformation. Both these methods can be effectively employed to avoid the deformation because of wall waviness. We employed the scanning speed method to fabricate gratings with straight walls that can be effectively used in our research, a diffractive optic element as shown in figure 6.10.

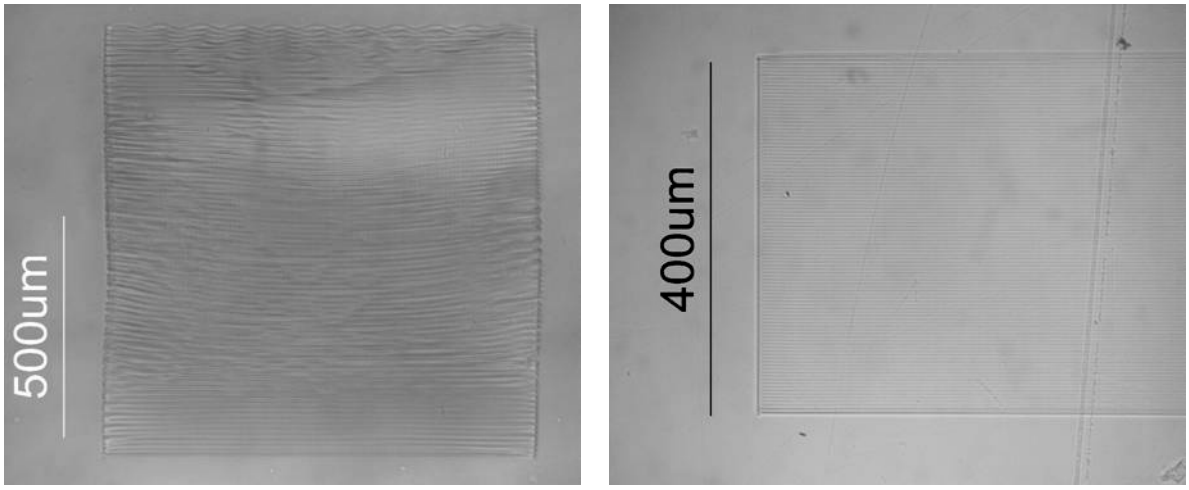

(a) (b)

Figure 6.10 Effect of aspect ratio on the fabricated diffraction grating (a) Deformed grating, and (b) Grating with straight walls

6.2.2 Surface tension effects

Another concern relating to high aspect ratio structures is the developing process. The high aspect ratio structures tend to collapse because of the surface tension of the liquid monomer. The surface tension produces a cohesive force that pulls the walls together thus deforming or even collapsing the structure. Deformation and collapse of patterned features in negative tone photoresist during the resist development stage of photolithography has been reported in the literature [75, 76]. In lithography, the resist material is solid and the structures are patterned in the resist. A liquid developer solution is used to remove the unexposed regions leaving the patterned structure behind. The surface tension of the liquid developer causes the

fabricated pattern to collapse due to the mismatch between cohesive and restoring forces. Developers with low surface tension are commonly employed to avoid this problem in lithography [76].

2PP is generally performed with liquid resins such as a liquid mixture of monomer and photoinitiator. The problem of collapsing pattern is more severe in single scan 2PP because of the high aspect ratio structures. Unlike the photolithography development process, the removal of unpolymerized liquid resin from the substrate could cause the deformation and collapsing of microstructures even before the developing step. The surface tension properties of the developer could be easily controlled but not so for the monomer as most of the multifunctional monomers have higher surface tension values compared to common solvents/developers [77]. Also, the monomer choice is limited and that also affects the physical and mechanical properties of fabricated structure. Deformed and collapsed high aspect ratio polymeric wall patterns (height ~800 µm) fabricated by the single laser scan methodology are shown in figure 6.11.

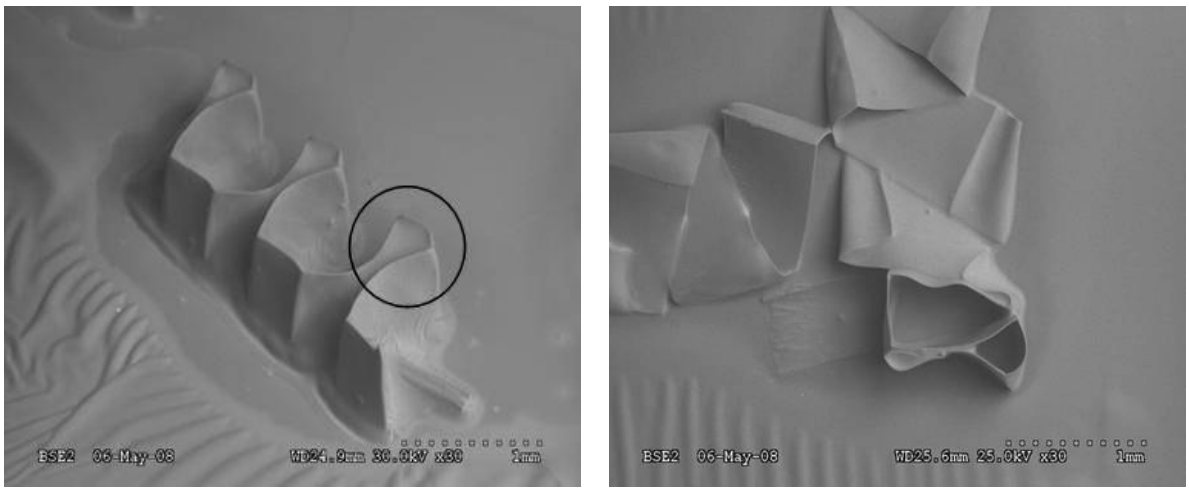

(a) (b)

Figure 6.11 Deformed and collapsed high aspect ratio structures (scale 1 mm) (a) Wall thickness ~ 25 µm, and (b) Wall thickness ~ 15 µm

2PP wall patterns with 25 µm and 15 µm thickness and 800 µm height shown in figure 6.7 did not survive the resin drainage process. The 15 µm thick wall pattern was completely

peeled off from the substrate, where the 25 µm thick pattern was deformed by the pulling cohesive forces. The deformation resulted in the inside and outside bowing of the longer and shorter walls respectively. The cohesive forces are produced because of the surface tension effect of the liquid resin on the polymerized walls. During draining, the receding level of liquid resin produces a concave meniscus between the patterned walls thus generating a pulling force on the walls causing the bowing of the walls as seen in figure 6.11 (a) and also observed by tanaka et al [75]. The pulling force effect is more severe for higher aspect ratio or thinner structures and might even cause the whole pattern to peel from the substrate as shown in figure 6.11 (b).

The surface tension effect is a serious problem for these high aspect ratio structures and remedial measures are crucial. The cohesive forces are directly related to the surface tension of the liquid and inversely related to the distance between the walls [75, 76]. The cohesive forces are counteracted by the restoring forces produced by the structure which is a function of the geometry of the polymerized feature. If the cohesive forces exceed the restoring force, the pattern will deform or collapse. The cohesive force can be estimated by equation 3 where F is the produced cohesive force, d is the distance between the polymerized walls, σ is the surface tension of resin and θ is the contact angle of the monomer and is also represented by the schematic shown in figure 6.12.

$$F = \frac{2\sigma \cos\theta}{d} \tag{3}$$

Hence, the cohesive forces can be reduced either by using a monomer with lower surface tension, reducing the angle of contact or by increasing the distance between the polymerized wall pattern. Most of the monomers commonly employed for 2PP have surface tension in the range of 30-40 dynes/cm [77]. Hence, there is not much control in modulating the coefficient of surface tension for reducing the magnitude of cohesive force. Similar to the coefficient of surface tension, the contact angle can not be easily modulated, as well since it depends on the

properties of monomer and the hydrophobicity of the polymerized structures. The distance between the walls can be increased to reduce the cohesive forces but it is dependent on the designed geometry of the structure.

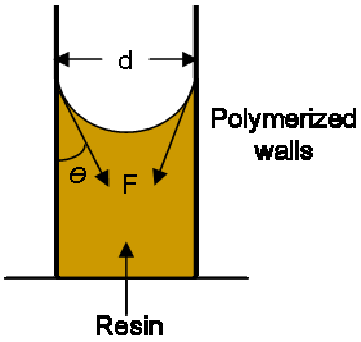

Figure 6.12 Cohesive forces produced by the liquid monomer

It is not easy to reduce the produced cohesive forces in 2PP as an experimenter does not have control over the choice of monomer and the designed geometry. The pattern deformation due to cohesive forces is also well studied for the photolithography process by various groups. In photolithography, the deformation is caused by the use of solvent during the developing phase. Methods like supercritical drying and freeze drying are commonly employed that effectively negate the surface tension effects [75, 76]. Though, the problem is much more severe in 2PP as the deformation is caused during the monomer drainage which is an inherent part of 2PP process. A mathematical model is developed by Tanaka et al that relates the cohesive forces with the rigidity of the polymerized structure to withstand structural deformation [75]. They have used a beam sway model to evaluate the expressions for cohesive force and the critical Young's modulus of the resist that can generate enough restoring forces to provide structural integrity.

Thus, decreasing the cohesive force or increasing the restoring forces produced by the polymerized structures leads to a solution to this problem. The restoring force is a function of the stiffness of polymerized part and can be increased by increasing the width and hence the cross-sectional moment of inertia of the walls. A wall pattern with a wall thickness of ~ 50 µm

(higher cross-sectional moment of inertia and high stiffness) and height of 800 µm was fabricated with a single laser scan using amplified laser pulses with an average power of 12 mW and a speed of 2 mm/min is shown in figure 6.13. The new polymerized pattern survived the drainage and developing process indicating good structural integrity as well as the effectiveness of single scan method to fabricate usable 2 ½ D structures in a very short time.

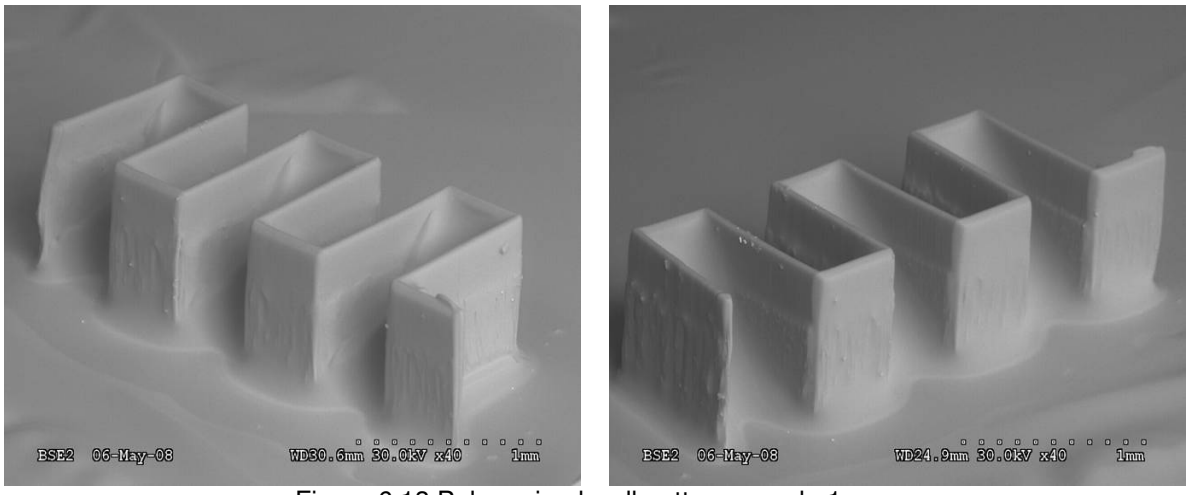

Figure 6.13 Polymerized wall pattern – scale 1 mm

This simple methodology can be effectively employed for the fabrication of high aspect ratio structures using 2PP. The single laser scan fabrication can be effectively applied for both the low and high repetition rate femtosecond laser system. The off-focus laser pulses from a low N.A. lens were used to initiate the polymerization process and produce the initial refractive index change that causes self-trapping of the laser pulses along the axis of propagation. Off-focused and self-trapped amplified laser pulses produce larger polymerization length along the optical axis. Polymerized walls with aspect ratio greater than 50 were easily fabricated in a single laser scan. Single scan fabrication of features with height in the millimeter order was effectively demonstrated by the amplified laser pulses attributed mostly to the higher energy and propagation of these pulses inside the liquid resin. The concern with the high aspect ratio structures is the wall waviness due to inertial effects and pattern collapse and peeling caused by the cohesive forces produced by the surface tension effect of monomer during drainage.

Measures to minimize or avoid feature deformation are presented, with one of the measures experimentally verified for both the deformation mechanisms. The proposed off-focus self-trapped laser pulses and single laser scan microfabrication methodology could be effectively used to fabricate high aspect ratio microstructures using 2PP while reducing fabrication time and increasing the throughput of the process.

CHAPTER 7

CONCLUSIONS AND RECOMMENDATIONS

In this research, a 3D micro/nano lithography technique utilizing two photon absorption of NIR laser source is presented. The two photon absorption by photoinitiator molecule generates active radicals that initiate a free radical chain polymerization reaction. The polymerization reaction is confined only at the focal volume because of the nonlinear dependence on input intensity and the confinement of polymerization reaction because of radical termination kinetics. The 2PP process is an excellent technique for the fabrication of complex 3D polymeric structures with great dimensional accuracy and minimum post/pre processing steps. This research focused on developing a mathematical model for the 2PP process, sensitivity analysis of the fabrication process based on experiments and development of a novel technique for the rapid fabrication of 2 ½ D microstructure using single laser scan.

7.1 Conclusions

This research presents the development, implementation and validation of a mathematical model that considers the various stages of the two photon polymerization process employing ultrashort pulsed laser systems. The effects of temperature dependent diffusion and polymerization kinetics are considered. Upon laser irradiation, the photoinitiator decomposes and the concentration is reduced at the irradiated volume. Radicals are generated and remain confined at the irradiated volume during the laser pulse width. It is observed that radical termination and monomer conversion take place at much longer time scales (micro-milliseconds) compared to the irradiation time. Three different modes of radical termination (combination, trapping and inhibition) were included in the developed model and their relative effects on the termination kinetics were analyzed. The surviving radicals diffuse outwards from

the irradiated volume during the dark period and define the volume where monomer concentration gradient is observed. Also, the limited replenishment of decomposed photoinitiator was observed would affect the radical generation for subsequent pulses. The degree of polymerization increases with subsequent pulses with a higher conversion rate at the center of focal volume. The mismatch in radial and axial conversion gives the voxel its experimentally demonstrated ellipsoidal shape. A comparison between the 1 kHz laser system and 80 MHz system is also presented. The underlying dynamics of each system is quite different because of the much shorter dark period for the later. The model also explores the effect of power and exposure time and thresholding effect introduced by inhibitor concentration. The developed model can be used for predicting process resolution and achieving a robust 2PP process.

A detailed statistical analysis is also employed using experimentally obtained data to understand the effect of common process parameters on the 3D resolution of 2PP process. Design of experiments approach was utilized to evaluate statistical significant effects of combinations of speed (1 mm/min, 3 mm/min, and 5 mm/min), photoinitiator concentration (2.56%, 3.78%, and 4.98%) and applied laser power (12.5 mW, 16 mW, 20 mW, 25 mW, 35 mW, and 50 mW). The model assumptions were tested from the residual plots and hypothesis testing. Difference in the average polymerized lateral and axial resolutions from various process parameter combinations were analyzed using the interaction plots and multiple comparison approach. It is concluded that the size of polymerized height is more sensitive to changes in the different levels of applied power, scanning speed and photoinitiator concentration. On the other hand, the size of polymerized width can be easily controlled by using lower power levels along with higher scanning speeds. The studied photoinitiator concentrations do not have any significant effect on the lateral resolution at high scanning speeds. The statistical model developed based on regression analysis approach was validated with the experimental results being within ± 5% error. The statistical model along with the information obtained from process

parameters analysis was successfully used to define the fabrication process parameters for fabricated microstructures with good dimensional accuracy.

A simple methodology for the fabrication of high aspect ratio structures using 2PP and single laser scan is also presented. Femtosecond laser pulses from an amplified laser source and an oscillator were used to fabricate polymerized high aspect ratio structures in a single laser scan. The off-focus laser pulses from a low N.A. lens were used to initiate the polymerization process and produce the gradient in refractive index that causes self-trapping of the laser pulses along the axis of propagation. Off-focused and self-trapped amplified laser pulses produce larger polymerization length along the optical axis. Polymerized walls with aspect ratio of ~ 100 were easily fabricated in a single laser scan. Single scan fabrication of microfeatures with height in the millimeter order was effectively demonstrated. The problem of pattern collapse and deformation during draining and development of un-polymerized liquid resin was discussed as it relates to the effect of cohesive forces due to surface tension and restoring forces. Measures to minimize or avoid feature deformation are presented, with one of the measures experimentally verified. The proposed off-focus self-trapped laser pulses and single laser scan microfabrication methodology could be effectively used for high aspect ratio microfabrication using 2PP while improving fabrication time.

This work effectively implements a mathematical framework to the 2PP process. The model adheres to the 3D confinement and nonlinearity which is inherent to the 2PP process and matches well with the experimental results obtained from the published research. The theoretical analysis also helps in explaining some of the unanswered phenomena published in open literature and noticed during the experiments and provides a deeper understanding on the 2PP process.

7.2 Recommendations

2PP is effectively used for the fabrication of complex micro/nano features with good geometrical and dimensional control. Feature sizes much smaller than the diffraction limit are

obtained by nonlinear excitation along with the combination of low dosage (exposure time and power) and thresholding conditions. Though, to achieve complete control, a complete understanding of the role of various process and material dependent parameters is required. The mathematical model developed in this work is effective in unraveling the effect of important process and material dependent parameters on the achievable resolution and also helps in understanding the dynamics of 2PP process. Though, it was understood from the validation study that the simulated and experimental results are reasonably close, there are certain improvements that can lead to precise resolution prediction. It will be advantageous to include the role of density change as the liquid resin transforms into high molecular weight polymer. The change in density may have an effect on the heat diffusion and also on the molecular diffusion of radicals. The model includes the effect of temperature on the molecular diffusion parameter, but it does not consider the effect of decreasing free volume as highly crosslinked structures are formed. The decreasing free volume will try to reduce the effect of molecular diffusion. Hence, by including the role of density change and decreasing free volume, the model will be able to more precisely depict the polymerization process and will lead to more accurate resolution prediction.

The effect of high powers on the polymerized height was discussed in chapters 5 and 6. As discussed, the higher powers lead to the rapid depletion in photoinitiator concentration from the irradiated volume. The depletion leads to a gradient in the degree of polymerization that acts as a low NA lens causing the trapping of laser pulses along the optical axis. This variation in refractive index based on the gradient in conversion ratio is not considered in the developed mathematical framework. Though, the change in refractive index is generally small, nonetheless its inclusion will improve the model and will help in predicting the increased polymerized height because of the trapping of laser pulses. Modeling of refractive index modification along with density change and available free volume will help in transforming the model to a next level.

Another critical issue with 2PP is to evaluate the mechanical properties of polymerized structures. It is understood that the choice of material has a significant effect on the mechanical properties of the polymerized features. Multifunction monomers are mostly employed for polymerization as they impart high crosslinking that increases the mechanical strength of polymerized features. But apart from the material, the choice of process parameters (applied laser power, exposure time) may also have significant effect on the mechanical properties. The crosslinking of polymerized features generally increases with high dosage conditions. But as the 2PP takes place with a delicate balance between various physical and chemical phenomena, their exact role on the mechanical properties of polymerized features is difficult to evaluate. A detailed experimental analysis is required that can decipher the role of controllable process parameters (applied power, exposure time/scanning speed, concentration of photoinitiator) on the mechanical properties of the polymerized structures. Especially, as fabrication using 2PP undergoes stacking of voxels, the average overlap between the consecutive voxels may have significant effect on the mechanical properties. The overlap between the consecutive voxels is governed by the scanning speed of the laser beam through the resin system and hence becomes one of the important parameters to be carefully analyzed.

Functionalization of polymerized structures has been explored by a few research groups using metallic deposition. The metallic deposition is performed on the polymerized structures in a secondary process that imparts electrical properties to the structures. Another method that can impart functionalization is by embedding metallic nanoparticles in the polymerized structures during the polymerization process. In this method, the functionalized nanoparticles are suspended in the photoresponsive resin in defined concentrations. The laser is scanned inside the resin containing nanoparticles and the polymerization is performed that embeds these nanoparticles in the fabricated features. The embedded nanoparticles can impart functionalization and may also help in improving the mechanical properties of the polymerized structures. Also, the embedded nanoparticles can produce localized heating and may be

effectively used for various biological applications that require in vivo localized heating. Though there are few issues like scattering and opacity by mixing nanoparticles that are needed to be addressed. But this method can easily lead to the fabrication of functionalized micro/nano features in a single step process.

2PP can also be effectively used as a secondary process where custom fabrication can be effectively performed on already fabricated microstructures. This can be very effective technique in combining different technologies for a single application. One of the examples is combining microfluidics along with custom fabricated diffraction optical elements for biological sensing and smart lab on chip applications. The applications of 2PP for micro/nano fabrication are endless and with good understanding of the process, this versatile fabrication technique can be effectively used for complex 3D fabrication with very high resolution.

This research has effectively presented an approach to better understand the role of various process and material dependent parameters on the 2PP process. The simulated results present valuable information that can not be effectively evaluated from experiments alone. There still remain some process and material dependent challenges (highly efficient materials, serial processing, and mechanical strength of polymerized structures) that limit the use of 2PP for mass fabrication in an industrial setting. But with the ongoing collaborative effort between different research groups and the versatility in fabrication provided by 2PP, it is believed that 2PP will transform this technique into one of the most adapted process for 3D micro/nano fabrication.

REFERENCES

[1] C. Liu, "Recent developments in polymer MEMS", *Advanced Materials*, **19**, 3783-3790 (2007).

[2] P. R. Patterson, "Optical MEMS and polymers: An overview", Proceedings of SPIE-The International Society for Optical Engineering, Optomechatronic Micro/Nano Devices and Components, **6050**, 60500P (2005).

[3] J. Zhou, N. V. Lafferty, B. W. Smith, and J. H. Burnett, "Immersion lithography with numerical aperture above 2.0 using high index optical materials", *Proceedings of SPIE--The International Society for Optical Engineering, Optical Microlithography*, **6520**, 65204T (2007).

[4] J. D. Madden, and I. W. Hunter, "Three-dimensional microfabrication by localized electrochemical deposition", Journal of Microelectromechanical Systems, **5(1)**, 24-32, (1996).

[5] F. Watt, M. B. H. Breese, A. A. Bettiol, and J. A. Van Kan, "Proton beam writing", *Materials Today*, **10(6)**, 20-29, (2007).

[6] A. Bertsch, P. Bernhard, and P. Renaud, "Microsterolithography: Concepts and applications", *IEEE Symposium on Emerging Technologies and factory Automation*, **2**, 289-298, (2001).

[7] Kuebler, S.M., Rumi, M., "Nonlinear Optics-Applications: Three Dimensional Microfabrication", Elsevier: Oxford, 189-206, (2004).

[8] Sun, H., Kawata, S., "Two Photon Laser Precision Microfabrication and Its Applications to Micro-Nano Devices and Systems", Journal of Lightwave Technology, **21(3)**, pp. 624-633, (2003).

[9] A. Diaspro, Confocal and Two-Photon Microscopy-Foundations, Applications, and Advances, Wiley-Liss, New York, (2002).

[10] W. Denk, J.H. Strickler, and W.W. Webb, "Two Photon Laser Scanning Fluorescence Microscopy", *Science*, **248**, 73-76 (1990).

[11] Maruo, S., Kawata, S., "Twp Photon Absorbed Photopolymerization for Three Dimensional Microfabrication", *Proceedings of IEEE Micro Electro Mechanical Systems (MEMS)*, 169-174, (1997).

[12] W. Denk, and Svoboda, "Photon upmanship: Why multiphoton imaging is more than a gimmick", *Neuron*, **18**, 351-357, (1997).

[13] J.H. Strickler, and W.W. Webb, "Three dimensional optical data storage in refractive media by two photon point excitation", *Optics Letters*, **16**, 1780-1782 (1991).

[14] Glezer, E.N., Milosavljevic, M., Huang, L., Finlay, R.J., Her, T., Callan, J.P., Mazur, E., "Three-Dimensional Optical storage Inside Transparent Materials", *Optics Letters*, **21**, 2023-2025, (1996).

[15] J-P. Fouassier, Photoinitiation, Photopolymerization, and Photocuring – Fundamentals and Applications, Hanser Publishers, Germany, 1995.

[16] G. Odian, *Principles of Polymerization,* Wiley-Interscience, Singapore, 2004.

[17] E. S. Wu, J. H. Strickler, W. R. Harrell, and W. W. Watt, "Two-photon lithography for microelectronic application", *Proceedings of SPIE--The International Society for Optical Engineering, Optical/Laser Microlithography*, **1674**, 776-782, (1992).

[18] S. Maruo, N. Osamu, and S. Kawata, "Two-photon-absorbed photopolymerization for three-dimensional microfabrication", Optics *Letters*, **22(2)**, 132-134, (1997).

[19] B. H. Cumpston, S. P. Ananthavel, S. Barlow, D. L. Dyer, J. E. Ehrlich, L. L. Erskine, A. A. Heikal, S. M. Kuebler, I. -Y. S. Lee, McCord-Maughon, D. J. Qin, H. R. Röckel, M. Rumi, X. -L. Wu, S. R. Marder, and J. W. Perry, "Two-photon polymerization initiators for three-dimensional optical data storage and microfabrication", *Nature*, **398**, 51-54, (1999).

[20] J. Serbin, B.N. Chichkov, and R. Houbertz, “Three dimensional nanostructuring of hybrid materials by Two Photon Polymerization”, *Nanocrystals, and Organic and Hybrid Nanomaterials, Proceedings of SPIE*, **5222**, 171-177 (2003).

[21] J. Serbin, A. Egbert, A. Ostendorf, B. N. Chichkov, R. Houbertz, G. Domann, J. Schulz, C. Cronauer, L. Frohich, and M. Popall, “Femtosecond laser-induced two-photon polymerization of inorganic-organic hybrid materials for applications in photonics”, *Optics Letters*, **28(5)**, 301-303 (2003).

[22] S. A. Pruzinsky, and P. V. Braun, “Fabrication and characterization two-photon polymerized features in colloidal crystals”, *Advanced Functional Materials*, **15**, 1995-2004, (2005).

[23] M. Deubel, G. V. Freymann, M. Wegener, S. Pereira, K. Busch, and C. M. Soukoulis, “Direct laser writing of three-dimensional photonic-crystal templates for telecommunications”, *Nature Materials*, **3**, 444-447 (2004).

[24] H-B. Sun, S. Matsuo, and H. Misawa, “Three-dimensional photonic crystal structures achieved with two-photon-absorption photopolymerization resin”, *Applied Physics Letters*, **74(6)**, 786-788 (1999).

[25] A. Tal, Y-S. Chen, H. E. Williams, R. C. Rumpf, and S. M. Kuebler, “Fabrication and characterization of three-dimensional copper metallodielectric photon crystals”, *Optics Express*, 15**(26)**, 18283-18293, (2007).

[26] S. Maruo, K. Ikuta, and H. Korogi, “Force-controllable, optically driven micromachines fabricated by single-step two-photon Microstereolithography”, *Journal of Microelectromechanical Systems*, **12(5)**, 2003.

[27] R. A. Farrer, C. N. LaFratta, L. Li, J. Praino, M. J. Naughton, B. E. A. Saleh, M. C. Teich, and J. T. Fourkas, “Selective functionalization of 3-D of polymer microstructures”, *Journal of American Chemical Society*, **128**, 1796-1797, (2006).

[28] A. Ovsianikov, A. Doraiswamy, R. Narayan, and B. N. Chichkov, “Two-photon polymerization for fabrication of biomedical devices”, *Proceedings of SPIE-The international*

Society for Optical Engineering, Microfluidics, BioMENS, and Medical Microsystems V, **6465**, 64650O (2007).

[29] S. Schile, A. Ngezahayo, A. Ovsianikov, T. Fabina, H. Kolb, H. Haferkamp, and B. N. Chichkov, "Three-dimensional cell growth on structures fabricated from ORMOCER [registered trademark] by two-photon polymerization technique", *Journal of Biomaterials Applications*, **22(3)**, 275-284 (2007).

[30] J-I. Kato, N. Takeyasu, Y. Adachi, H-B. Sun, and S. Kawata, "Multiple-spot parallel processing for laser micronanofabrication", *Applied Physics Letters*, **86**, 044102, (2005).

[31] C. N. LaFratta, T. Baldacchini, R. A. Farrer, J. T. Fourkas, M. C. Teich, B. E. A. Saleh, and M. J. Naughton, "Replication of two-photon-polymerized structures with extremely high aspect ratios and large overhangs", *Journal of Physical Chemistry B*, **108(31)**, 11256-11258, (2004).

[32] C. N. LaFratta, J. T. Fourkas, T. Baldacchini, and R. A. Farrer, "Multiphoton fabrication", *Angewandte Chemie*, **46**, 6238-6258 (2007).

[33] C. A. Leatherdale, and R. J. DeVoe, "Two-photon microfabrication using two-component photoinitiaton systems: effect of photosensitizer and acceptor concentrations", *Nonlinear Optical Transmission and Multiphoton Processes in Organics, Proceedings of SPIE*, **5211**, 112-123 (2003).

[34] T. Baldacchini, C. N. LaFratta, R. A. Farrer, M. C. Teich, B. E. A. Saleh, M. J. Naughton, J. T. Fourkas, "Acrylic-based resin with favorable properties for three-dimensional two-photon polymerization", *Journal of Applied Physics*, **95(11)**, 6072-6076 (2004).

[35] G. Witzgall, R. Vrijen, E. Yablonovitch, V. Doan, and B. J. Schwartz, "Single-shot two-photon exposure of commercial photoresist for the production of three-dimensional structures", *Optics Letters*, **23(22)**, 1745-1747 (1998).

[36] K-S. Lee, R. H. Kim, D-Y. Yang, and S. H. Park, "Advances in 3D nano/microfabrication using two-photon initiated polymerization", *Progress in Polymer Science*, **33**, 631-681, (2008).

[37] R. J. DeVoe, H. Kalweit, C. A. Leatherdale, and T. R. Williams, "Voxel shapes in two-photon microfabrication", Proceedings of SPIE-The international Society for Optical Engineering, Multiphoton Absorption and Nonlinear Transmission Processes: Materials, Theory and Applications, **4797**, 310-316, (2003).

[38] K. Lee, D. Yang, S.H. Park, and R.H. Kim, "Recent developments in the use of two-photon polymerization in precise 2D and 3D microfabrication", *Polymers for Advanced Technologies*, **17**, 72-82 (2006).

[39] H. Sun, T. Tanak, and S. Kawata, "Three-dimensional focal spots related to two-photon excitation", *Applied Physics Letters*, **80(20)**, 3673-3675 (2002).

[40] H. Sun, K. Takada, M. Kim, K. Lee, and S. Kawata, "Scaling laws of voxels in two-photon polymerization nanofabrication", *Applied Physics Letters*, **83(6)**, 1104-1106 (2003).

[41] J-F. Xing, X-G. Dong, W-Q. Chen, X-M. Duan, N. Takeyasu, T. Tanaka, and S. Kawata, "Improving spatial resolution of two-photon microfabrication by using photoinitiator with high initiating efficiency", *Applied Physics Letters*, **90(13)**, P131106 (2007).

[42] G. Kamlage, T. Bauer, A. Ostendorf, and B. N. Chichkov, "Deep drilling of metals by femtosecond laser pulses", *Applied Physics A: Materials Science and Processing*, **77(2)**, 307-310, (2003).

[43] G. Dumitru, V. Romano, H. P. Weber, M. Sentis, and W. Marine, "Femtosecond ablation of ultrahard materials", *Applied Physics A: Materials Science and Processing*, **74(6)**, 729-739, (2002).

[44] Newport-Spectra Physics, "MaiTai user's manual", 2002.

[45] Newport-Spectra Physics, "Hurricane user's manual", 2002.

[46] N. Uppal, P. S. Shiakolas, and S. Belligundu, “Femtosecond laser micromachining as a rapid prototyping environments-System development and initial results”, *Proceedings of International Mechanical Engineering Congress and Exposition, Design and Manufacturing*, (2006).

[47] Sartomer Application Bulletin, “Ethoxylated TMPTA monomers: Properties and performance”, 2008.

[48] C. R. Mendonca, D. S. Correa, T. Baldacchini, P. Tayalia, and E. Mazur, “Two-photon absorption spectrum of the photoinitiator Lucirin TPO-L”, *Applied Physics A: Materials Science and Processing*, **90(4)**, 633-636 (2008).

[49] R. E. Medsker, M. Chumacero, E. R. Santee, A. Sebenik, and H. J. Harwood. “P-NMR characterization of chain ends in polymers and copolymers prepared using Lucirin TPO as a photoinitiator”, *Acta Chimica Slovenica*, **45(4)**, 371-388, (1998).

[50] T. Cauffman, “The effects polymerization inhibitors have on acrylate monomers and formulations”, *Sartomer Company Inc.*, 2008.

[51] G. Witzgall, R. Vrijen, E. Yablonovitch, V. Doan, and B. J. Schwartz, “Single-shot two-photon exposure of commercial photoresist for the production of three-dimensional structures”, *Optics Letters*, **23(22)**, 1745-1747 (1998).

[52] M. D. Goodner, and C. N. Bowman, “Development of a comprehensive free radical photopolymerization model incorporating heat and mass transfer effects in thick films”, *Chemical Engineering Science*, **57**, 887-900 (2002).

[53] A. O’Brien, and C. N. Bowman, “Modeling thermal and optical effects on photopolymerization systems”, *Macromolecules*, **36**, 7777-7782 (2003).

[54] M. F. Perry, and G. W. Young, “A mathematical model for photopolymerization from a stationary laser light source”, *Macromolecular Theory Simulations*, **14**, 26-39 (2005).

[55] P. F. Jacobs, and D. T. Reid, *Rapid Prototyping and Manufacturing: Fundamentals of Stereolithography*, Society of Manufacturing Engineers, 1992.

[56] N. Fang, C. Sun, and X. Zhang, "Diffusion-limited photopolymerization in scanning micro-stereolithography", *Applied Physics A*, **79**, 1839-1842 (2004).

[57] J. D. Hoffman, *Numerical methods for engineers and scientists*, Marcel Dekker Inc., Second Edition, 2001.

[58] H. Sun, M. Maeda, K. Takada, J. W. M. Chon, M. Gu, and S. Kawata, "Experimental investigation of single voxels for laser nanofabrication via two-photon polymerization", *Applied Physics Letters*, **83(5)**, 819-821 (2003).

[59] K. Takada, K. Kaneko, Y. Li, S. Kawata, Q. Chen, and H. Sun, "Temperature effects on pinpoint photopolymerization and polymerized micronanostructures", *Applied Physics Letters*, **92**, 041902 (2008).

[60] J. Brandrup, E. H. Immergut, *Polymer handbook*, John Wiley and Sons, Second Edition, 1975.

[61] D. R. Lide, ed., *CRC Handbook of Chemistry and Physics*, CRC Press, Boca Raton, FL, 2005.

[62] F. Qi, Y. Li, H. Guo, H. Yang, and Q. Gong, "Wavy lines in two-photon photopolymerization microfabrication", *Optics Express*, **12(20)**, 4725-4730, (2004).

[63] T. Mappes, S. Achenbach, and J. Mohr, "X-ray lithography for devices with high aspect ratio polymer submicron structures", *Microelectronic Engineering*, **84**, 1235-1239, (2007).

[64] J. Mohr, P. Bley, M. Strohrmann, and U. Wallrabe, "Microactuators fabricated by LIGA process", *Journal of Micromechanics and Microengineering*, **2 (4)**, 234-241, (1992).

[65] R. Boucher, U. Hübner, W. Morgenroth, H. Roth, H.-G. Meyer, M. Schmidt, and M. Eich, "Etching a sub-micron high aspect ratio holes in oxides and polymers", *Microelectronic Engineering*, **73-74**, 330-335, (2004).

[66] C. N. LaFratta, T. Baldacchini, R. A. Farrer, J. T. Fourkas, M. C. Teich, B. E. A. Saleh, and M. J. Naughton, "Replication of two-photon-polymerized structures with extremely high

aspect ratios and large overhangs", *Journal of Physical chemistry B*, **108 (31)**, 11256-11258, (2004).

[67] C.-H. Lee, T.-W. Chang, K.-L. Lee, J.-Y. Lin, and J. Wang, "Fabrication of high-aspect-ratio sub-diffraction-limit structures on silicon with two-photon photopolymerization and reactive ion etching", *Applied Physics A: Materials Science and Processing*, **79(8)**, 2027-2031, (2004).

[68] E.-Y. Pan, N.-W. Pu, Y.-P. Tong, and H.-F. Yau, "Fabrication of high-aspect-ratio sub-diffraction-limit microstructures by two-photon-absorption photopolymerization", *Applied Physics B: Lasers and Optics*, **77(5)**, 485-488, (2003).

[69] F. Qi, Y. Li, H. Guo, H. Yang, and Q. Gong, "Wavy lines in two-photon photopolymerization microfabrication", *Optics Express*, **12(20)**, 4725-4730, (2004).

[70] B. E. A. Saleh, and M. C. Teich, *Fundamentals of Photonics*, New York: John Wiley and Sons, (1991).

[71] R.W. Boyd, *Nonlinear Optics,* Academic Press, San Diego, (2003).

[72] A. S. Kewitsch, and A. Yariv, "Self-focusing and self-trapping of optical beams upon photopolymerization", *Optics Letters*, **21 (1)**, 24-26, (1996).

[73] T. Yamashita, and M. Kagami, "Fabrication of light-induced self-written waveguides with w-shaped refractive index profile", *Journal of Lightwave Technology*, **23 (8)**, 2542-2548, (2005).

[74] A. Saliminia, N. T. Nguyen, S. L. Chin, and R. Vallée, "The influence of self-focusing and filamentation on refractive index modifications in fused silica using intense femtosecond pulses", *Optics Communications*, **241 (4-6)**, 529-538, (2004).

[75] T. Tanaka, M. Morigami, and N. Atoda, "Mechanism of resist pattern collapse during development process", *Japanese Journal of Applied Physics*, **32**, 6059-6064, (1993).

[76] A. Jouve, J. Simon, A. Pikon, H. Solak, C. Vannuffel, and J-H. Tortai, "Overcoming pattern collapse on E-beam and EUV lithography", *Advances in Resist Technology and Processing, Proceedings of SPIE*, **61531**, (2006).

[77] Sartomer Application Bulletin, "Surface Tensions of Sartomer Monomers", Sartomer Company, Inc., (2004).

BIOGRAPHICAL INFORMATION

Nitin Uppal received his Bachelor of Engineering degree in Mechanical Engineering from the Maharishi Dayanand University, India in 2002. He worked as a Trainee Engineer for Amtek Auto Ltd., India for the period of one year before joining Mechanical and Aerospace Engineering Department at the University of Texas at Arlington in the Fall of 2003. For his Master of Science research, he worked on the Femtosecond laser assisted ablation study and rapid prototyping. He received his Master of Science in Mechanical Engineering in the Spring of 2005 and continued to stay at The University of Texas at Arlington for his PhD. studies. His research interests include novel methods for micro/nano fabrication, ultrashort laser induced material ablation, optical sensing, process development and simulation. He is also interested in using the numerical computation and statistical analysis for process validation and improvement. He will receive his Doctorate in Mechanical Engineering in August 2008.